Saint Petersburg State University

Pochkaeva Evgeniia Igorevna

Synthesis, identification and physicochemical properties of the C_{60} fullerene adduct with L-arginine

Scientific specialty 1.4.15. Solid-state chemistry

The dissertation is submitted for the degree of Candidate of Chemical Sciences

Translation from Russian

Academic supervisor:
Doctor of Biological Sciences, Associate Professor,
Sharoyko Vladimir Vladimirovich

Saint Petersburg
2024

Contents

Introduction

The prospects for using fullerenes in biomedicine became obvious almost from the moment of their discovery [1,2]. The fullerene molecule has a high reactivity due to the large number of double bonds to which various radicals can attach [3,4], the ability to penetrate cell membranes [5,6], modulate ion transport [5,6], and overcome the blood-brain barrier [7,8]. Thus, fullerenes are considered promising scaffolds for the production of new high-tech nanomaterials and drugs for medicine.

The study of the physicochemical properties of fullerenes and their derivatives is a necessary condition for understanding the mechanisms of their action, biodistribution and pharmacokinetics, etc. [9]

The main difficulty in the biomedical use of fullerenes is associated with the insolubility of fullerene molecules in water and aqueous solutions [5,6]. A way to solve this problem is the synthesis of water-soluble fullerene adducts [5,6,10]. Analysis of the literature shows that the most promising classes of water-soluble fullerene adducts are carboxylated and polyhydroxylated adducts [5,6,11], adducts of fullerenes with amino acids [12], peptides and proteins [13–17].

It has been established that water-soluble fullerene adducts exhibit antibacterial properties [18], pro- and antioxidant activity [4,19], and also have prospects for use as scaffolds for obtaining antitumour [20,21], neuroprotective [7,8,22], antiviral drugs [23–25]. Moreover, water-soluble fullerene adducts have great potential for use in the creation of microfertilisers due to their ability to carry out transmembrane transport of macro- and microelements, as well as due to their pronounced antioxidant activity [11,26–28].

According to the data presented in the Scopus database, there is an increase in scientific publications in the field of production and application of water-soluble adducts of light fullerenes with amino acids, peptides and proteins (Fig. 1).

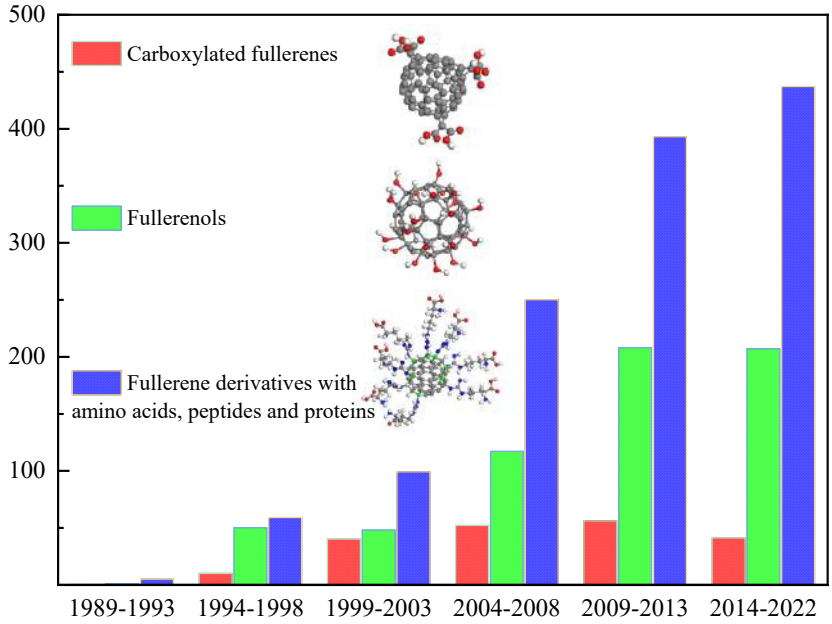

Fig. 1. Number of scientific publications (by year) in the field of production and application of water-soluble adducts of light fullerenes with amino acids, peptides and proteins.

Purpose and objectives of the work

The purpose of the work is to develop a method for the synthesis of the C_{60} fullerene adduct with L-arginine, its identification, and the study of thermodynamic properties, as well as the physicochemical properties of aqueous solutions.

To achieve this goal, the following tasks were set:

1. Development of a method for one-step synthesis of a water-soluble adduct of fullerene C_{60} with L-arginine, allowing to obtain a product with high yield (more than 90 %).

2. Identification of the C_{60} fullerene adduct with L-arginine using a complex of physicochemical methods of analysis, namely: elemental analysis, IR and ^{13}C NMR spectroscopy, high-performance liquid chromatography (HPLC), thermogravimetric analysis.

3. Study of the thermodynamic properties of the adduct of fullerene C_{60} with L-arginine in the temperature range T = 13–326 K using adiabatic vacuum calorimetry.

4. Conducting a comprehensive study of the physicochemical properties of aqueous solutions of the C_{60} adduct with L-arginine in a wide range of temperatures and concentrations (density, viscosity, refractive index, particle size distribution, ζ-potential).

5. Study of the biocompatibility of the C_{60} fullerene adduct with L-arginine, including the study of cyto- and genotoxicity, antiradical activity and binding to human serum albumin (HSA).

Scientific novelty

1. A method has been developed for obtaining the adduct of fullerene C_{60} with L-arginine, characterised by high yield (more than 90 %). Dialysis was used for the first time to purify the adduct.

2. Identification of the synthesised adduct using a complex of modern physicochemical methods of analysis allows us to conclude that the resulting compound is an adduct of C_{60} fullerene with L-arginine. The method of solid-state 13C NMR spectroscopy was used for the first time to characterise adducts of fullerenes with amino acids.

3. For the first time, the thermodynamic properties of the C_{60} fullerene adduct with L-arginine were studied in a wide temperature range T = 13–326 K using adiabatic vacuum calorimetry.

4. Experimental data on the study of the physicochemical properties of solutions of the synthesised adduct of fullerene C_{60} with L-arginine are the basis for the creation of materials for biomedical use.

5. Based on data on the study of cyto- and genotoxicity, it is shown that the adduct of fullerene C_{60} with L-arginine is non-toxic.

Reliability and testing of research results

The results were published in four papers in peer-reviewed scientific journals, indexed in the Scopus and Web of Science databases, and presented at ten international and all-Russian scientific conferences.

List of publications

1. Iurev G.O., Lelet M.I., Pochkaeva E.I., Petrov A.V., Semenov K.N., et. al. Thermodynamic and thermal properties of the C_{60}-L-Arg derivative // *J. Chem. Thermodyn.* — 2018. — Vol.127. — P. 39–44 (Q1, IF 2.6).

2. Pochkaeva E.I., Anufrikov Yu.A., Faenkova V.P., Sharoyko V.V., Charykov N.A., Murin I.V. Isothermal calorimetric titration of human serum albumin with C_{60}-L-arginine adduct // *Journal of General Chemistry*. — 2019. — Vol.89. — №8. — P.1309–1312 (Q4, IF 0.9).

3. Pochkaeva E.I., Meshcheriakov A.A., Ageev S.V., Podolsky N.E., Petrov A.V., et. al. Polythermal density and viscosity, nanoparticle size distribution, binding with human serum albumin and radical scavenging activity of the C_{60}-L-arginine ($C_{60}(C_6H_{13}N_4O_2)_8H_8$) aqueous solutions // *J. Mol. Liquids*. — 2020. — Vol.297. — P.111915 (Q1, IF 6.0).

4. Pochkaeva E.I., Podolskiy N.E., Zakusilo D.N., Andrusenko E.V., Petrov A.V. et. al. Fullerene derivatives with amino acids, peptides and proteins: from synthesis to biomedicinal application // *Prog in Solid State Chem.* — 2020. — Vol.57. — P.100255 (Q1, IF 12.0).

List of conferences

1. Materials of the LXXIX scientific-practical conference with international participation ‘Current issues of experimental and clinical medicine — 2018’ April 1–27, 2018. Pochkaeva E.I., Meshcheryakov A.A., Yuryev G.O., Pechnikova N.A. ‘Study of hemocompatibility of water-soluble adducts of light fullerenes *in vitro*’, St. Petersburg, Russian Federation, 2018.

2. Materials of the II All-Russian Conference ‘Baikal School-Conference in Chemistry’ September 24–28, 2018. Pochkaeva E.I., Meshcheriakov A.A., Yur’ev G.O., Pechnikova N.A., Leonova Y.V., Nurutdinov A.Z. ‘*In vitro* hemocompatibility and antioxidant properties of water-soluble adducts of light fullerenes with L-arginine’, Irkutsk, Russian Federation, 2018.

3. Proceedings of the international student conference ‘Science and Progress — 2018’ November 12–14, 2018. Pochkaeva E. ‘Antioxidant activity and binding of the C60-Arg

derivative with human serum albumin (HSA)', St. Petersburg, Russian Federation, 2018.

4. Materials of the LIII PNPI School on Condensed Matter Physics March 11–16, 2019. Pochkaeva E.I., Semenov K.N., Charykov N.A., Sharoyko V.V. 'Biomedical study of the C_{60}-L-arginine derivative', St. Petersburg, Russian Federation, 2019.

5. Materials of the IX scientific and technical conference of students, graduate students, young scientists with international participation 'Science Week 2019' April 1–3, 2019. Pochkaeva E.I., Charykov N.A., Sharoyko V.V. 'Study of the physicochemical properties of aqueous solutions of fullerene derivative C_{60} with L-arginine ($C_{60}(C_6H_{13}N_4O_2)_8H_8$)', St. Petersburg, Russian Federation, 2019.

6. Materials of the VI international conference 'Modern biotechnologies for science and practice' April 25–26, 2019. Pochkaeva E.I., Semenov K.N., Anufrikov Yu.A., Sharoyko V.V. 'Study of the interaction of C_{60}-L-arginine with human serum albumin by isothermal titration calorimetry,' St. Petersburg, Russian Federation, 2019.

7. Materials of the national medical innovation forum 'Almazov Youth Medical Forum — 2019' May 16–18, 2019. Pochkaeva E.I., Pechnikova N.A., Semenov K.N. 'Study of the interaction of the C_{60}-L-arginine derivative ($C_{60}(C_6H_{13}N_4O_2)_8H_8$) with blood components', St. Petersburg, Russian Federation, 2019.

8. Materials of the XII All-Russian school-conference of young scientists 'Theoretical and experimental chemistry of liquid-phase systems' October 7–11, 2019. Pochkaeva E.I., Semenov K.N., Sharoyko V.V., Lelet M.I. 'Thermodynamic study of the fullerene derivative C_{60} with L-arginine ($C_{60}(C_6H_{13}N_4O_2)_8H_8$)', Ivanovo, Russian Federation, 2019.

9. Materials of the XXVI All-Russian Conference of Young Scientists with International Participation 'Current Problems of Biomedicine — 2020' March 26–27, 2020. Pochkaeva E.I., Semenov K.N., Vasina L.V., Solovtsova I.L. 'Biological activity of the adduct of fullerene C_{60} with L-arginine ($C_{60}(C_6H_{13}N_4O_2)_8H_8$)', St. Petersburg, Russian Federation, 2020.

10. Materials of the XXVII All-Russian Conference of Young Scientists with International Participation 'Current Problems of Biomedicine — 2021' March 25–26,

2021. Pochkaeva E.I., Meshcheryakov A.A., Ageev S.V. ‘Adduct of fullerene C_{60} with L-arginine: study of physicochemical properties and biological activity’, St. Petersburg, Russian Federation, 2021.

The work was carried out with financial support from the Ministry of Health of the Russian Federation (state task on the topic ‘Development of a radioprotector based on water-soluble forms of nanocarbon modified with L-amino acids’, registration No. 123020800170-8).

The author’s personal contribution was the analysis of literature data, the synthesis and identification of the adduct of light fullerene C_{60} with L-arginine, the study of the physicochemical properties and biocompatibility of the resulting adduct, the discussion of experimental results and the preparation of scientific publications based on the dissertation materials.

Structure of the dissertation: the dissertation consists of a list of abbreviations, introduction, three chapters, conclusion, appendix; the first chapter presents a review of the literature, the second chapter describes the materials and research methods, the third chapter presents the results on the synthesis, identification and physicochemical properties of the individual C_{60} fullerene adduct with L-arginine and its solutions, as well as the results on the study of biocompatibility. The dissertation is presented on 117 pages, contains 79 figures, 17 tables, 130 literature references.

Main scientific results

1. A new method for obtaining a water-soluble adduct of fullerene C_{60} with l-arginine has been developed and its identification has been carried out using a complex of physicochemical methods of analysis: ^{13}C NMR, IR spectroscopy, thermogravimetric analysis, elemental analysis and HPLC. See works [122,123] from the dissertation reference list (in particular, section 2.1 in [122] and section 2.2 in [123]; personal contribution is at least 80%).

2. The thermodynamic properties of the C_{60} fullerene adduct with l-arginine were studied in a wide temperature range T = 13–326 K using adiabatic vacuum calorimetry. See works [96,122] from the dissertation reference list (in particular, section 3.1 in [96] and section 2.2 in [122]; personal contribution is at least 60%).

3. A study was carried out of the physicochemical properties of aqueous solutions of the adduct of fullerene C_{60} with l-arginine: densities, viscosities, refractive indices, particle size distribution and ζ-potentials were studied. See sections 3.1, 3.2, 3.3 in [122] from the dissertation reference list (personal contribution is at least 80%).

4. The biocompatibility of the C_{60} fullerene adduct with l-arginine was studied. See work [126] from the dissertation reference list (personal contribution is at least 80%).

5. The interaction of the C_{60} fullerene adduct with l-arginine with the stable DPPH radical was studied. See section 3.8 in [123] from the dissertation reference list (personal contribution is at least 70%).

Provisions for defence

1. A one-step method for the synthesis of the C_{60} fullerene adduct with L-arginine, which makes it possible to obtain a water-soluble nanomaterial with a yield of more than 90 %, as well as data on its identification.

2. Results of thermodynamic study of the adduct of fullerene C_{60} with L-arginine in the temperature range T = 13–326 K.

3. Data on the study of the physicochemical properties of aqueous solutions and phase equilibria in binary systems of fullerene C_{60} adduct with L-arginine-water.

4. Results of the study of the biocompatibility of the C_{60} fullerene adduct with L-arginine, including the study of cyto- and genotoxicity, antiradical activity and binding to HSA.

Chapter 1. Literature review

1.1. Synthesis of fullerene adducts with amino acids, peptides and proteins

In the first studies devoted to the study of the reactivity of individual light fullerenes (C_{60} and C_{70}), it was found that fullerenes easily enter into nucleophilic addition reactions with primary and secondary amines [29,30]. In works [31–43], C_{60} adducts with the following amino acids and peptides were obtained using a one-step synthesis (Fig. 2): glycine, *p*-aminobenzoic acid, ω-aminocaproic acid, γ-aminobutyric acid, L-proline, L-alanine-*N*-methyl-L-alanine, DL-serine, D-arginine, L-arginine, β-alanine, valine, cystine, phenylalanine, folacin, carnosine and glutathione. Identification of the obtained compounds was carried out using a complex of physicochemical methods (IR spectroscopy, mass spectrometry, HPLC, NMR spectroscopy, elemental analysis, dynamic light scattering). The disadvantage of the work is the lack of data on the yields of the final adducts.

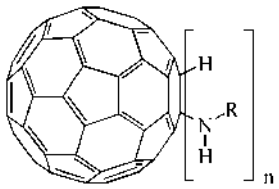

1. R = CH_2COOH n = 1
2. R = pC_6H_4COOH n = 1
3. R = $(CH_2)_5COOH$ n = 1
4. R = $(CH_2)_5COONa$
5. R = $(CH_2)_3COOH$ n = 1
6. R = $(CH_2)_5COONa$
7. R = C_4H_6COOH
8. R = $(CH_2)_2COOH$ n = 1
9. R = L,D-$CH(CH_3)COOCH_3$ n = 1
10. R = L,D-$C(CH_2OH)COOH$ n = 1
11. R = L,D-$C(=NH)NH(CH_2)_3CH(NH_2)COOH$ n = 1
12. R = CH_3-$CH(CH_3)CHCOOH$ n = 1
13. R = $C_5H_9NO_2S_2COOH$ n = 1
14. R = C_8H_8COOH n = 1
15. R = C_8H_5OCOOH n = 4
16. R = $C_9H_{10}O_4SCOOH$ n = 3

Fig. 2. C_{60} adducts with amino acids and peptides [31–43].

Khalikov *et al.* [44] as a result of a one-step reaction between fullerene and amino acids in an alkaline medium, obtained sodium salts of fullerene C_{60} with glycine and L-lysine: $C_{60}(Gly\text{-}ONa)_6 \cdot 10H_2O$, $C_{60}(Lys\text{-}ONa)_4 \cdot 10H_2O$, as well as adducts of mixed composition: $C_{60}[(Gly\text{-}ONa)_3(Lys\text{-}ONa)_2] \cdot 10H_2O$ and $C_{60}[(Gly\text{-}ONa)_3(Asp\text{-}ONa)_2Arg\text{-}ONa] \cdot 10H_2O$. Identification of the obtained compounds was carried out using IR, NMR spectroscopy, and mass spectrometry.

The patent [45] presents a method for producing a new class of compounds — fullerene polycarbonate anions with the general formula $C_{60}H_n[NH(CH_2)_mC(O)O^-]_n$,

where m = 1–5, n = 2–12. The resulting adducts were characterised by NMR spectroscopy (^{1}H NMR and ^{13}C NMR). In the patent [46], crystalline hydrates of C_{60} adducts with aminocarboxylic acids with the general formula $C_{60}(H)_3\{NH(CH_2)_nCOOH\}_3 \cdot xH_2O$ were obtained, where n = 5–7; x = 8–10 (Fig. 3).

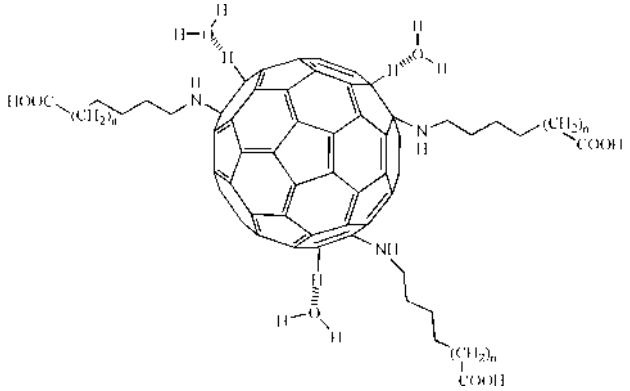

Fig. 3. General structural formula of C_{60} adducts with amino acids [46].

These adducts were characterised using IR spectroscopy, elemental analysis and thermogravimetry. Hsieh *et al.* [7] synthesised salt forms of water-soluble adducts of fullerene C_{60} with L-phenylalanine (Fig. 4*a*), L-serine (Fig. 4*b*), β-alanine (Fig. 4*c*) and with γ-phenylbutyric acid (Fig. 4*d*). The authors found that the resulting adducts contain five highly polar solubilising groups attached to one hemisphere of the fullerene core, while the second hemisphere remains non-functionalised and highly hydrophobic. This unique molecular structure distinguishes these compounds from most other water-soluble fullerene adducts, giving the compounds amphiphilicity leading to self-assembly in polar solvents. The obtained adducts were characterized by NMR.

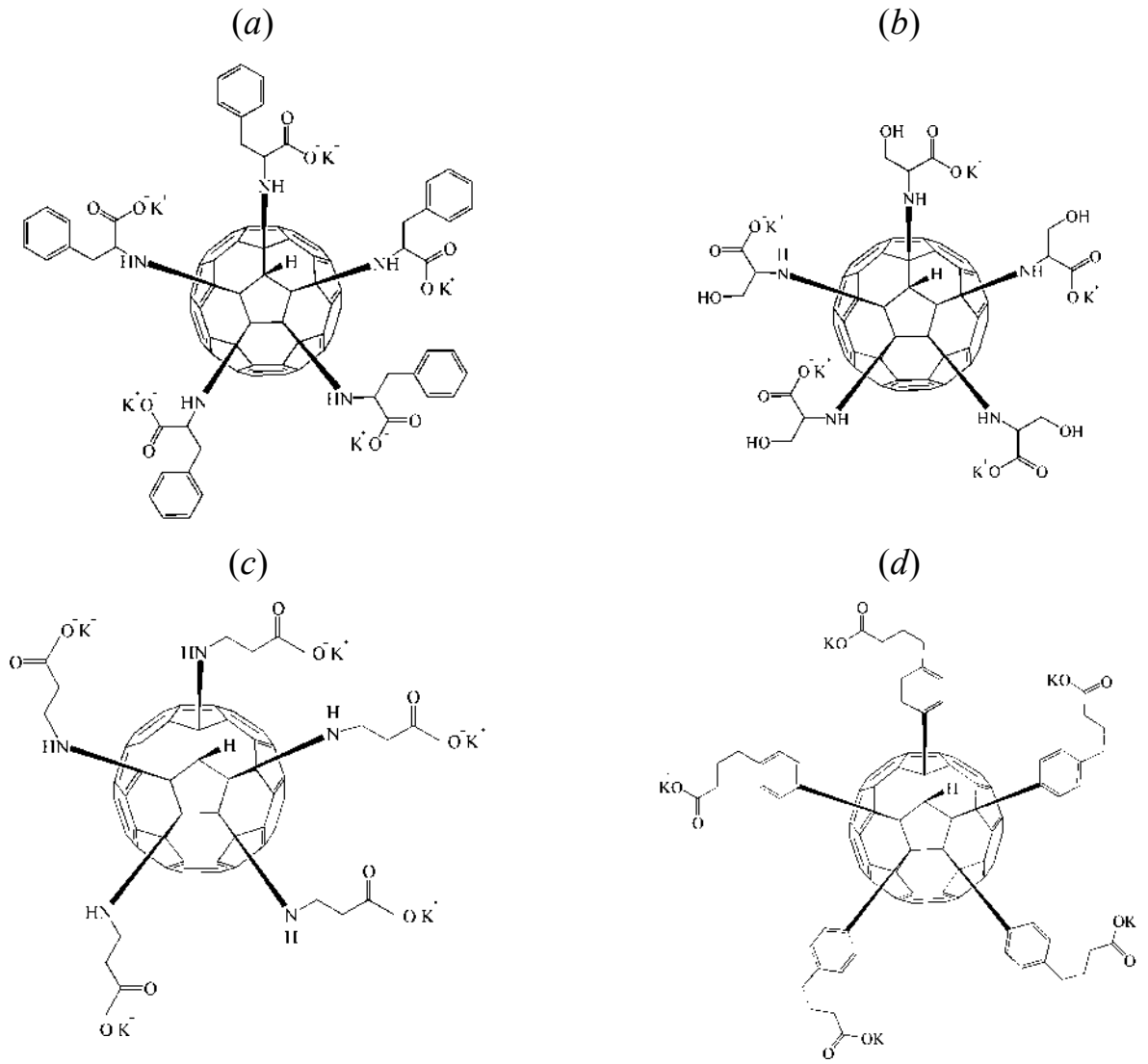

Fig. 4. Water-soluble adducts of light C_{60} fullerenes with amino acids: L-phenylalanine (*a*), L-serine (*b*), β-alanine (*c*) and γ-phenylbutyric acid (*d*) [7].

Maggini *et al.* [47] obtained a fulleroproline adduct as a result of the 1,3-dipolar cycloaddition of azomethine ylides to C_{60} fullerene (Prato reaction) (Fig. 5).

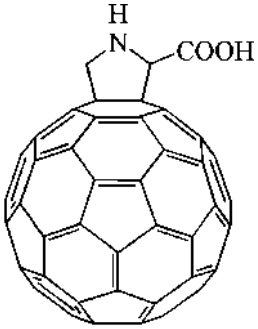

Fig. 5. Fulleroproline adduct [47].

The resulting adduct was characterised by 1H NMR, 13C NMR and UV spectroscopy. Watanabe *et al.* [48] proposed methods for using the Prato reaction to

synthesise fullerene adducts with amino acids containing 4–6 methylene units (Fig. 6). The resulting adducts were characterised by ^{1}H NMR, ^{13}C NMR and mass spectrometry.

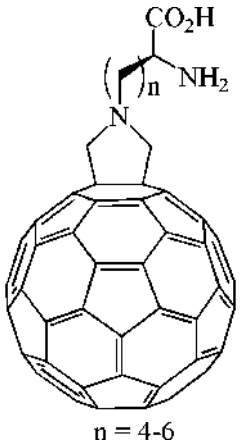

Fig. 6. Adduct of fullerene with amino acids containing 4–6 methylene units [48].

Zhang *et al.* [49] carried out the condensation of *N*-substituted fulleropyrrolidine with L-aspartic (Fig. 7*a*) and L-glutamic acids (Fig. 7*b*) containing protected α-amino and α-carboxy groups. The product yields (Fig. 7*a*) and (Fig. 7*b*) were 82 and 83 %, respectively. The resulting compounds were characterised using mass spectrometry, UV, IR and NMR spectroscopy.

(*a*) (*b*)

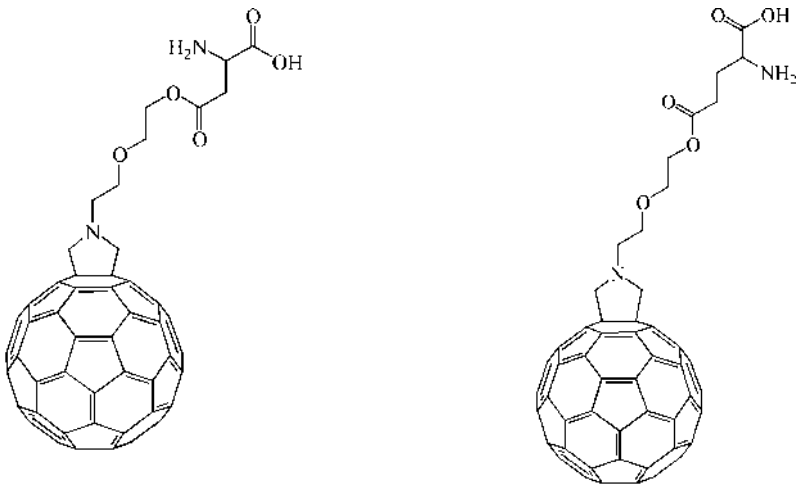

Fig. 7. Adducts of C_{60} with L-aspartic (*a*) and L-glutamic (*b*) acid [49].

Currently, there are two methods for the synthesis of C_{60} fullerene adducts with peptides. The simplest method is the functionalisation of fullerene with a pre-synthesised peptide. A more complex method is the synthesis of peptides with the introduction of a C_{60} peptide into the amino acid sequence.

Romanova *et al.* [32] were the first to perform a direct functionalisation reaction of C_{60} fullerene with a peptide. The reaction mechanism for the interaction of C_{60} with various dipeptides (L-Ala-L-Ala, D,L-Ala-D,L-Ala, and Gly-L-Val) is nucleophilic addition (Fig. 8). The resulting compounds were characterised by NMR spectroscopy.

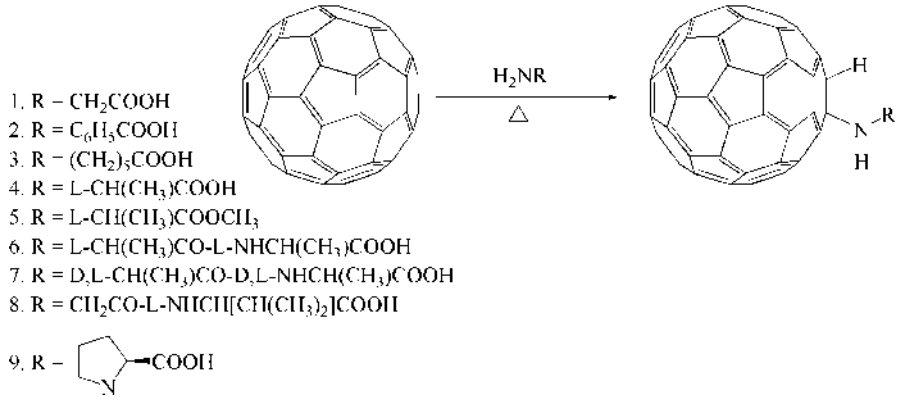

Fig. 8. Scheme for preparing C_{60}-based adducts with peptides [32].

Wang *et al.* [50] obtained the adduct of C_{60} with glycylglycine methyl ester (Fig. 9) as a result of the interaction of an aqueous solution of methylglycylglycinate with C_{60} in an alkaline medium upon heating. Identification of the resulting adduct was carried out using IR, UV, NMR spectroscopy, and mass spectrometry.

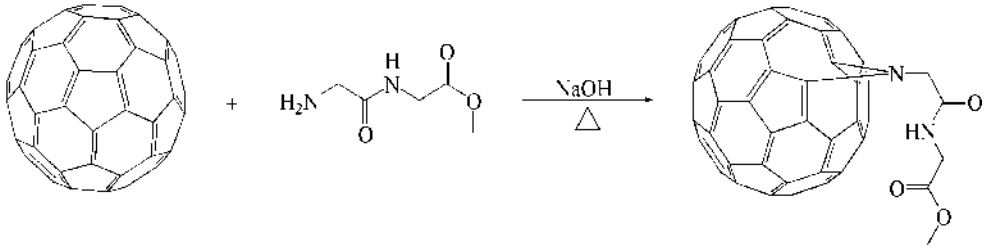

Fig. 9. Scheme for the preparation of the C_{60} adduct with glycylglycine methyl ether with C_{60} fullerene [50].

The fullerenopeptide (Fig. 10) was synthesised as a result of the addition of the *N*-terminus of a pentapeptide with an alternating –Ala-Aib sequence to methanofullerene [51].

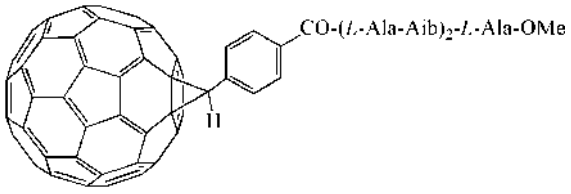

Fig. 10. Fullerenopeptide [51].

Identification of the resulting compound was carried out using UV, IR, and NMR spectroscopy methods.

Toniolo *et al.* [14] described a two-step synthesis of a water-soluble oligopeptide (Fig. 11). First, the authors obtained methanofullerene carboxylic acid, which was then bound by the standard method (using DCC/HOBt [52]) to the α-amino group of peptide T. Identification of the resulting compound was carried out using UV and NMR spectroscopy.

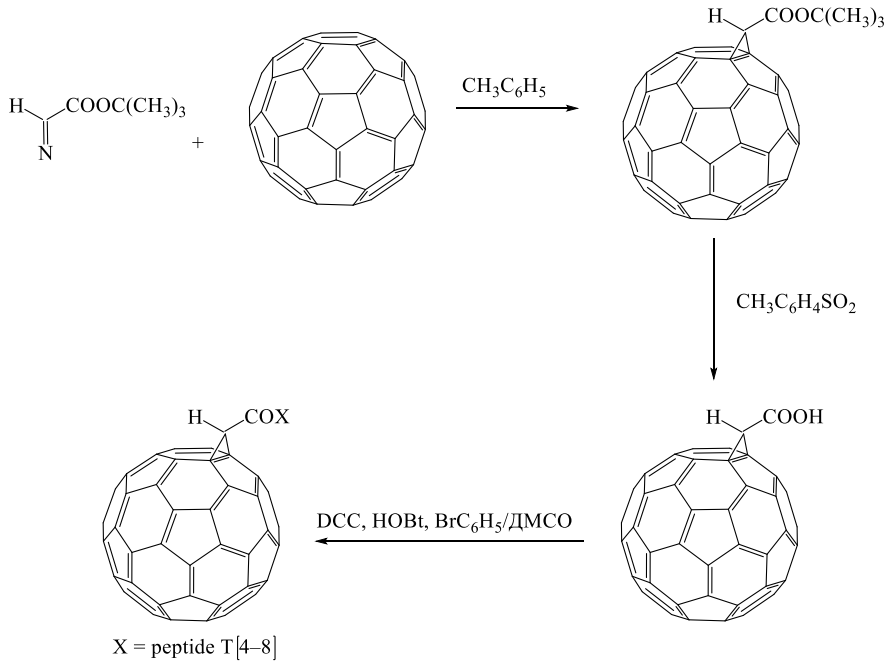

Fig. 11. Scheme for the synthesis of the C_{60} adduct with peptide T [14].

The patent [53] describes a method for preparing the fullerene-containing glycopeptide GlcNac-MurNac-Ala-DiGln[Lys-ε-CO$(CH_2)_5$NHC_{60}-H] from the adduct of fullerene with ε-aminocaproic acid and Lys-containing glycopeptide. The formula of the final product is presented in Fig. 12. Identification of the resulting compound was carried out using NMR spectroscopy.

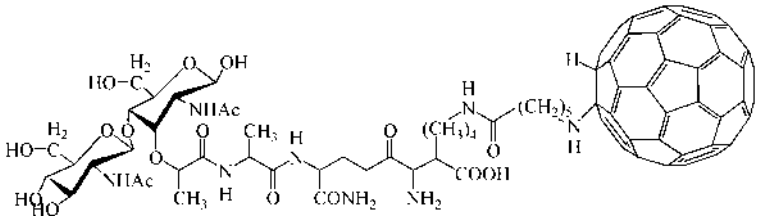

Fig. 12. Fullerene-containing glycopeptide [53].

Polese *et al.* [54] described the synthesis and photophysical properties of the $[Ru(bpy)_3]^{2+}$-hexapeptide-C_{60} complex (bpy = 2,2'-bipyridine) (Fig. 13).

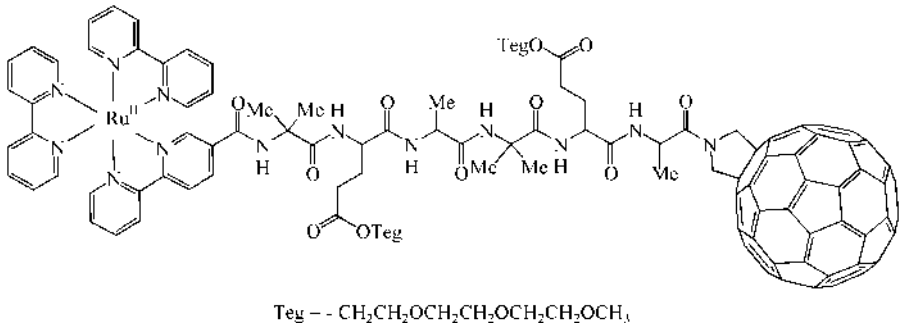

Fig. 13. $[Ru(bpy)_3]^{2+}$-hexapeptide-C_{60} (bpy = 2,2'-bipyridine) [54].

The synthesis of the adduct was carried out in several stages: (*1*) preparation of unsubstituted fulleropyrrolidine by the Prato reaction; (*2*) carrying out the reaction of interaction of unsubstituted fulleropyrrolidine with Boc-protected alanine; (*3*) deprotection and reaction with bipyridine pentapeptide; (*4*) reacting the resulting adduct with a ruthenium-bipyridine complex. Identification of the resulting compound was carried out using IR, UV, and NMR spectroscopy methods.

Usaka *et al.* [55] obtained C_{60} adducts with *N*-Boc-protected hexapeptides L-Leu-Aib-L-Leu_2-Aib-Gly (Fig. 14*a*) and D-Leu-Aib-D-Leu_2-Aib-Gly (Fig. 14*b*).

(*a*)

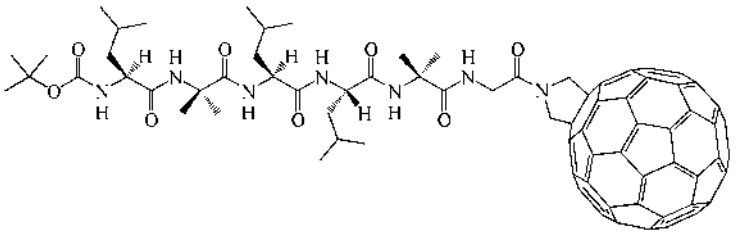

(*b*)

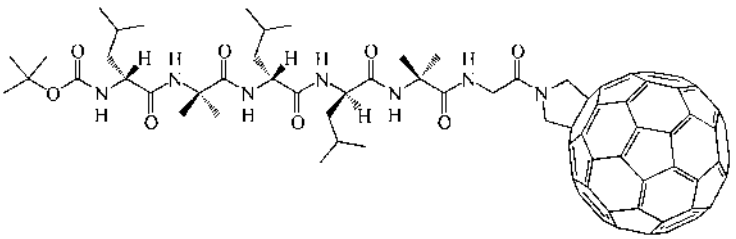

Fig. 14. C_{60} adducts with *N*-Boc-protected hexapeptides L-Leu-Aib-L-Leu_2-Aib-Gly (*a*) and D-Leu-Aib-D-Leu_2-Aib-Gly (*b*) [55].

The enantiomeric adducts (Fig. 14*a*) and (Fig. 14*b*) were then encapsulated into the helical cavity of syndiotactic polymethyl methacrylate (st-PMMA) (Fig. 15) to

produce unique optically active helix-in-helix supramolecular complexes. Next, the complexes were characterised using a set of physicochemical methods: NMR spectroscopy, mass spectrometry, IR spectroscopy, circular dichroism spectroscopy, X-ray diffraction analysis, as well as using differentiating scanning calorimetry.

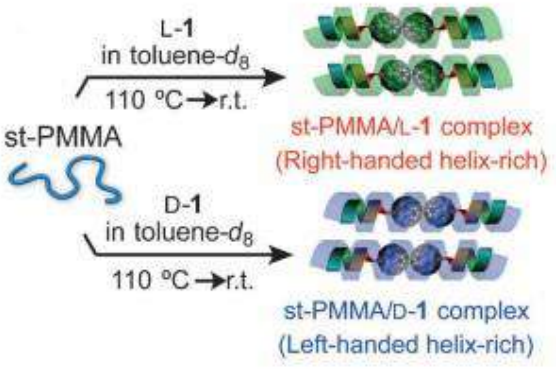

Fig. 15. Scheme of encapsulation of C_{60} adducts with *N*-Boc-protected hexapeptides *N*-Boc-L-Leu-Aib-L-Leu_2-Aib-Gly and *N*-Boc-D-Leu-Aib-D-Leu_2-Aib-Gly into the spiral cavity st-PMMA [55].

Mazzoni *et al.* [56] synthesised a fulleropyrrolidine-nitroxide conjugate, in which the TEMPO (2,2,6,6-tetramethylpiperidin-1-yl)oxyl radical and fulleropyrrolidine are connected through a peptide spacer — Z (carbobenzoxy group)-Asp-Aib-Ala-TOAC-Ala-OtBu (Fig. 16).

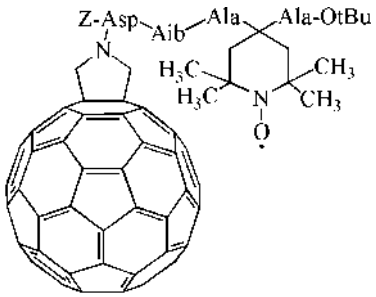

Fig. 16. Fulleropyrrolidine-TEMPO conjugate.

Kurtz *et al.* [57] synthesised a cysteine-containing redox protein (azurin mutant S118C) labelled with a C_{60}-based thiol-selective reagent. To do this, *N*-(triphenylmethyl)-3,4-fulleropyrrolidine was reacted with 3-maleimidopropionyl chloride to obtain thiol-selective fullerene maleimide [58]. Next, the resulting compound was mixed with a solution of azurin S118C in HEPES buffer at pH 7 (Fig.

17). The reaction progress was monitored by electrophoresis under denaturing conditions in a polyacrylamide gel.

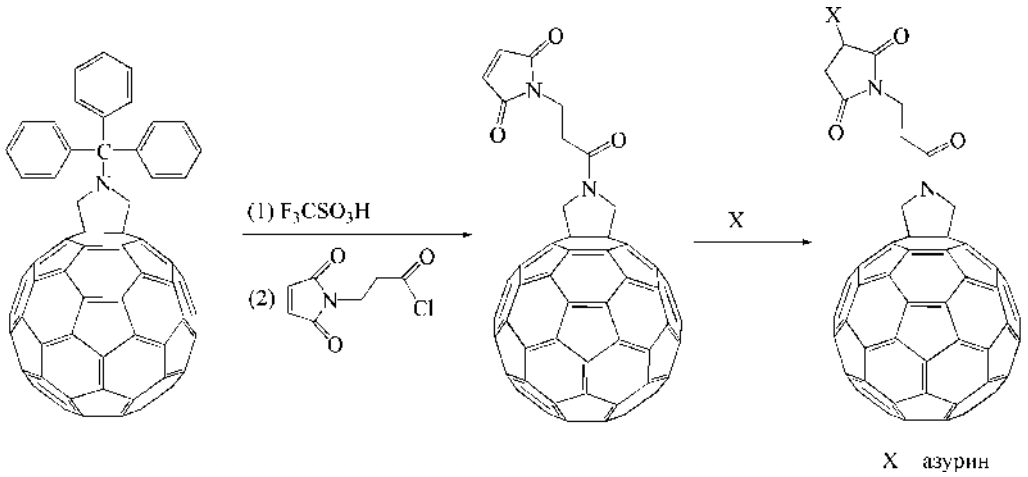

Fig. 17. Scheme for the preparation of a cysteine-containing redox protein labeled with a thiol-selective reagent based on C_{60} [57].

The authors of [59,60] synthesised C_{60} complexes with a stable COP tetramer (C_{60}-organising peptide) containing the following sequence of 30 amino acids — AEAESALEYAQQALEKAQLALQAARQALKA) (Fig. 18).

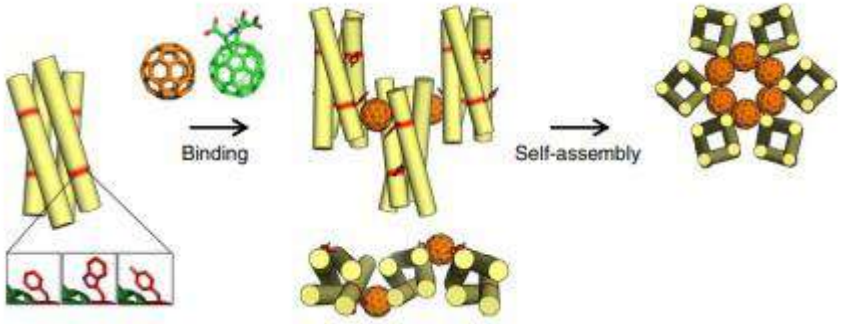

Fig. 18. Assembly diagram of the complex C_{60}-COP [59].

As shown in Fig. 18, the COP tetramer interacts with the individual C_{60} molecule, as well as with the fullerene core of fullerene-pyrrolidine acid (Fig. 19) through a surface binding site containing Tyr residues (the fullerene core interacts with aromatic fragments of the amino acid) and then the process of organising a crystalline joint with the fullerene occurs structures to produce C_{60}-COP.

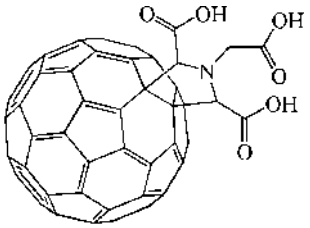

Fig. 19. Fullerene-pyrrolidic acid [59].

For the synthesised structures, the authors carried out X-ray diffraction analysis using the PHASER program.

Xu *et al.* [61] obtained an aqueous dispersion of the C_{60}-GluEG adduct (Fig. 20) as a result of a thiolene click reaction in the presence of GluEG *N*-carboxyanhydride and subsequent ring-opening polymerisation.

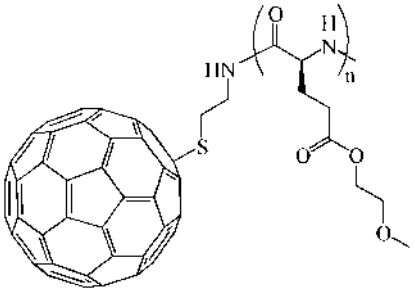

Fig. 20. C_{60}-GluEG adduct [61].

The resulting compound was characterised using IR, NMR spectroscopy, and thermal analysis. The authors found that the particle size of the synthesised adduct was about 4.0 ± 1.2 nm; the adduct has high dispersibility in water, intense fluorescence and high photostability in solution.

Jung *et al.* [62] synthesised the C_{60} adduct with alamethicin (Fig. 21).

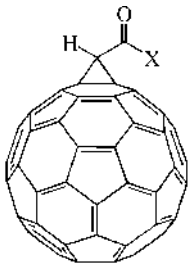

X – Ac-Aib-Pro-Aib-Ala-Aib-Ala-Gln-Aib-Val-Aib-Gly-Leu-Aib-Pro-Val-Aib-Aib-Glu-Gln-Phl

Fig. 21. C_{60} adduct with alamethicin [62].

To carry out the synthesis, succinimidyl ester of fullerene carboxylic acid was reacted with the peptide in methylene chloride, then the products were precipitated with

n-hexane and purified by flash chromatography. The resulting compounds were characterised using NMR spectroscopy and mass spectrometry. The authors of [63] as a result of a three-stage synthesis, including the Prato reaction, acylation with anhydrides or acid chlorides and conjugation using (EDC·HCl, HOAt, H-L-Ala-OEt) obtained a mixture of two diastereomeric dipeptides (Fig. 22). Identification of the obtained compounds was carried out using UV and NMR spectroscopy methods.

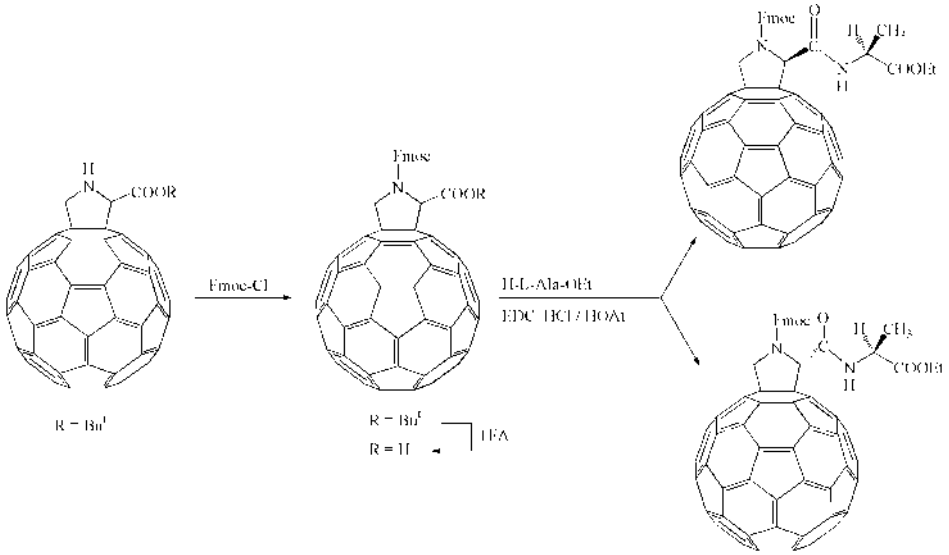

Fig. 22. Scheme for obtaining diastereomeric dipeptides [63].

Pellarini *et al.* [64] performed solid-phase peptide synthesis for the first time. To carry out the reaction, the C_{60} adduct containing a free amino group was condensed with α-tert-butyl ester of *N*-Fmoc-L-glutamic acid to obtain the fulleropeptide Fgu-(Gly-Orn)$_6$-Gly-NH_2, where Fgu is fulleropyrrolidino-glutamic acid (Fig. 23). The resulting compound was characterised using mass spectrometry and UV spectroscopy.

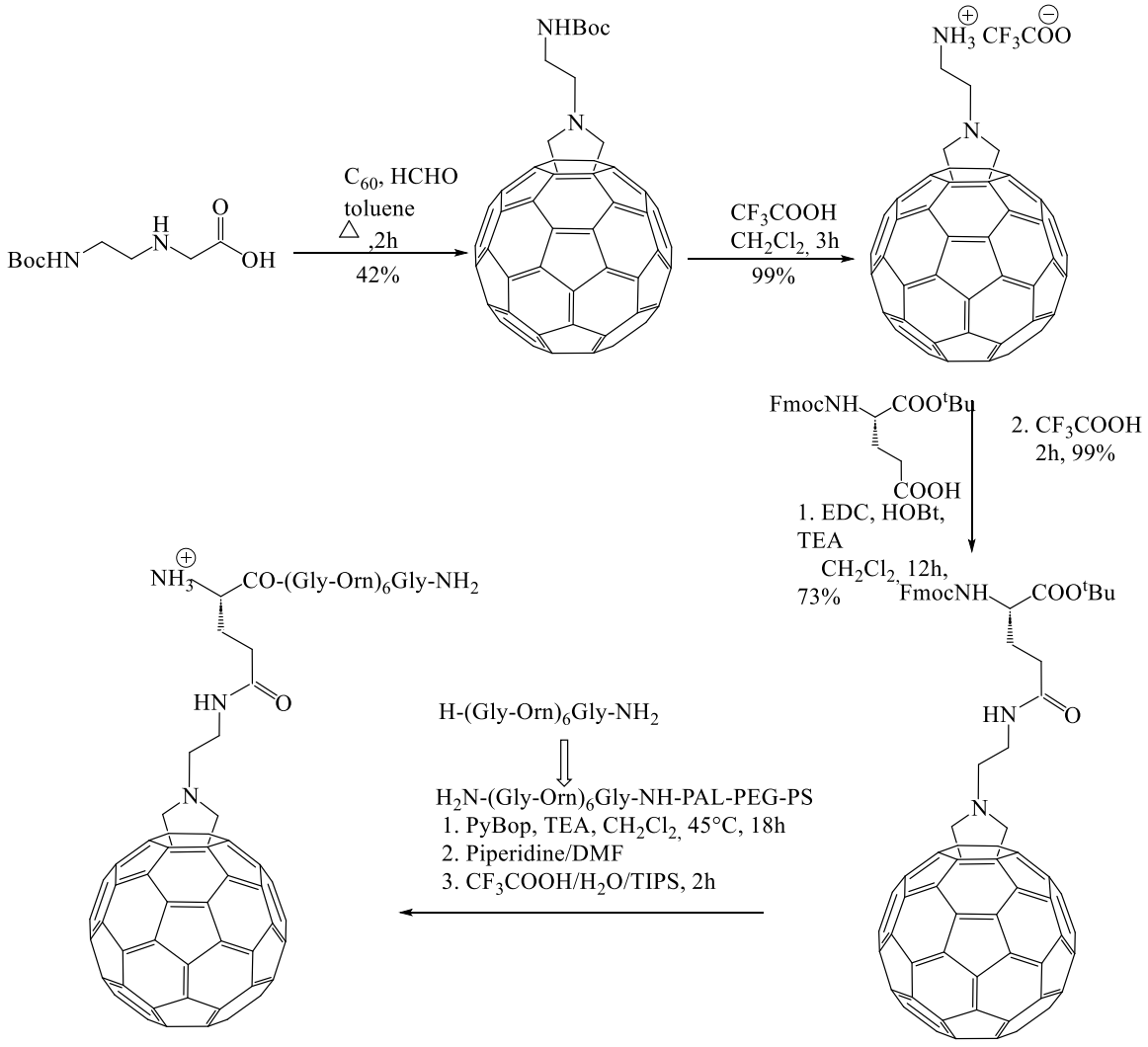

Fig. 23. Fgu-(Gly-Orn)$_6$-Gly-NH$_2$ synthesis scheme [64].

Pantarotto *et al.* [65] conducted a systematic study of the solid-phase synthesis of two classes of fullerene-containing peptides based on Fgu acid (Fig. 24).

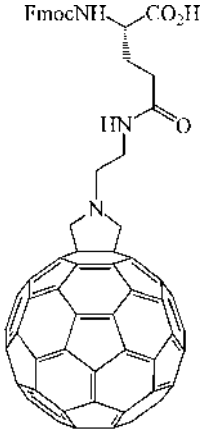

Fig. 24. Fgu acid [65].

Peptide synthesis reactions were carried out using different resins to analyse the role of the solid support on the reaction yield (Table 1). The first class of peptides (1–3)

consisted of analogues of the natural opioid peptide Leu_5-Enkephalin (H-Tyr-$(Gly)_2$-Phe-Leu-NH_2 and H-Tyr-$(Gly)_2$-Phe-Leu-OH). As can be seen from Table 1, in peptides (1–3), the authors replaced the hydrophobic residues Tyr^1 and Phe^4 with Fgu acid. The second class of peptides (4–6) included cationic peptides of various lengths, in which an Fgu acid residue was introduced either at the *N*-terminal position or in the middle of the sequence, to assess the effect of the position of the fullerene core on the biological activity of fullerene-containing peptides. The resulting compounds were characterised using mass spectrometry methods.

Table 1. Fgu-containing peptides synthesised using various resins [65].

No.	Synthesised peptides	Resin[a]	Product yield
1	H-Tyr-$(Gly)_2$-**Fgu**-Leu-NH_2	PAL-PEG-PS	<25 %
2	H-Tyr-$(Gly)_2$-**Fgu**-Leu-OH	NovaSyn-HMP POEPOP HMP	<25 %
3	H-**Fgu**-$(Gly)_2$-Phe-Leu-NH_2	PAL-PEG-PS POEPOP HMP	48 %
4	H-**Fgu**-$(Nle)_2$-Gln-Orn-Nle-Gly-$(Orn)_2$-Nle-$(Orn)_2$-Nle-Gly-$(Orn)_2$-Nle-Gly-Tyr-NH_2	PAL-PEG-PS	88 %
5	H-Gly-$(Nle)_2$-Gln-Orn-Nle-Gly-$(Orn)_2$-**Fgu**-$(Orn)_2$-Nle-Gly-$(Orn)_2$-Nle-Gly-Tyr-NH_2	PAL-PEG-PS	46 %
6	H-Gly-Orn-Gly-**Fgu**-Gly-Orn-Gly-NH_2	PAL-PEG-PS POEPOP HMP	49 %

[a]Type of resin used for solid phase peptide synthesis.

Bianco *et al.* [17] described a method for the solid-phase synthesis of a histone H3 protein analogue containing L-fulleropyrrolidinoglutamic acid. To obtain the compound, the authors replaced the Glu68 fragment with Fgu (Fig. 25). The resulting compound was characterised using UV spectroscopy and mass spectrometry.

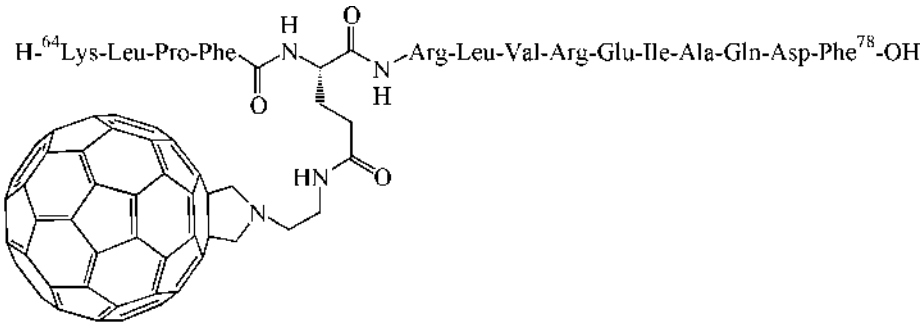

Fig. 25. Histone H3 analogue containing L-fulleropyrrolidinoglutamic acid [17].

Xu *et al.* [66] obtained adducts of fullerene C_{60} with tuftsin (Thr-Lys-Pro-Arg). The relevance of this study is related to the study of the effect of the fullerene core on the immunomodulatory effect of the tetrapeptide under study. Depending on the reaction conditions, two conjugates were obtained: NH_2-Thr-Lys-Pro-Arg-C_{60} (Fig. 26*a*) and C_{60}-Thr-Lys-Pro-Arg-COOH (Fig. 26*b*). The resulting compounds were characterised using mass spectrometry.

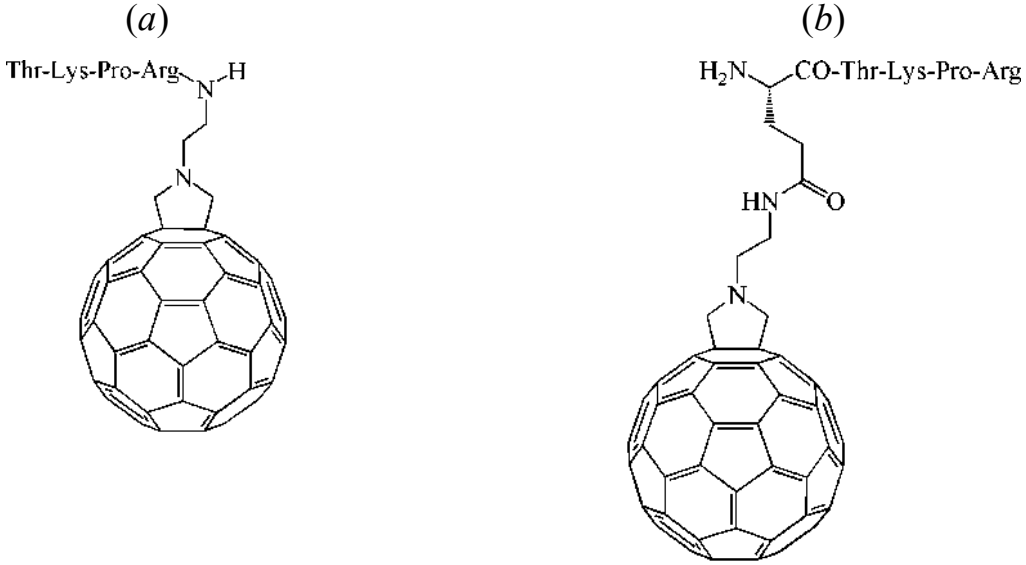

Fig. 26. Adducts NH_2-Thr-Lys-Pro-Arg-C_{60} (*a*) and C_{60}-Thr-Lys-Pro-Arg-COOH (*b*).

Dostalova *et al.* [67] synthesised six modifications of the maximin H5 peptide by replacing the l -aspartic acid residue with the following amino acids: L-histidine, L-tyrosine, L-alanine, glycine or L-valine. Next, the authors conjugated the resulting compounds with carboxylated fullerene C_{60}. To bind peptides, the surface of C_{60} fullerene was activated with nitric or trimesic acids. It was found that modification of fullerene with trimesic acid leads to the formation of a larger number of carboxyl groups on the surface of C_{60} fullerene, which makes it possible to increase the amount of

peptide associated with fullerene. The authors conducted a physicochemical study of aqueous solutions of synthesised conjugates and obtained concentration dependences, particle size distribution and zeta potential values.

Genepalli *et al.* [68] synthesised fullerenyldihydropyrrole peptides (Fig. 27*a–f*) from mono- and *bis*[60]fullerenedihydropyrrolecarboxylic peptides. The compounds were characterised by NMR spectroscopy and mass spectrometry.

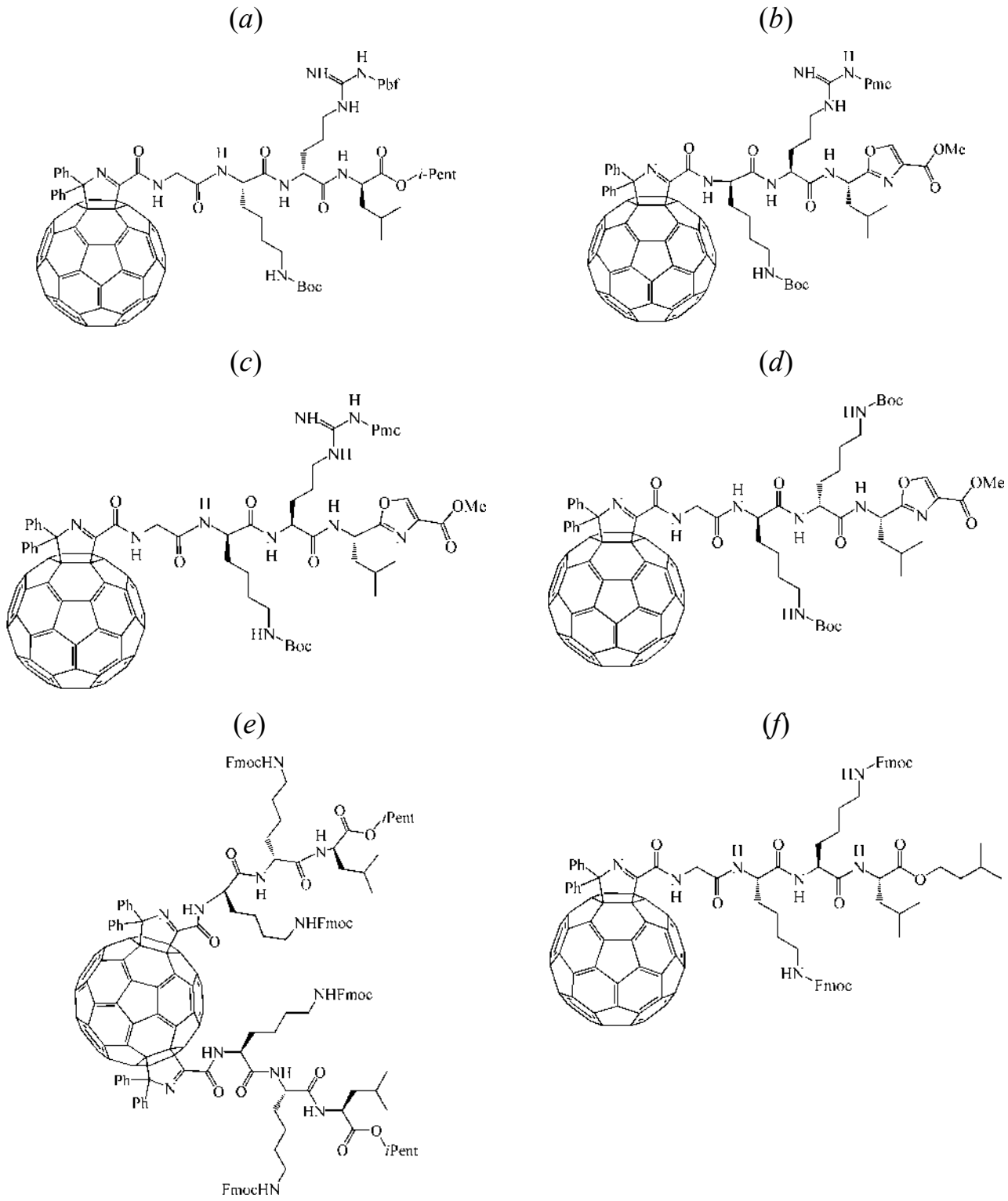

Fig. 27. Fullerenyldihydropyrrole peptides from mono- and *bis*[60]fullerenedihydropyrrolecarbon peptides: protected fullerenyl peptides (*a–d*), dipeptide (*e*) and peptide (*f*).

Sofou *et al.* [16] obtained a fullerene peptide enriched in Pro as a result of a four-stage synthesis (Fig. 28). The compound was characterised by NMR spectroscopy and mass spectrometry.

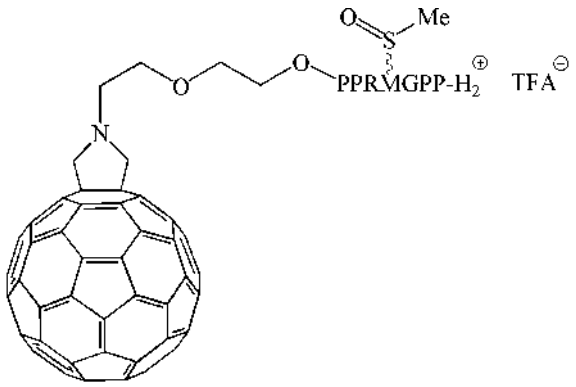

Fig. 28. Fullerene peptide enriched with Pro [16].

Arua *et al.* [69] as a result of the Prato reaction followed by deprotection of *tert*-butyl, they obtained a fulleropyrrolidine adduct (Fig. 29) and on its basis a fuller dipeptide was synthesised (Fig. 30).

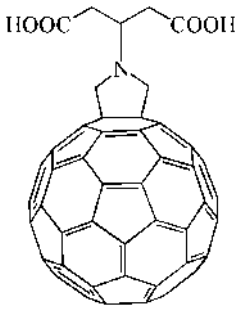

Fig. 29. Fulleropyrrolidine adduct [69].

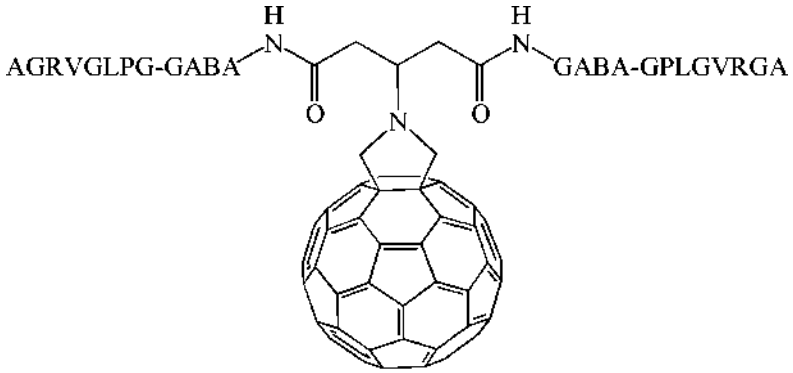

Fig. 30. Fullerodipeptide [69].

The resulting compound (Fig. 30) was characterised using NMR spectroscopy and mass spectrometry.

Strom *et al.* [70] obtained two *N*-Boc- and *N*-Fmoc protected aza- and aziridine-adducts of fullerene with L-lysine and L-phenylalanine by reacting fullerene C_{60} with azide derivatives of L-lysine and L-phenylalanine. After deprotection of the aza derivative of L-phenylalanine, aza-C_{60}-Phe acid was obtained (Fig. 31), which was reacted with glycine *tert*-butyl ester to form a dipeptide (Fig. 32).

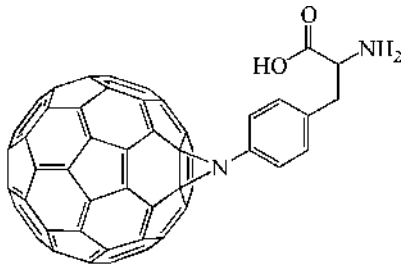

Fig. 31. Aza-C_{60}-Phe acid [70].

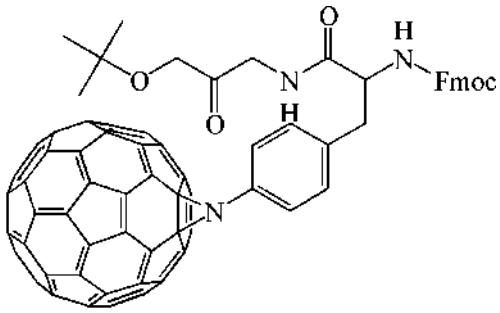

Fig. 32. Conjugate of aziridinofullerene with a dipeptide containing protective groups [70].

The resulting derivatives were characterised using CV and UV spectroscopy.

Tsumoto *et al.* [71] described the synthesis of *N*-hydroxysuccinimide C_{60} esters from methanofullerene carboxylic acids. When using a DMAP catalyst, such esters selectively react with the amino or hydroxy groups of an amino acid or peptide to produce various adducts (Fig. 33). The resulting compounds were characterised using NMR spectroscopy and mass spectrometry.

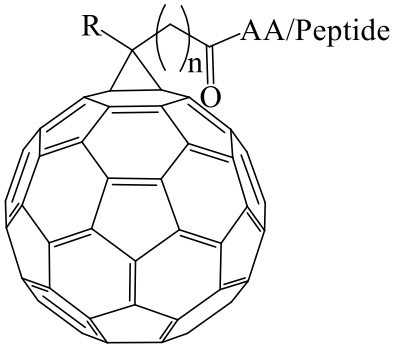

R = H, n=0, AA/Peptide = Gly/Gly-Gly-Gly/Z-Lys/Bz-Gly-Lys/Gly-Gly-Tyr-Arg/Tyr-Gly-Gly-Phe-Leu
R = C_6H_5, n=3, AA/Peptide = Gly/Gly-Gly-Gly/Z-Lys/Bz-Gly-Lys/Gly-Gly-Tyr-Arg/Tyr-Gly-Gly-Phe-Leu
R = C_6D_5, n=3, AA/Peptide = Gly
R = C_6H_4Br, n=3, AA/Peptide = Gly

Fig. 33. *N*-hydroxysuccinimide C_{60} adducts derived from methanofullerene-carboxylic acids [71].

Reiriz *et al.* [72] developed a method for the synthesis of two types of peptide nanotubes from α,γ-cyclic octapeptides bound to methanofullerene. To do this, hydrophilic amino acids were introduced into a solid-phase peptide synthesis reaction using Wang resin. Next, the resulting cyclic octapeptides participated in the assembly of nanotubes. The authors showed that fullerene fragments can be located on one side of the tube (model a) or on two (model b) (Fig. 34). The resulting compounds were characterised using AFM, STM and TEM methods. It was found that the synthesised adducts have prospects for use in the creation of optical and electronic devices.

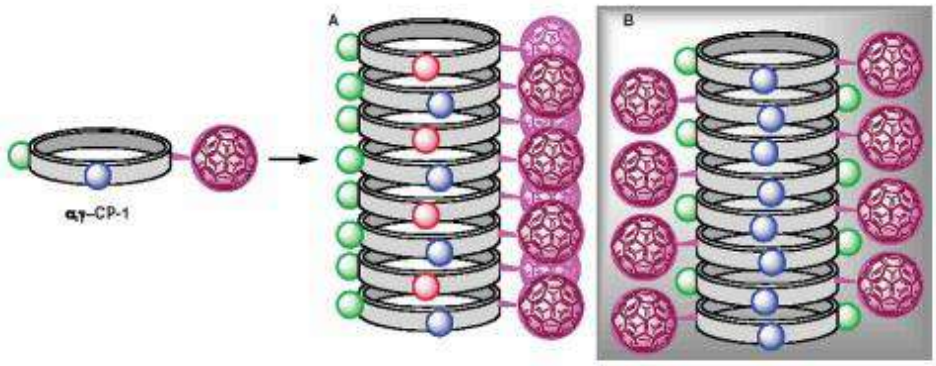

Fig. 34. Model of peptide nanotube formation. The self-assembly process can be controlled by ionic interactions between amino acid molecules (red and blue balls) (*a*), and can also be induced by the surface properties of fullerene molecules (*b*) [72].

Garbuyo *et al.* [73] described the solid-phase synthesis of two types of 310-helix fullerene peptides containing intramolecular C–O···H–N hydrogen bonds and a nitroxyl radical (Fig. 35).

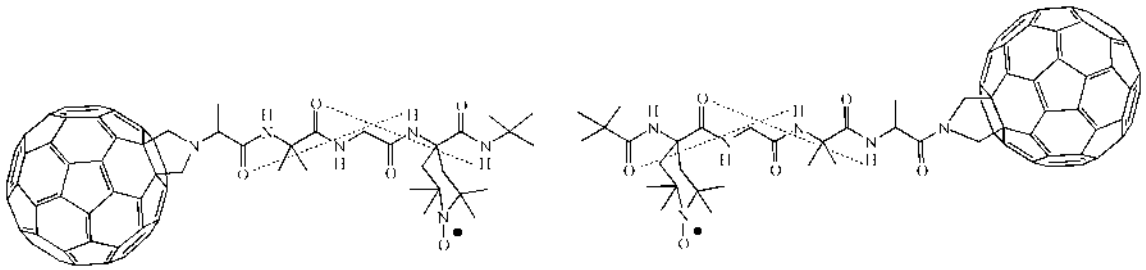

Fig. 35. Helical fullerene peptides [73].

The resulting peptides were characterised using IR, NMR and EPR spectroscopy.

Fujii *et al.* [74,75] described the liquid-phase synthesis of two cyclic fulleropeptides with a polyethylene glycol chain: (cyclo8-C_{60}+PEG) (Fig. 36*a*) and (C_{60}+PEG) (Fig. 36*b*).

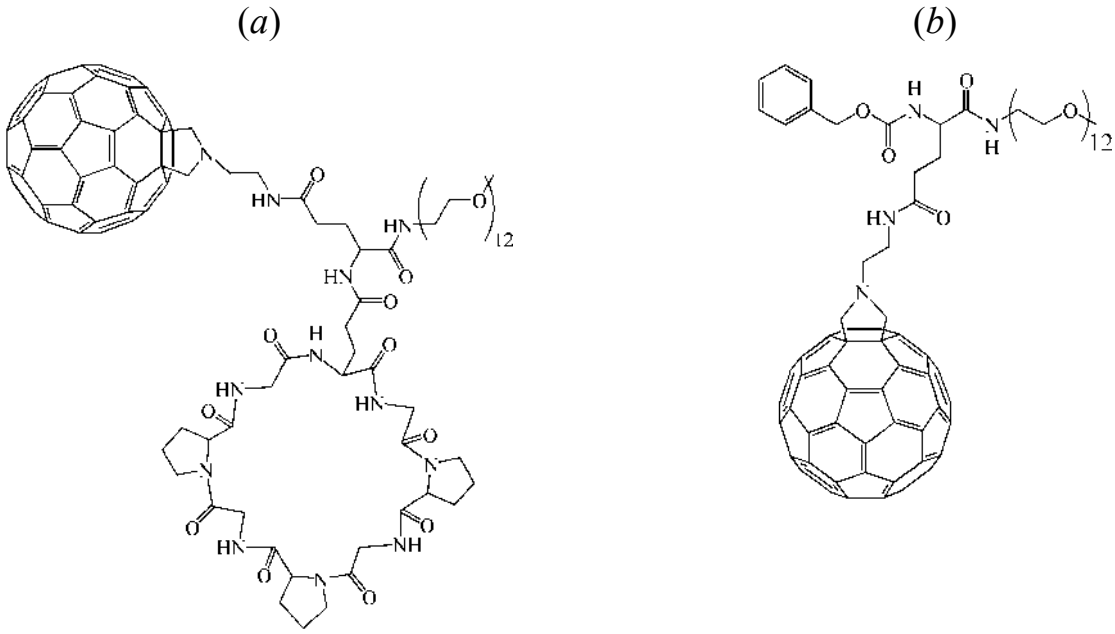

Fig. 36. Fulleropeptides with polyethylene glycol chain: (cyclo8-C_{60}+PEG) (*a*) and (**(**C_{60}+PEG) (*b*) [74,75].

As a result of binding of C_{60}-pyrrolidine tris acid to the N-terminus of the peptide containing hexahistidines, the peptide $H_2NGSGA_3GLSH_6$ was obtained (Fig. 37) [76]. The resulting compound was characterised using NMR spectroscopy and mass spectrometry.

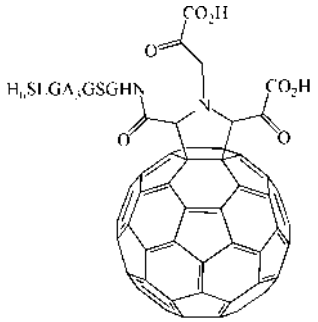

Fig. 37. $H_2NGSGA_3GLSH_6$ peptide [76].

Minois *et al.* [77] proposed a new method for the preparation of amino acid and peptide adducts of fullerenes by hydrophosphination using secondary phosphine-borane as a cross-linking agent (Fig. 38). The resulting compounds were characterised by NMR spectroscopy. Additionally, the electrochemical properties of the resulting adducts were studied.

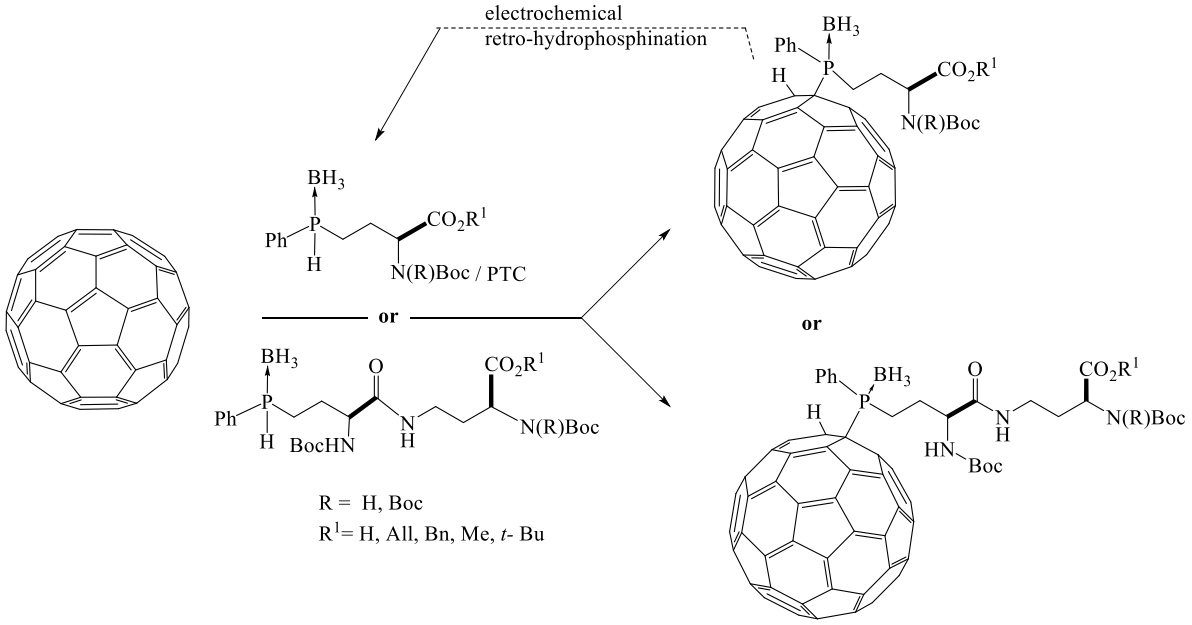

Fig. 38. Scheme for the preparation of amino acid and peptide adducts C_{60} using the hydrophosphinisation reaction [77].

Siepi *et al.* [78] developed a method for preparing C_{60} nanoparticles modified with lysozyme isolated from hen egg white (HEWL), as well as lysozyme in which the cysteine groups were alkylated with 3-bromopropylamine, resulting in the introduction of eight additional positive charges. The authors carried out a physicochemical study of the resulting nanoparticles and their aqueous dispersions using AFM, TEM, DLS and UV spectroscopy, and the values of ζ-potentials were also calculated. As a result of the research, effective solubilising agents were found that make it possible to create biologically active dispersions of fullerenes without the use of aromatic solvents, polymers or surfactants.

Chen *et al.* [79] obtained a conjugate of fullerene with bovine thyroglobulin (Fig. 39). The resulting conjugate was characterised using UV spectroscopy.

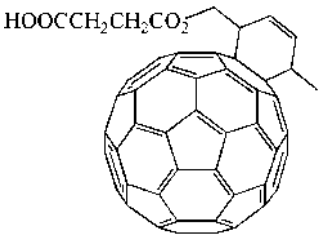

Fig. 39. Fullerene conjugate with bovine thyroglobulin [79].

Benyamini *et al.* [80] conducted studies of the interaction of the C_{60} fullerene and the C_3 isomer of C_{60}-trismalonic acid with four proteins: HIV protease, fullerene-

specific antibody, HSA and bovine serum albumin using the PatchDock algorithm. Using the MultiBind method, the authors established a correlation between the physicochemical properties and surface geometry for the binding sites of fullerene with HIV protease, human and bovine serum albumin.

1.2. Physicochemical properties of fullerenes with amino acids and peptides

1.2.1. Thermodynamic properties of fullerenes and their adducts

The study of the thermodynamic properties of fullerenes is an actual task, since they are fundamental characteristics of matter and are necessary for solving various kinds of thermophysical and technological problems. Let us consider the basic thermodynamic properties of fullerene C_{60}. The values of the enthalpy of combustion ($\Delta_c H°$, κJ·mol^{-1}) and formation (Δ_fH° kJ·mol^{-1}) fullerene C_{60} at 298.15 K and standard pressure, as well as the values of entropy ($\Delta_f S°$,J·mol^{-1}·K^{-1}), Gibbs energy ($\Delta_f G°$, kJ·mol^{-1}) and logarithm of the equilibrium constant ($\lg K_f^0$) of the reaction of formation of fullerene C_{60} from graphite are given in Table. 2.

Table 2. Values of enthalpies of combustion and formation of fullerene C_{60} at 298.15 K and standard pressure, as well as entropy, Gibbs energy and logarithm of the equilibrium constant of the reaction of formation of fullerene C_{60} from graphite [81].

$\Delta_c H°$ / kJ·mol^{-1}	$\Delta_f H°$ / kJ·mol^{-1}	$\Delta_f S°$ / J·mol^{-1}·K^{-1}	$\Delta_f G°$ / kJ·mol^{-1}	$\lg K_f^0$
C_{60} fullerene				
−25937 ± 17	2327 ± 16	420.8 ± 1.2	2202 ± 17	0.306

Fig. 40 shows the temperature dependence of the isobaric heat capacity of fullerene C_{60}.

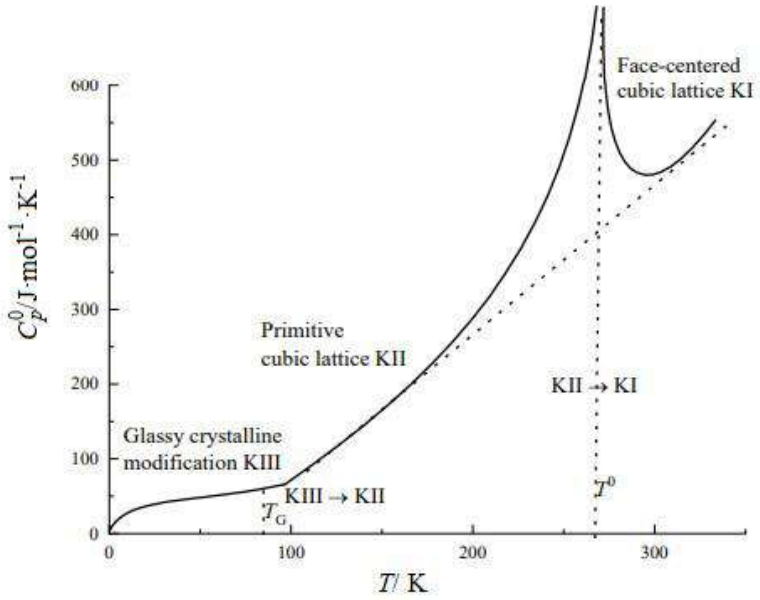

Fig. 40. Temperature dependence of the isobaric heat capacity of fullerene C_{60}.

Analysis of Fig. 40 allows us to conclude that, depending on the temperature, the C_{60} fullerene exists in three physical states: (*i*) in the form of plastic crystals (KI), having a face-centred cubic lattice, at the nodes of which the C_{60} molecules perform almost free rotation; (*ii*) in the form of crystals (KII), having a simple cubic lattice and characterised by the orientational ordering of C_{60} molecules; (*iii*) in the form of glass-like crystals (KIII). It has been established that in the temperature range 0–340 K two phase transitions are observed: a second-order phase transition KIII→KII (at 86 K) and a first-order phase transition KII→KI (at 260.7 K).

To date, not much data on the thermodynamic properties of fullerene adducts has been presented in the literature. Let us look at the main results. In [82], the authors studied the temperature dependence of the heat capacity C_p^o of hydrofullerene $C_{60}H_{36}$ in the region of 4.8–340 K. It was found that the dependence of C_p^o on T does not have any anomalies. Works [83–85] present the results of a thermodynamic study of adducts of light fullerenes with L-lysine, as well as water-soluble fullerenols $C_{60}(OH)_{40}$ and $C_{70}(OH)_{12}$ in a wide temperature range. Based on experimental data on the temperature dependence of isobaric heat capacity, standard thermodynamic functions of compounds were calculated (entropy $S_m°(T)$, enthalpy $[H_m°(T) - H_m°(0)]$ and Gibbs energy $[\Phi_m°(T) - \Phi_m°(0)]$).

As an example, Fig. 41 shows the temperature dependence of the isobaric heat capacity of fullerenol $C_{60}(OH)_{40}$, as well as the temperature dependence of the isobaric heat capacity of $C_{60}(OH)_{40}$ isomers with a uniform distribution of hydroxyl groups, and an isomer in which the hydroxyl groups are located in the equatorial region ('Saturn-like'), calculated by the DFT method. It can be seen that, unlike the C_{60} fullerene, no phase transitions are observed in the temperature dependence of the isobaric heat capacity.

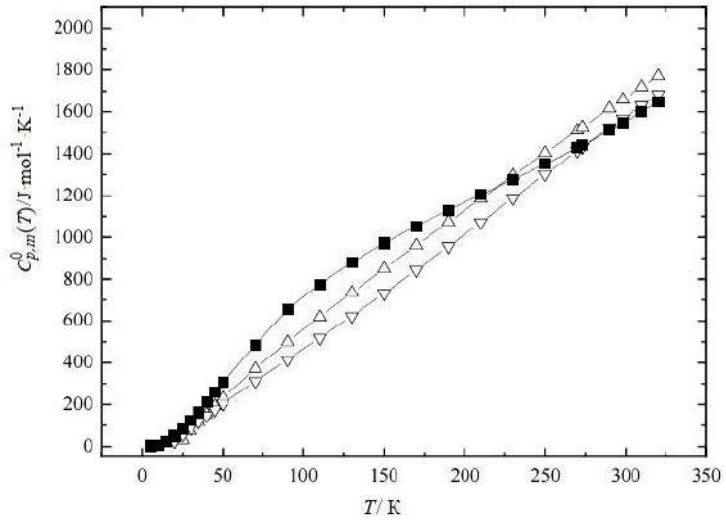

Fig. 41. Temperature dependence of the isobaric heat capacity of $C_{60}(OH)_{40}$ in the temperature range T = 5–326 K. ■ — experimental data, ▽ — calculation by DFT method for fullerenol with a uniform distribution of hydroxyl groups; □ — calculation by DFT method for fullerenol, in which hydroxyl groups are located in the equatorial region ('Saturn-like').

1.2.2. Physicochemical properties of aqueous solutions of fullerene adducts with amino acids and peptides

An analysis of the literature shows a limited number of works devoted to the physicochemical study of aqueous solutions of adducts of light fullerenes with amino acids and peptides, as well as the study of phase equilibria in systems containing these adducts. Let us briefly discuss the main results obtained.

In [86–88], the degree of association of fullerene adducts was studied depending on the concentration and nature of the substituent for aqueous solutions of the following fullerene adducts: C_{60} adducts with amino acids (glycine, L-alanine) and peptides

(glycylglycine, glycyl-L-alanine, glycyl-L-valine and L-alanyl-L-alanine), containing a free carboxyl group [89]; methyl esters of peptide-containing maleimidofullerenes (*N*-maleimidofullerenyl-L-valyl-L-valine, *N*-maleimidofullerenyl-L-alanyl-L-leucine, *N*-ma-lei-midofullerenyl-DL-alanyl-DL-alanine, *N*-maleimidofullerenylglycyl-L-valine, *N*-mal-eimido-fullerenyl-L-valyl-L-valyl-L-valine) [87]; mono- and disubstituted adducts C_{60} with propionic, γ-aminobutyric, and ε-aminocaproic acids (sodium salt of *N*-monohydrofullerenyl-ω-aminocaproic acid, sodium *N*-monohydrofullerenyl-γ-aminobu-ty-rate, sodium L-*N*-monohydrofullerenylpropionate, sodium *N*-2-hydroxyethyl-fullerenyl-ω-aminocaproate, methyl-*N*-2-hydroxyethylfullerenyl-ω- amino-caproate, so-dium *N*-2- hydr-oxylethylfullerenyl-γ-aminobutyrate, methyl-L-*N*-2-hydroxylethylfu-llerenylpropionate, methyl-L-*N*-2-nitroxyethylfullerenylpropionate, 2-nitro-xyethyl-L-*N*-2-nitroxyethylfullere-nepropionate, 2-nitroxyethyl-L-*N*-2-hydroxyethylfullerenylpropi-onate) [88].

Timofeeva *et al.* [89] conducted a study of the degree of association of C_{60} adducts with amino acids and peptides (*N*-monohydrofullerenyl-DL-serine, *N*-monohydrofullerenyl-L-arginine, *N*-monohydrofullerenyl-DL-alanil-DL-alanine and *N*-monohydrofullerenyl-L-alanine) in aqueous solutions depending on pH, ionic strength and concentration.

The thermodynamic approach proposed by St. Petersburg State Technological Institute Professor N. A. Charykov for calculating excess thermodynamic functions and the concentration limit of the thermodynamic stability of solutions of water-soluble fullerene adducts of relative phase separation, including adducts of light fullerenes with amino acids, deserves special attention. This approach is based on the use of the semi-empirical VD-AS (Virial Decomposition Asymmetric Model) model, based on the virial expansion of the excess molar Gibbs energy of a solution into mole fractions of the components:

$$\frac{G^{ex}}{RT} = (n_1 + n_2)\sum_{i=1}\sum_{j=1} x_1^i x_2^j \cdot \lambda_{ij} = \frac{\sum_{i=1}\sum_{j=1} n_1^i n_2^j \cdot \lambda_{ij}}{(n_1 + n_2)^{i+j-1}}, \quad (1)$$

where G^{ex} is total molar excess Gibbs energy of solution, R = 8.31 J·K^{-1}, T is absolute temperature (K), n_i and x_i are number of moles and mole fraction of the i-th component (subscript *1* refers to the fullerene adduct, subscript *2* refers to water), λ_{ij} is ij-virial coefficient in expansion $\frac{G^{ex}}{RT}$ in terms of the number of moles of components (the upper limits of summation in the general case are not limited and can be arbitrary), λ_{ij} is identified with the reduced (to RT) nonspecific interaction energy of i particles of the 1st component and j particles of the 2nd component.

It should be noted that when using only one term in such an expansion, the well-known model of strictly regular solutions is realised, when assuming the temperature dependence of the only virial coefficient — the model of quasi-regular solutions, when using third virial coefficients — the model of subregular solutions and the EFLCP model, and finally, with the additional use in the expansion of the contribution of electrostatic nonspecific interactions according to the Debye–Hückel theory — the Pitzer model in various modifications.

The authors of [90] obtained the following equations for calculating the activity coefficients of fullerene adducts (subscript 1) and solvent (subscript 2) on an 'asymmetric' normalisation scale:

$$\ln \gamma_1^{ass} \approx 2\Lambda_2 x_1 + 3\Lambda_3 x_1^2 + 4\Lambda_4 x_1^3, \quad (2)$$

$$\ln \gamma_2^{ass} \approx -\Lambda_2 x_1^2 - 2\Lambda_3 x_1^3 - 3\Lambda_4 x_1^4, \quad (3)$$

where $\Lambda_i(T) = \sum_{i=1} \lambda_{ij}$.

Based on equations 2, 3, the stability condition for solutions of fullerene adducts with respect to phase separation (separation) can be obtained:

$$g_{11}^{mix} = \frac{\partial^2 \left(\frac{G^{mix}}{RT} \right)}{\partial x_1^2} = 12\Lambda_4 x_1^3 + 6\Lambda_3 x_1^2 + 2\Lambda_2 x_1 + 1 = 0. \quad (4)$$

Equation 4 is a cubic equation that can be solved for x_1 using Cardano's formula. Fig. 42, as an example, shows the concentration dependences of the activity coefficients of aqueous solutions of fullerene adducts with L-hydroxyproline ($C_{60}(C_5H_9NO_3)_2$) and

L-lysine ($C_{60}(C_6H_{14}N_2O_2)_2$, $C_{70}(C_6H_{14}N_2O_2)_3$). Fig. 43 shows the concentration dependences of the function $F(x_1) = 12\Lambda_4 x_1^3 + 6\Lambda_3 x_1^2 + 2\Lambda_2 x_1 + 1 = 0$ for binary systems $C_{60}(C_5H_9NO_3)_2$–H_2O, $C_{60}(C_6H_{14}N_2O_2)_2$–$H_2O$ and $C_{70}(C_6H_{14}N_2O_2)_3$)–$H_2O$ at 273.15 K.

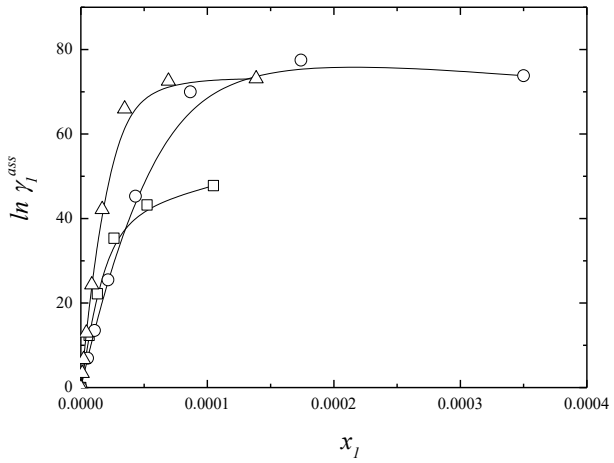

Fig. 42. Concentration dependences of functions $\ln \gamma_1^{ass}$ for binary systems $C_{60}(C_5H_9NO_3)_2$–H_2O (□), $C_{60}(C_6H_{14}N_2O_2)_2$–$H_2O$ (○), $C_{70}(C_6H_{14}N_2O_2)_3$–$H_2O$ (△) [90,91].

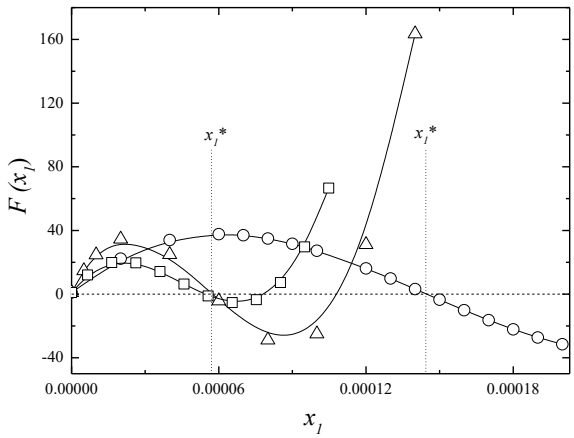

Fig. 43. Concentration dependences of functions $F(x_1) = 12\Lambda_4 x_1^3 + 6\Lambda_3 x_1^2 + 2\Lambda_2 x_1 + 1 = 0$ for binary systems $C_{60}(C_5H_9NO_3)_2$–H_2O (□), $C_{60}(C_6H_{14}N_2O_2)_2$–$H_2O$ (○), $C_{70}(C_6H_{14}N_2O_2)_3$–$H_2O$ (△). x_1^* corresponds to the loss of thermodynamic stability of solutions of fullerene adducts with respect to phase separation [90,91].

Fig. 43 clearly shows the intersection of the function $F(x_1)$ with the abscissa axis, the intersection point (x_1^*) corresponds to the loss of thermodynamic stability (solution stratification). When comparing data on dynamic light scattering with data obtained

from independent cryometric measurements, it can be stated with some confidence that in these systems there are three concentration zones:

(*1*) at $x_1 < x_1^*$ $x_1 \approx (0.8–1.5)\ 10^{-4}$ in solutions there are only 1st order associates with linear dimensions of tens of nm and, possibly, monomeric hydrated molecules in very small quantities nanoclusters. Solutions are thermodynamically stable;

(*2*) at comparable values of $x_1 \approx x_1^*$ in solutions, in addition to 1st order associates, 2nd order associates with linear dimensions of hundreds of nm appear, and the solutions begin to lose stability with respect to phase separation, in other words, the solutions begin to prestratify;

(*3*) finally, at $x_1 > x_1^*$, third-order associates with linear dimensions of a unit of microns appear in solutions and the solutions begin to stratify.

An analysis of the literature shows a limited amount of data on the physicochemical properties of solutions of water-soluble fullerene adducts. The authors of [83–85,91–97] studied the physicochemical properties of fullerenols, carboxylated fullerenes, adducts of fullerenes with L-amino acids and obtained experimental data on the concentration dependences of heat capacities, densities, refractive indices, electrical conductivity, dissociation constants, apparent degree of dissociation, particle size distributions, diffusion coefficients, viscosity, etc., and also studied solubility diagrams in binary and ternary systems containing water-soluble fullerene adducts. The authors of [98–105] studied the solubility of fullerenols $C_{60}(OH)_{22–24}$ and $C_{70}(OH)_{12}$ in water in the temperature range 293–353 K, as well as in ternary systems fullerenol $C_{60}(OH)_{22–24}$–inorganic salt ($Pr(NO_3)_3$, YCl_3, $CuCl_2$, UO_2SO_4)–water. As an example, in Fig. 44 presents experimental data on solubility in binary fullerenol-water systems.

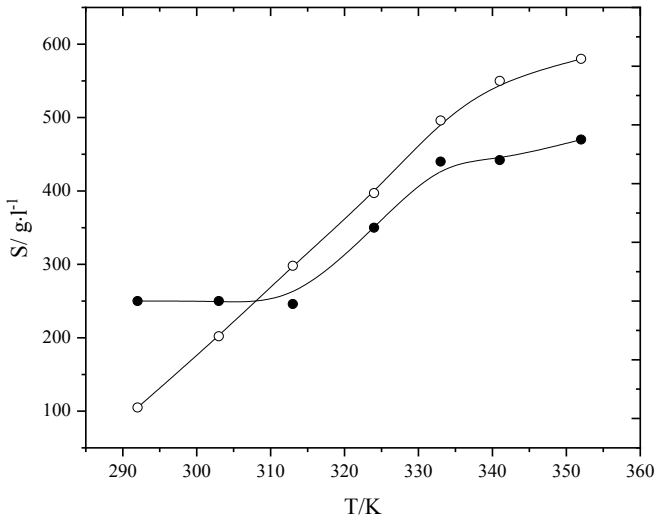

Fig. 44. Temperature dependences of the solubility of fullerenols ($C_{60}(OH)_{22–24}$ (●), $C_{70}(OH)_{12}$ (○)) in water. *S* is the volume concentration of fullerenols in a saturated solution.

From Fig. 44, it follows that the solubility of fullerenols monotonically increases with increasing temperature, while the shapes of the *S*(*T*) curves have a complex sigmoidal character. This experimental fact is not surprising, since similar dependences were obtained for the binary systems C_{70}-*o*-xylene (on the C_{70} crystallisation branch) and C_{60}-α-chloro(bromo)naphthalene (on the solvated fullerene crystallisation branch) [106,107].

In work [108], the solubility of *bis*-adducts of light fullerene C_{60} and essential amino acids: lysine, threonine and hydroxyproline — $C_{60}(C_6H_{13}N_2O_2)_2$, $C_{60}(C_4H_8NO_3)_2$, $C_{60}(C_5H_9NO_2)_2$ in water in the temperature range was studied using the isothermal saturation method in ampoules 20–80 °C. Solubility polytherms contain one invariant point each, corresponding to saturation with two solid phases at once — crystalline hydrate and anhydrous bis-adduct.

1.3. Biomedical study of fullerene adducts with amino acids, peptides and proteins

Let us briefly describe the biological activity of fullerene adducts with amino acids and peptides [96].

Kotelnikova *et al.* [34] studied the inhibitory effect of the fullerene adduct C_{60}-ε-aminocaproate sodium (Fig. 2) against HIV protease in *in vitro* experiments. It was

found that the sodium C_{60}-ε-aminocaproate adduct is capable of inhibiting HIV protease by suppressing the activity of the viral enzyme.

Strom *et al.* [109] studied the inhibitory effect of tripeptides (Fig. 45*a–c*): Fmoc-Phe(4-*aza*-C_{60})-Lys_3-OH, Fmoc-Phe(4-*aza*-C_{60})-Pro-Hyp-Lys-OH, Fmoc-Phe(4-*aza*-C_{60})-Hyp-Hyp-Lys-OH against HIV-1 protease (Fig. 45).

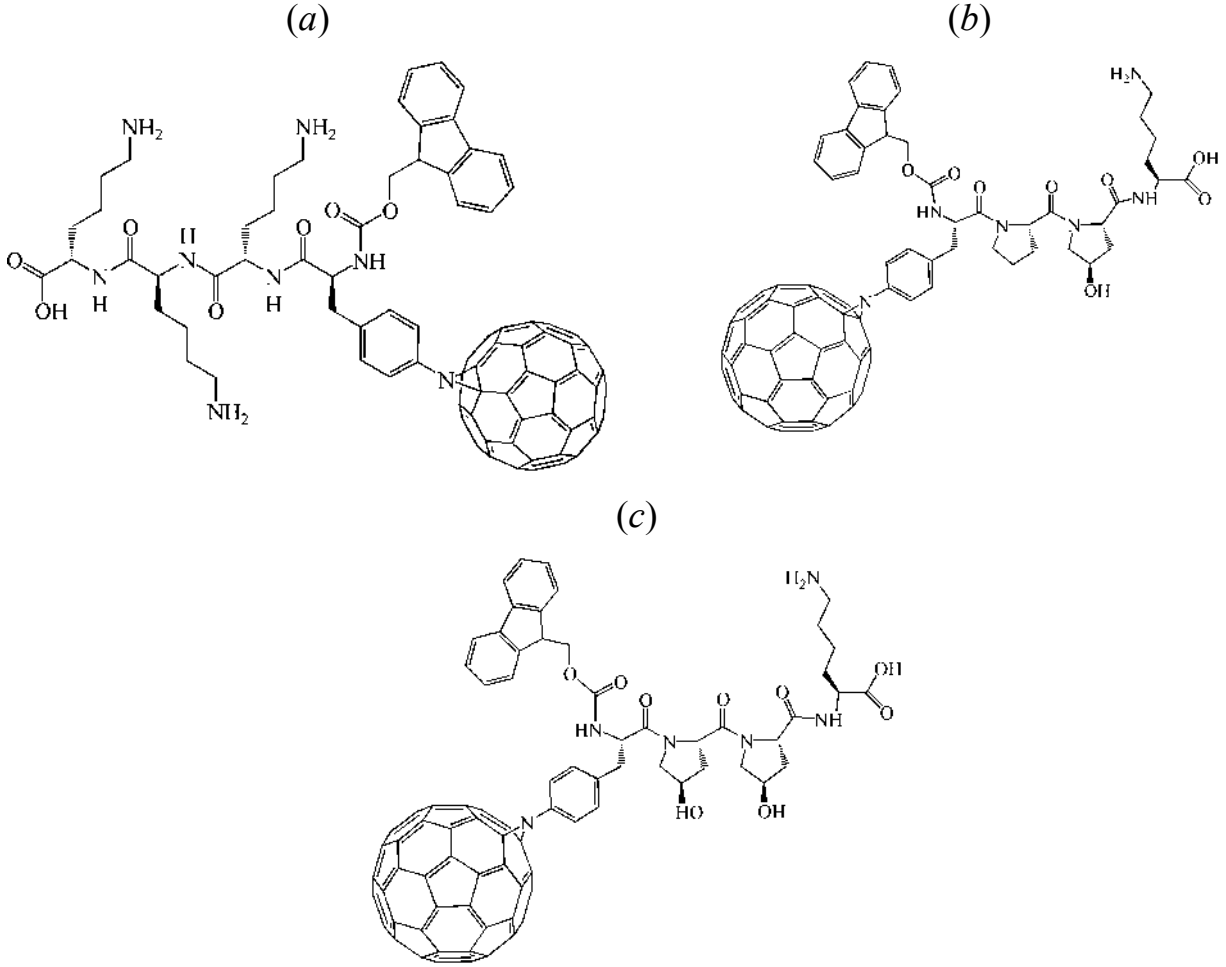

Fig. 45. Structural formulae of adducts: Fmoc-Phe(4-*aza*-C_{60})-Lys_3-OH Fmoc-Phe(4-*aza*-C_{60})-Lys_3-OH (*a*), Fmoc-Phe(4-*aza*-C_{60})-Pro-Hyp-Lys-OH (*b*) and Fmoc-Phe(4-*aza*-C_{60})-Hyp-Hyp-Lys-OH (*c*) [109].

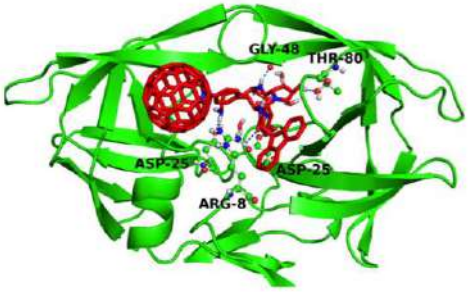

Fig. 46. Crystal structure of HIV-1 protease containing Fmoc-Phe (4-*aza*-C_{60})-Lys_3-OH (Fig. 45*a*) in the active site of the enzyme [109].

It was found that the adducts presented in Fig. 45*a–c* cause suppression of HIV-1 protease activity. Greatest inhibitory effect (K_i = 76 nmol·l^{-1}) was shown by the Fmoc-Phe(4-*aza*-C_{60})-Hyp-Hyp-Lys-OH adduct (Fig. 45*c*) due to the presence of the largest number of Hyp residues in its amino acid sequence. In addition, it was shown that the adducts (Fig. 45*a–c*) have a higher inhibition constant (K_i (Fig. 45*a*) = 85 nmol·l^{-1}; K_i (Fig. 45*b*) = 120 nmol·l^{-1}; K_i (Fig. 45*c*) = 76 nmol·l^{-1}) compared with traditionally used protease inhibitors - ritonavir (K_i of ritonavir = 4.8 nmol·l^{-1}), saquinavir (K_i of saquinavir = 24 nmol·l^{-1}) and atazanavir (K_i of atazanavir = 2.66 nmol·l^{-1}) [110]. In this regard, further research is needed aimed at creating C_{60} adducts with peptides that have greater affinity for HIV-1 protease.

In the patent [46], the authors established that hydrated adducts of fullerene C_{60} with acids with the general formula$C_{60}(H)_3\{NH(CH_2)_nCOOH\}_3 \cdot xH_2O$, where n = 5–7; x = 8–10, have antiviral activity against HSV, influenza viruses of various natures, HIV, as well as antitumour and antipsoriatic activity.

Mashino *et al.* [23] studied the inhibitory effect of various fullerene adducts: C_{60}-dimalonic acid; regio-isomers C_{60}-*bis*(*N*,*N*-dimethylpyrrolidinium iodide) (Fig. 47*a–c*); a mixture of regio-isomers C_{60}-*bis*(2-alkyl-*N*,*N*-dimethylpyrrolidinium iodide) (Fig. 47*d*,*e*); a mixture of stereo-isomers of proline-fullerene (Fig. 47*f*,*g*); against HIV reverse transcriptase, and also compared the biological activity of these adducts with the inhibitor nevirapine, which is actively used in clinical practice.

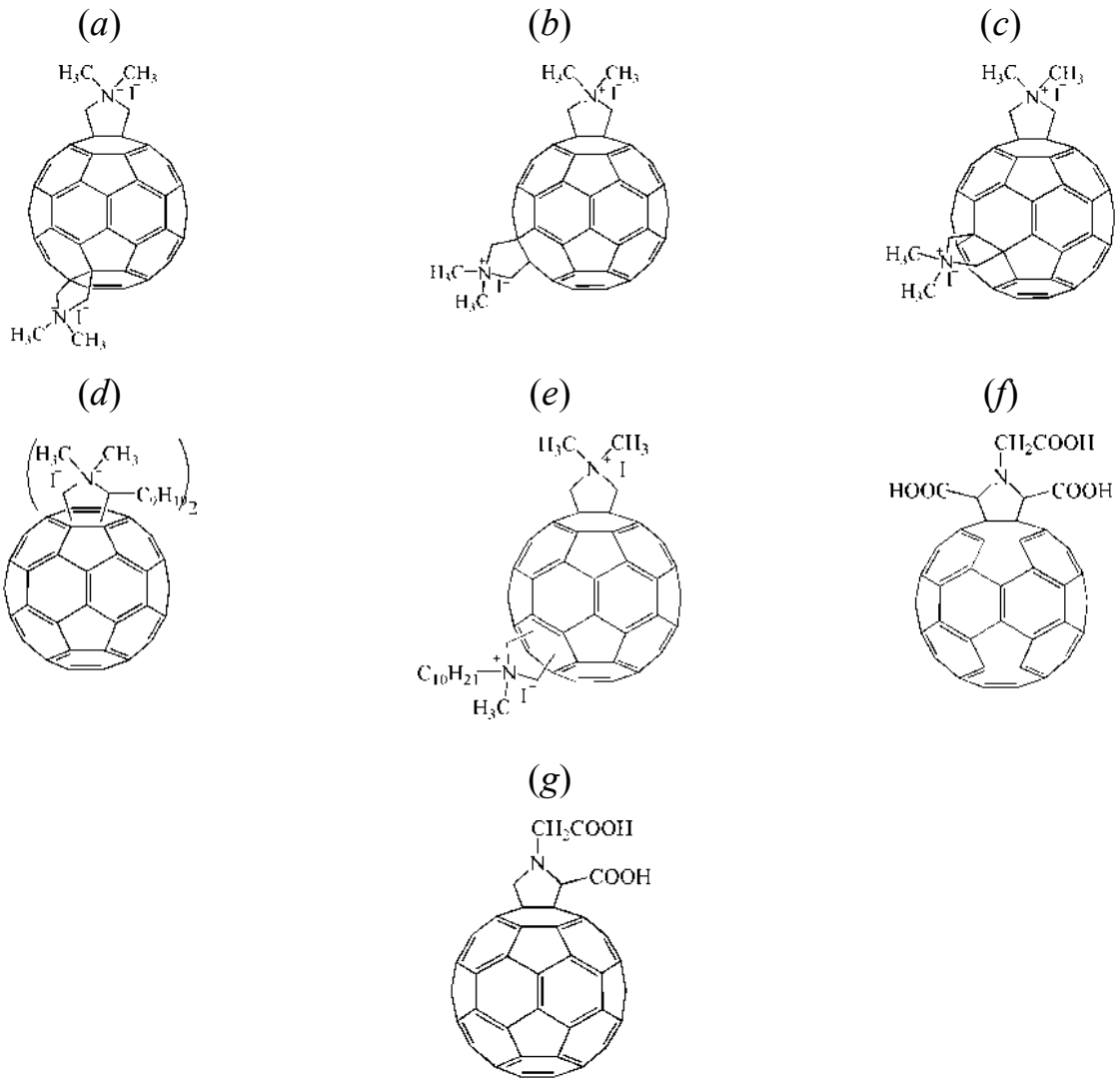

Fig. 47. Regio-isomers of C_{60}-*bis*(*N*,*N*-dimethylpyrrolidinium iodide) (*a*–*c*); mixture of regio-isomers C_{60}-*bis*(2-alkyl-*N*,*N*-dimethylpyrrolidinium iodide) (*d*, *e*); mixture of stereo-isomers proline-fullerene (*f*, *g*) [23].

It was found that all fullerene adducts have an inhibitory effect compared to the non-nucleoside analogue of the HIV reverse transcriptase inhibitor nevirapine. The highest inhibitory activity (IC_{50} = 0.029 μM) was shown by the fullerene adduct with L-proline (Fig. 47*e*). According to the authors of [23,111], this is explained by the fact that the biological activity of fullerene adducts with amino acids depends on the type and position of substituents in the fullerene core.

An important advantage of anti-HIV drugs based on fullerene adducts with amino acids is the almost complete absence of resistance to them in viruses [112].

In addition to work related to the inhibition of HIV protease and reverse transcriptase, studies are being conducted on the effects of fullerene adducts with amino

acids on the development of CMV infection. In works [35,36], the antiviral activity of C_{60} fullerene adducts with sodium salts of γ-aminobutyric and ε-aminocaproic acids (see Fig. 2) was studied against CMV infection, as well as hybrid structures based on the C_{60} fullerene adduct with carnosine dipeptide (see Fig. 2). It was found that the sodium salt of fullerenylaminobutyric acid more effectively inhibits the development of CMV infection compared to the clinical drug for the treatment of CMV infection — ganciclovir.

Kotelnikova *et al.* [35] were the first to show a significant correlation between the development of CMV infection and the intensity of lipid peroxidation in infected human lung fibroblast cells. It was found that the studied adducts of fullerene C_{60} with sodium salts of γ-aminobutyric and ε-aminocaproic acids (see Fig. 2) reduce the amount of malondialdehyde formed in mitochondria. It is known that malondialdehyde is one of the end products of lipid peroxidation and is formed during the oxidative degradation of fatty acids. The accumulation of malondialdehyde can indicate the activation or inhibition of LPO [113]. The most effective antioxidant of all adducts was the adduct of fullerene C_{60} with carnosine (see Fig. 2); carnosine by itself is less effective than the adduct of C_{60} fullerene with carnosine.

Adducts of fullerene C_{60} with sodium salts of ε-aminocaproic and γ-aminobutyric acids (see Fig. 1) have pronounced antiviral activity against the herpes virus, various influenza viruses and HIV [35,36]. Thus, Khalikov *et al.* [44] studied the antiviral activity of sodium salts of fullero-(C_{60}) amino acids against the H5N1 virus using the PEKC cell line model in *in vitro* experiments. These compounds have been shown to inhibit the replication of the H5N1 virus. The virucidal activity of the compounds is due to the direct inactivation of virions in a population of viruses, which partially or completely suppress their infectious activity.

Under certain conditions, many of the fullerene compounds are capable of protecting cells from various types of ionising radiation [114,115]. The possibility of using fullerenes in photodynamic therapy is determined both by the physicochemical properties of a particular adduct and by the experimental conditions: time, power of the radiation source, concentration of the substance, size of nanoparticles [114]. Currently,

studies of C_{60} fullerene adducts with amino acids are widely carried out in this area. Hu *et al.* [31] studied the biological effect of adducts of fullerene C_{60} with folacin, L-phenylalanine and L-arginine (see Fig. 2)) against HeLa tumour cells. It has been shown that when HeLa cells are irradiated with visible light, there is a decrease in mitochondrial membrane potential, cell viability, and the activity of the enzymes SOD, catalase, and glutathione peroxidase, which leads to the activation of caspase-3 and, accordingly, the launch of the apoptosis program.

Jiang *et al.* [38] studied the biological effect of the adduct of fullerene C_{60} with glycine (see Fig. 2) in relation to the HeLa and Lm8 cell lines. Cytotoxicity was compared for the adduct of fullerene C_{60} with glycine at various concentrations (0–100 $\mu g \cdot ml^{-1}$) based on growth rate inhibition of the Lm8 cell line, as shown in Fig. 48. In addition, cytotoxicity at different irradiation powers was compared *in vitro* using the HeLa cell line (Fig. 49).

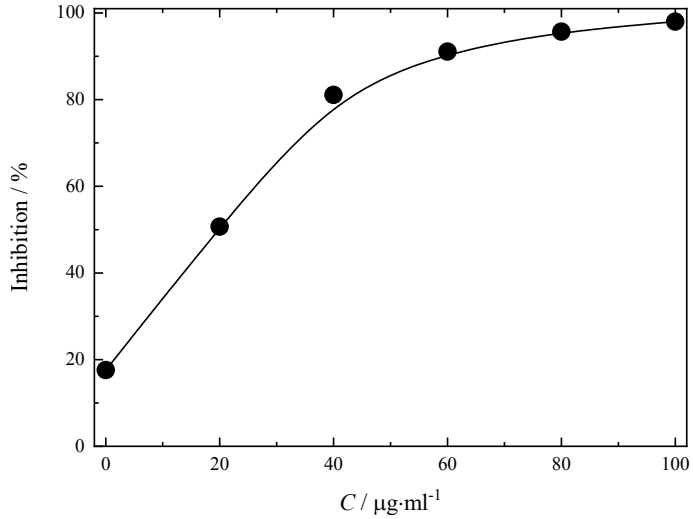

Fig. 48. Dependence of growth inhibition of the HeLa cell line on concentration (0–100 $\mu g \cdot ml^{-1}$) in the presence of the C_{60} fullerene adduct with glycine [38].

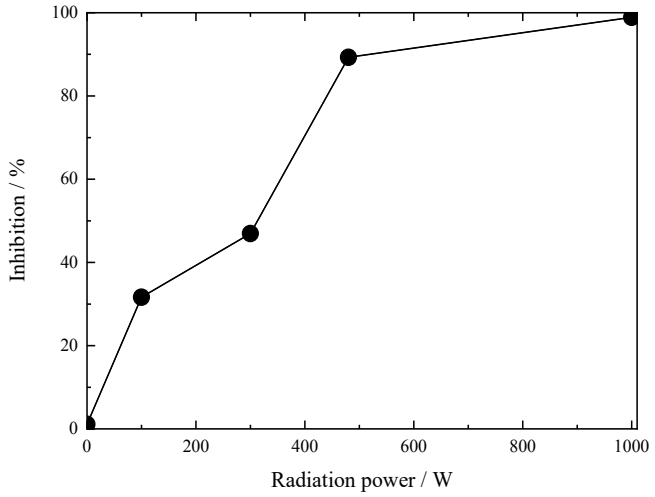

Fig. 49. Dependence of growth inhibition of the Lm8 cell line on radiation power (λ = 500–600 nm) in the presence of a C_{60} fullerene adduct with glycine [38].

As a result of research, it was found that the adduct of fullerene C_{60} with glycine under irradiation (λ = 500–600 nm) causes the death of cell lines Lm8 and HeLa.

According to the authors, cell death occurs mainly due to damage to phospholipids and proteins of the cell membrane. When irradiated, the adduct of fullerene C_{60} with glycine passes from an excited singlet state to an excited triplet state, which is subsequently quenched by oxygen, transferring it to the singlet state. Singlet oxygen then immediately reacts with proteins, nucleic acids and membrane phospholipids, leading to cell damage and death.

Lee *et al.* [39] studied the biological effect of fullerene C_{60} adducts with L-phenylalanine and glycine (see Fig. 2). It was found that these adducts can act as photosensitisers for photodynamic therapy. The study was conducted on the SMMC-7721 cell line. Apoptotic cell death was assessed 30 min, 24–72 h after irradiation; C_{60} fullerene adducts with L-phenylalanine and glycine were used at concentrations of 80–300 $\mu g \cdot ml^{-1}$. It was found that the inhibition of cell division in the presence of fullerene adducts with amino acids is significantly higher after 48 h of incubation compared to incubation of cells for 24 h. Thus, the research results show that C_{60} fullerene adducts with amino acids can be considered as promising compounds for the treatment of cancer diseases.

Hu *et al.* [61] studied the biological activity of C_{60}-GluEG (see Fig. 20) against the HeLa cell line at various concentrations and incubation times of 12 and 24 h. The study showed that C_{60}-GluEG has low cytotoxicity and high biocompatibility.

Siepi *et al.* [78] studied the biocompatibility of C_{60} nanoparticles modified with hen egg white lysozyme (HEWL) and lysozyme in HaCaT and HeLa cell lines. It was shown that C_{60} fullerene nanoparticles modified with lysozyme in the concentration range of 0.5–3.0 μmol·l^{-1} do not have cytotoxicity (incubation time 24 and 48 h).

One of the most important properties of C_{60} fullerene adducts with amino acids is their ability to penetrate biological membranes and distribute in various cell compartments [116]. Kotelnikova *et al.* [117] studied the membranotropic properties of fullerene adducts C_{60}-Ala (($C_{60}(C_3H_6NO_2)_nH_n$, where n = 1) and (C_{60}-Ala-Ala ($C_{60}(C_6H_{12}N_2O_3)_nH_n$, where n = 1). It was shown that these adducts penetrate into liposomes through the lipid bilayer of membranes and are able to carry out active transmembrane transport of Co^{2+} ions, forming complexes with it.

Hu *et al.* [40–42] studied the biological effect of adducts of fullerene C_{60} with β-alanine, L-cystine and tripeptide glutathione (see Fig. 2) in relation to the PC12 cell line. The results of the study showed that C_{60} fullerene adducts in the concentration range from 0.5 to 100 μg·ml^{-1} have an anti-apoptotic effect against PC12 cells when exposed to hydrogen peroxide. The antiapoptotic effect of fullerene adducts is primarily associated with their activity and the morphology of the aggregates. The size of the aggregates of the C_{60} fullerene adduct with L-alanine (see Fig. 2) is the smallest among other adducts, which makes it easier for it to penetrate the cell membrane and have a protective effect by capturing ROS.

Kumar *et al.* [118] studied the ability of a conjugate of fullerene C_{60} with L-lysine (Fig. 50) to cause breaks in covalent bonds in the supercoiled DNA molecule of plasmid pBR322 in the presence of the coenzyme NADH under the influence of visible radiation (irradiation time is 3 h).

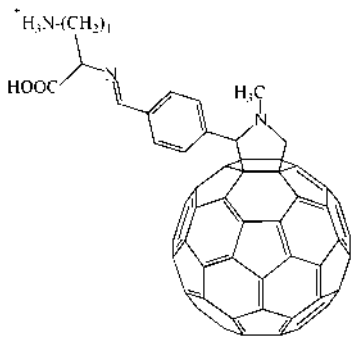

Fig. 50. Conjugate of fullerene C_{60} with L-lysine [118].

Fullerene adducts with amino acids effectively penetrate the blood-brain barrier and therefore can act as drug carriers into nervous tissue [7]. In this regard, the creation and study of adducts based on fullerenes is a promising approach in the pharmacotherapy of diseases of the nervous system. The authors of [7] in experiments *in vitro* and *in vivo*, found that adducts of fullerene C_{60} with various amino acids: (L-phenylalanine (Fig. 4*a*), L-serine (Fig. 4*b*), β-alanine (Fig. 4*c*) and γ-phenylbutyric acid (Fig. 4*d*)) inhibits the proliferation of glioblastoma cells and reduces its growth rate in Zebrafish. It was also found that the adduct of fullerene C_{60} with L-phenylalanine inhibits the growth of glioblastoma without slowing down the recovery of neurons and does not affect neuronal stem cells. Presumably, the antitumour mechanism of action of C_{60} fullerene adducts with amino acids is explained by their participation in the regulation of free radical processes.

In the patent [53], the authors studied the biological activity of the fullerene-containing glycopeptide GlcNac-MurNac-Ala-DiGln[Lys-ε-$CO(CH_2)_5NHC_{60}$-H] (see Fig. 12). Experiments conducted on mice (female Balb/c line) showed that at low doses of 1 and 10 nmol/animal, the fullerene-containing glycopeptide has high adjuvant properties. When a high dose of the compound was administered (1 mg/animal), no death of animals was observed, which indicates the non-toxicity of this adduct.

The literature review summarizes the available data on the synthesis, identification, physicochemical and biological study of fullerene C_{60} adducts with amino acids, peptides and proteins. An analysis of the work on the functionalization of light fullerenes allows us to draw the following conclusion:

– not all of the reviewed works provide complete identification data of the synthesized C_{60} fullerene adducts, and thus, it is impossible to judge the chemical composition of the compounds obtained;

– only a small number of papers present data on the physicochemical study of fullerene adducts, despite the fact that their physicochemical properties underlie the understanding of the mechanisms of action of the created nanoparticle;

– the study of the biological activity of fullerene adducts is fragmentary and unsystematic.

It is obvious that the development of single-stage methods for the synthesis of water-soluble fullerene adducts, as well as a complex study of their properties, is relevant for the creation of high-tech medical materials based on them.

Chapter 2. Experimental part

2.1. Materials and research methods

2.1.1. Synthesis of the adduct of light fullerene C_{60} with L-arginine

To carry out the synthesis, a sample of L-arginine (4.65 g) and sodium hydroxide (15.75 g) was dissolved in 54 ml of water. Sodium hydroxide was used to convert the amino acid to sodium form. Then ethanol (270 ml) was added to the resulting solution (to ensure the mutual solubility of *o*-xylene and water) and a saturated solution of fullerene C_{60} in *o*-xylene (for this, 1 g of C_{60} was dissolved in 131.5 ml of *o*-xylene). Then the resulting reaction mixture was stirred on a magnetic stirrer at room temperature for a week in an argon atmosphere. The reaction scheme for the synthesis of the fullerene adduct is shown in Fig. 51.

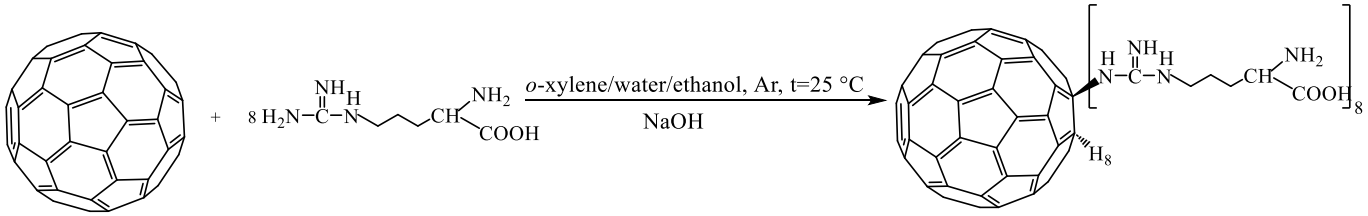

Fig. 51. Scheme of the reaction for producing the C_{60} fullerene adduct with L-arginine.

Then the reaction product was isolated. The resulting mixture was separated from the solvents using a rotary evaporator RV3V (IKA, Germany) and then the resulting precipitate was dissolved in water. After that, the resulting solution was filtered from insoluble impurities and the adduct of light fullerene C_{60} with L-arginine was recrystallised using ethanol. The resulting precipitate was washed from alkali with ethanol until the medium was neutral (pH 7). The adduct of C_{60} with L-arginine was dried at 60 °C in air (Fig. 51). The yield of the target product was up to 90 %. Then the product was purified from impurities by dialysis using a dialysis bag, MWCO = 1000 g/mol, at $t°$ = 25 °C, against deionised water for 24 h. The water was replaced every 6 h.

2.1.2. Identification of the adduct of light fullerene C_{60} with L-arginine

Identification of the resulting adduct was carried out using a complex of physicochemical methods of analysis: elemental analysis, IR and ^{13}C NMR spectroscopy, HPLC, thermogravimetric analysis.

Determination of the carbon, nitrogen and hydrogen content in the sample was carried out using a C, H, N analyser EuroEA3028-NT (Italy). IR spectra were recorded using a Nicolet 8700 IR Fourier spectrometer (USA). To identify the adduct, solid-state 13C NMR spectroscopy was also used (NMR spectrometer Avance III 400 WB, Bruker (Massachusetts, USA).

Thermogravimetric analysis was carried out using a synchronous thermal analyser Netzsch STA 449 F3 Jupiter (Germany) in the temperature range 303.62–10274.95 °C at heating rate 5 °C/min in air.

2.1.3. Study of the thermodynamic properties of the adduct of light fullerene C_{60} with L-arginine

The temperature dependence of the isobaric heat capacity of the adduct of light fullerene C_{60} with L-arginine was studied by adiabatic vacuum calorimetry in the low temperature range T = 5–328 K (AK-9.02/BCT-21 calorimeter, TERMAX, Russia). The instrument was calibrated by measuring the isobaric heat capacities of standard samples—benzoic acid (purity 0.99999) and synthetic sapphire α-Al_2O_3 (purity 0.99999). The heat capacity was determined in a titanium ampoule evacuated and filled with dry helium.

2.1.4. Study of the physicochemical properties of the adduct of light fullerene C_{60} with L-arginine

The density (ρ) of aqueous solutions of the adduct of light fullerene C_{60} with L-arginine was measured using an Anton Paar DMA 5000 M density meter (Anton Paar GmbH, Austria) in the temperature range T = 278.15–323.15 K and in the concentration range C = 0.3–40 g·dm^{-3}). Before each series of measurements, the device was calibrated under isothermal conditions (at atmospheric pressure). The accuracy of density determination was $7 \cdot 10^{-6}$ g·cm^{-3} (reproducibility $5 \cdot 10^{-6}$ g·cm^{-3}), temperature control of the samples was controlled with an accuracy of 0.01 K. The presented density values are the average of three independent experiments.

The study of the concentration dependence of viscosity (η) of aqueous solutions of the adduct of light fullerene C_{60} with L-arginine in the temperature range T = 278.15–313.15 K and in the concentration range C = 0.25–40 g dm^{-3} was carried out using a

microviscometer Anton Paar LOVIS 2000 M. The viscometer was calibrated using deionised water; The temperature control accuracy was 0.02 K; the accuracy of viscosity measurement did not exceed 0.5%. Viscosity measurements were carried out three times for each sample.

The refractive index (n_D) was measured using an Anton Paar Abbemat Multi-Wavelength WR-MW refractometer (Austria) at a wavelength of 589.3 nm (sodium D line) in the temperature range T = 278.15–323.15 K and in concentration range C = 0.06–30 g·dm^{-3}. The device was calibrated at atmospheric pressure using dry air. The refractive index values presented are the average of three independent experiments.

The study of the concentration dependence of electrophoretic mobility and the concentration dependence of the sizes of associates of the adduct of light fullerene C_{60} with L-arginine in aqueous solutions was carried out on a Malvern Zetasizer 3000 device (Great Britain).

The study of solubility in the binary system adduct C_{60} with L-arginine-water was carried out by the method of isothermal saturation in ampoules in the temperature range 293.15–333.15 K. Saturation was carried out in a water shaker-thermostat LAUDA ET 20 (Germany), the temperature control accuracy was ΔT = ±0.1 K, shaking frequency 2 Hz, saturation time 8 h. The adduct concentration was determined spectrophotometrically at a wavelength of 330 nm [108].

2.1.5. Biocompatibility and biological activity of the adduct of light fullerene C_{60} with L-arginine

2.1.5.1. Cytotoxicity

The cytotoxicity of the C_{60} adduct with L-arginine was studied using the MTT reagent (3-(4,5-dimethylthiazol-2-yl)-2,5-diphenyltetrazolium bromide) on the HEK293 cell line (human embryonic kidney cells). The cell line was obtained from the Russian Collection of Vertebrate Cell Cultures, Institute of Cytology, Russian Academy of Sciences, St. Petersburg.

The cell line was cultured in a CO_2 incubator at +37 °C in a humidified atmosphere containing air and 5 % CO_2 in a DMEM nutrient medium containing 10 %

heat-inactivated fetal bovine serum, 1 % L-glutamine, 50 $U \cdot ml^{-1}$ penicillin and 50 $\mu g \cdot ml^{-1}$ streptomycin.

To conduct the experiment, cells were seeded into a 96-well plate and placed for incubation overnight in a CO_2 incubator: during this time, cells were attached to the surface of the wells (5000 cells were added to each well in 200 µl of DMEM medium). Cell number counting was performed using a BioRad TC10 cell viability analyser (Bio-Rad Laboratories, USA). Then a solution containing the adduct of fullerene C_{60} with L-arginine was added to the wells. Incubation of cells in plates lasted 48 h in a CO_2 incubator at +37 °C. Next, the DMEM culture medium was drained by inverting the plate and 100 µl of DMEM medium and 20 µl of MTT reagent were added to the wells, after which the plates with cells were incubated for 1 h in a CO_2 incubator at +37 °C.

After removing the supernatant, the formazan crystals were dissolved for 15 min with stirring in 200 µl/well of DMSO and the optical density was measured on a BioRadxMarx plate spectrophotometer (Bio-Rad Laboratories, USA) at wavelengths of 540 nm and 690 nm. To correct the background, the absorbance values at 540 nm for the corresponding wells were subtracted from the absorbance values at 540 nm. Data were normalised as percentages relative to control cells [119].

2.1.5.2. Genotoxicity

The genotoxicity of the adduct of light fullerene C_{60} with L-arginine was studied using the DNA comet method, based on measuring the effect of the adduct on the integrity of the DNA molecule of human peripheral blood mononuclear cells (PBMC) using electrophoresis [120,121]. The comet DNA was visualised using a Mikromed 3 LYUM fluorescence microscope (Russia). DNA comet tail lengths were measured using CASP software. The DNA content of the tail and the length of the tail were determined experimentally, and the tail moment was calculated as the percentage of DNA in the tail multiplied by the distance between the centre of the comet's head and tail.

2.1.5.3. Binding to HSA

The interaction of HSA and the C_{60} fullerene adduct with L-arginine was studied at 298.15 K by isothermal titration calorimetry using a Nano ITC 2G device (TA Instruments, USA) equipped with a 1 ml gold measuring cell. An HSA solution (C =

10^{-4} mol·l^{-1}) was placed in the cell. After equilibrium was established, the adduct solution ($C = 10^{-3}$ mol·l^{-1}) was added to the contents of the cell with continuous stirring by successive injections of 10 μl. A phosphate buffer solution of PBS was used as a medium for the reaction under study. The interval between injections was 2400 s, the stirrer rotation speed was 250 rpm. The accuracy of maintaining temperature during the experiment was ±0.0003 K [119].

2.1.5.4. Antiradical activity

A study of the antiradical activity of the C_{60} fullerene adduct with L-arginine (240 μM) in a model reaction with a stable diphenylpicrylhydrazyl (DPPH) radical (120 μM) was carried out on a BioRadxMark spectrophotometer. To obtain the kinetic curve of DPPH reduction by the test substance, the reaction mixture was pipetted into a 96-well plate and the optical density was recorded at a wavelength of 515 nm every min for 10 min, every 10 min for the next 170 min, and also 6 days after the start. reactions. Mixing of the reaction mixture was carried out on a Multi Bio 3D orbital shaker [119].

Chapter 3. Results

3.1. Identification of the light fullerene C_{60} adduct with L-arginine

3.1.1. Elemental analysis

The results of elemental analysis of the adduct showed good agreement between calculated and experimental data (experimental content: C 61.3 %, H 5.3 %, N 21.2 %, theoretical content: C 61.3 %, H 5.3 %, N 21.2 %). Thus, we can conclude that for one molecule of C_{60} there are eight residues of the L-arginine molecule.

3.1.2. IR spectroscopy

Fig. 52 shows the IR spectrum of the adduct of fullerene C_{60} with L-arginine: a broad peak at 3449 cm^{-1} is attributed to the stretching vibrations of the NH bond of the guanidine group; the peak at 2926 cm^{-1} can be attributed to the stretching vibrations of the amino group of the L-arginine molecule; the peak at 1618 cm^{-1} corresponds to the stretching vibrations of the C–N bond in the guanidine group; the peak at 1574 cm^{-1} can be attributed to the stretching vibrations of the C=O bond of the carboxyl group of the L-arginine molecule; the peak at 1401 cm^{-1} is due to bending vibrations of CH_2–NH in the guanidine group; the peak at 1190 cm^{-1} corresponds to the stretching vibrations of the C–N bond of the guanidine group; the peak at 596 cm^{-1} corresponds to vibrations of the C–C bonds of the fullerene molecule.

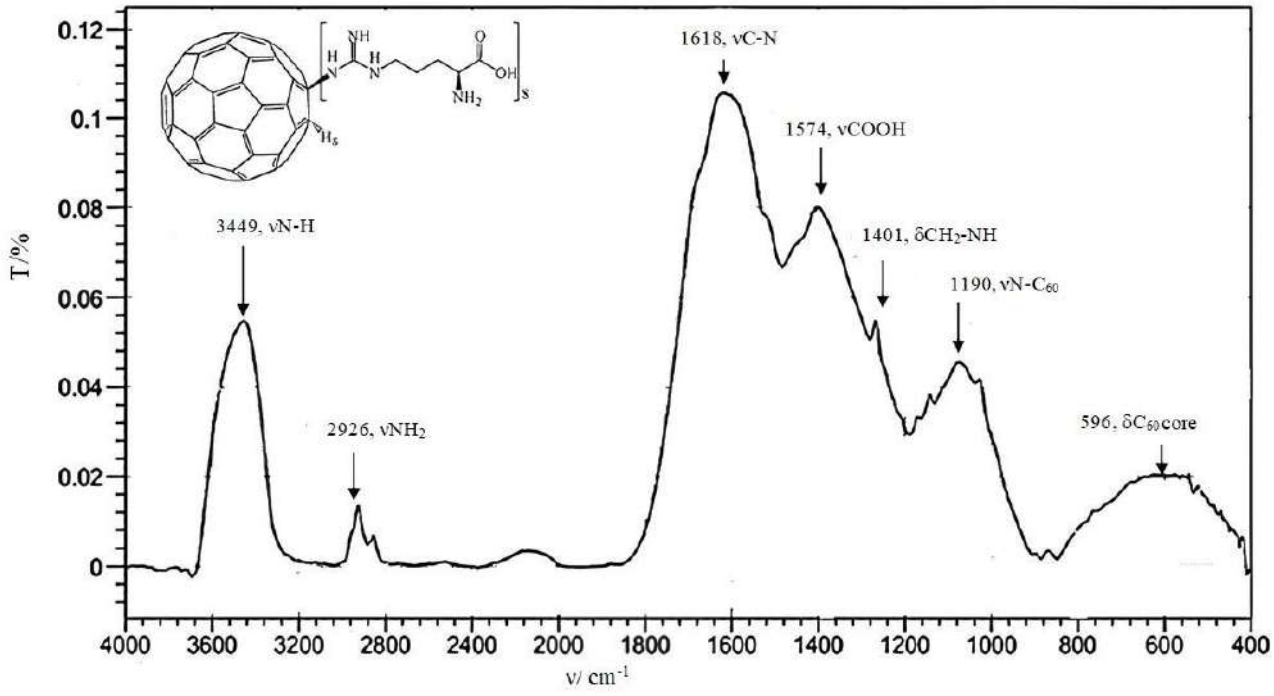

Fig. 52. IR spectrum of the adduct of fullerene C_{60} with L-arginine.

3.1.3. ^{13}C NMR spectroscopy

Since during the dissolution of the adduct, the formation of large associates with sizes of hundreds to thousands of nm (depending on the concentration) is observed, which prevents high-speed spin diffusion processes, as well as averaging of dipole-dipole interaction, leading to the impossibility of recording a high-resolution NMR spectrum (in the liquid phase). Therefore, the method of solid-state NMR spectroscopy was used to record the spectra. To record spectra on ^{13}C nuclei, a cross-polarisation sequence of exciting pulses was used (CP/MAS technique). Tetramethylsilane was used as an external reference.

Fig. 53 shows a set of CP/MAS NMR spectra obtained at different contact times. It can be seen that at short contact times (from 7 to 10 μs), signals corresponding to two –CH_2– structural elements of the L-arginine molecule are observed. When the contact time is greater than 20 μs, a signal appears that corresponds to the –CH– structural element of the L-arginine molecule. At the next stage, when the contact time exceeds 100 μs, peaks corresponding to the carbon atoms in the guanidine and carboxyl groups

of the L-arginine molecule are visible in the spectrum. The remaining signals at a contact time of 500 μs refer to the carbon atoms of the fullerene core.

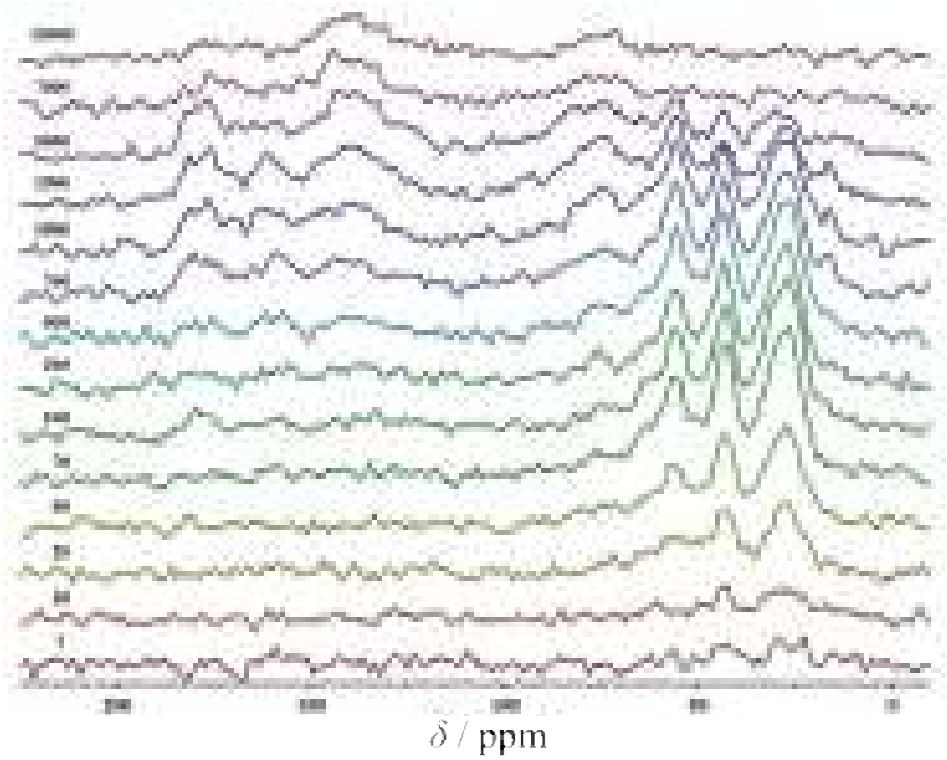

Fig. 53. A set of CP/MAS NMR spectra of C_{60}-L-arginine obtained at different contact times (indicated to the left of the spectra in μs).

Fig. 54 shows the ^{13}C NMR spectrum of the adduct obtained by the CP/MAS method (contact time 2 μs). The spectrum is represented by the following peaks: the signal at 176.4 ppm corresponds to the carbon atom in the carboxyl group, the signal at 158 ppm corresponds to the carbon atoms in the guanidine group, the signal at 76.2 ppm can be attributed to carbon atoms of the fullerene core bonded to a hydrogen atom, the signal at 56 ppm corresponds to the –CH– structural element of the L-arginine molecule, the signal at 27.5 ppm corresponds to the $–CH_2–$ structural element of the L-arginine molecule. The remaining signals at 139.6, 76.2, 63.7 and 16.4 ppm correspond to the fullerene core.

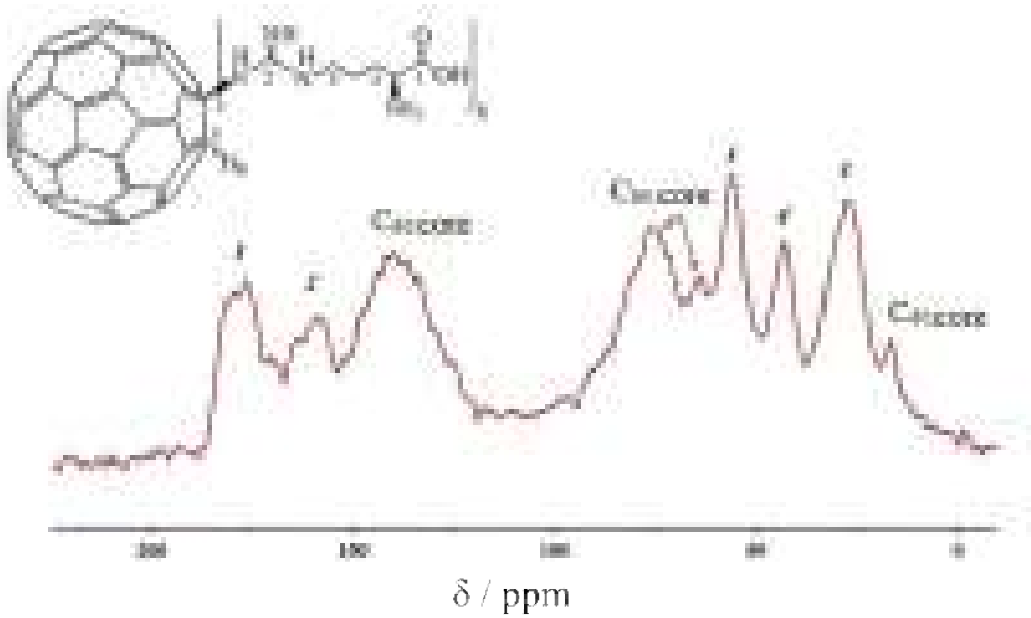

Fig. 54. ^{13}C NMR spectrum of the adduct of fullerene C_{60} with L-arginine, obtained by the CP/MAS method (contact time was 2 μs).

3.1.4. High performance liquid chromatography

The results of the chromatographic analysis showed that the purity of the adduct of light fullerene C_{60} with L-arginine is 99.8 % (Fig. 55).

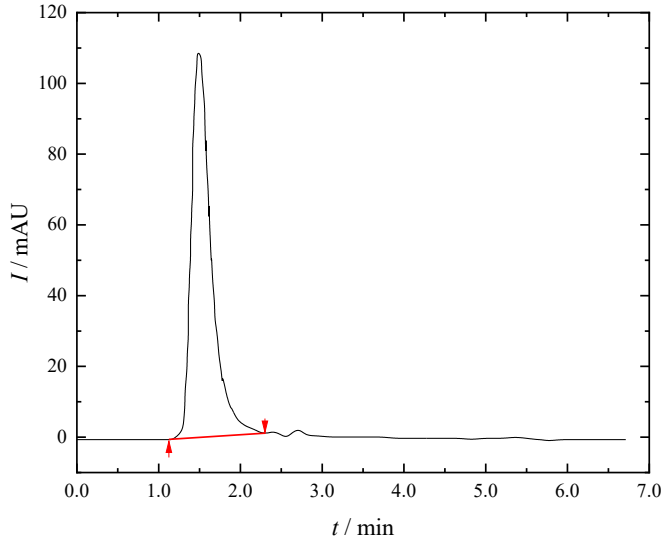

Fig. 55. Chromatogram of the adduct of fullerene C_{60} with L-arginine.

3.1.5. Thermogravimetric analysis

Fig. 56 presents the results of thermogravimetric analysis of the adduct of C_{60} with L-arginine.

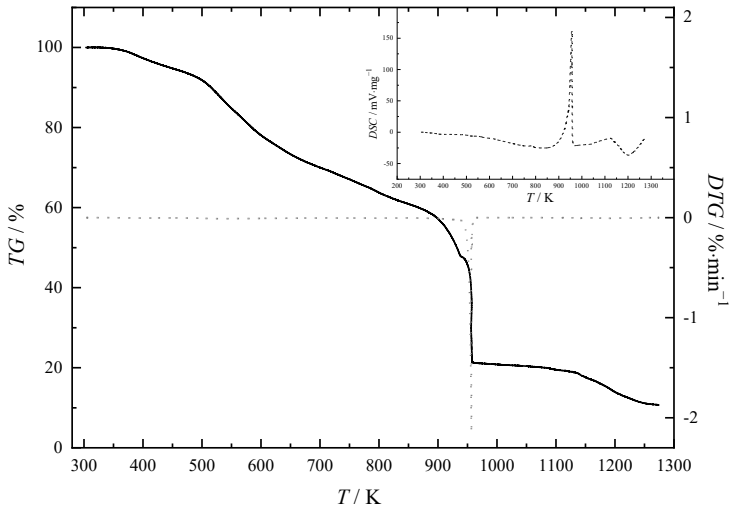

Fig. 56. Thermogravimetric analysis of the adduct of light fullerene C_{60} with L-arginine in the temperature range T = 303.62–1274.95 K in air. The *TG* curve is a solid line, the *DTG* curve is a dotted line.

Analysis of Fig. 56 reveals the following: (*1*) in the temperature range up to 340 K, the adduct is thermally stable; (*2*) in the temperature range T = 340–950 K, multistage adduct decomposition processes occur, including dehydration ($-nH_2O$), decarboxylation ($-nCO_2$), denitrogenation ($-N_2$), and dehydrogenation ($-H_2$). The mass loss of 65.9 % (Fig. 56) corresponds to the decomposition of eight L-arginine residues; (*3*) in the temperature range T = 950–1270 K, oxidation of the fullerene core (C_{60}) occurs.

3.2. Thermodynamic characteristics of the adduct of light fullerene C_{60} with L-arginine

Fig. 57 shows the temperature dependence of the isobaric heat capacity of the adduct in the temperature range T = 5–328 K. The experimental data obtained indicate that no phase transitions are observed in the studied temperature range. For comparison, an individual fullerene C_{60} exists in three physical states: in a glassy crystalline state, in the form of monoclinic crystals and in the form of plastic crystals, and two-phase transitions take place: a second-order 'order-disorder' transition (at 86 K) and a first-order phase transition (at 260.7 K) (see section 1.2.1) [81].

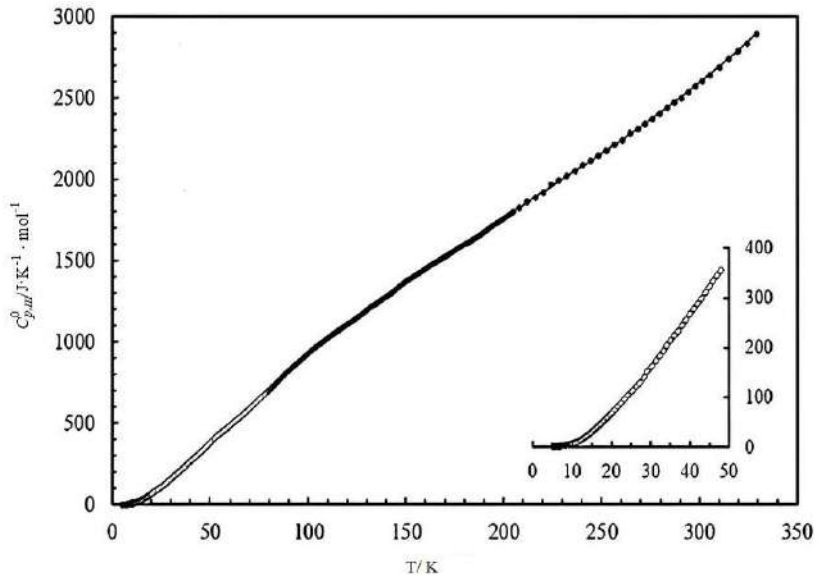

Fig. 57. Temperature dependence of the isobaric heat capacity of the adduct of light fullerene C_{60} with L-arginine in the temperature range T = 5–328 K.

Extrapolation of the heat capacity to T = 0 K was carried out using the polynomial equation 5:

$$C^o_{p,m} = A \cdot T^n, \quad (5)$$

where A and n are empirical coefficients calculated based on experimental heat capacity values in the temperature range T = 6–10 K.

Logarithmic form of equation 5 has the following form:

$$\ln(C^o_{p,m} / J \cdot K^{-1} \cdot mol^{-1}) = 2,88346 \cdot \ln(T / K) - 0,010126, \quad (6)$$

Standard deviations of the calculated coefficients (A and n) from equation 5 is less than 1.2 %. Numerical form of equation 5 has the following form:

$$C^o_{p,m} = 0,989925 \cdot T^{2,88346}, \quad (7)$$

The temperature dependence of the isobaric heat capacity was described using the polynomial equation 8 for the following temperature ranges: T = 5–14 K, T = 1–81 K and T = 82–328 K:

$$C^o_{p,m} = k_0 + k_1 T^{-3} + k_2 T^{-2} + k_3 T^{-0,5} + k_4 T + k_5 T^2 + k_6 T^3, \quad (8)$$

where k_i are polynomial coefficients.

The values of polynomial coefficients are presented in Table 3.

Table 3. Values of polynomial coefficients k_i in the temperature ranges T = 5–14 K, T = 15–81 K and T = 82–328 K.

T / K	k_0	k_1	k_2	k_3	k_4	k_5	k_6
5–14	3515.76	−29494.3	20428.2	−7195.9	−217.887	9.28502	−0.156846
15–81	−6907.51	3088030	−575915	27599.6	110.993	−0.97727	0.00388589
82−328	−12630.8	472098000	−21656200	108085	55.5848	−0.125264	0.000140997

The calculation of the standard molar entropy $S_m°(T)$ of the adduct was carried out in accordance with equation 9, subject to $S^{T=0K}=0$:

$$S_0 - S^{T=0K} = \int_0^{298,15} \frac{C_p^0}{T} dT \ , \qquad (9)$$

Thus, it was found that at T = 298.15 K the standard molar entropy of the adduct ($S_m°(T)$) is 2396 ± 5 $J \cdot K^{-1} \cdot mol^{-1}$.

The entropies of simple substances (C (gr.), H_2 (g), O_2 (g), N_2 (g)) (Table 4) were used to calculate the standard molar entropy of formation of $C_{60}(C_6H_{14}N_4O_2)_8$ in the crystalline state at T = 298.15 K by equation 10:

$$108C_{(gr.)} + 56H_{2(g)} + 16N_{2(g)} + 8O_{2(g)} = C_{60}(C_6H_{14}N_4O_2)_{8(cr.)}, \qquad (10)$$

where gr. is graphite, g is gas, cr. is crystal.

Table 4. Standard molar entropies of simple substances.

Substance	$S_m°$(298 K) / $J \cdot K^{-1} \cdot mol^{-1}$
C, *gr.*	5.6 ± 0.5
H_2, *g.*	130.680 ± 0.003
O_2, *g.*	205.152 ± 0.005
N_2, *g.*	191.609 ± 0.004

As a result, the following value was obtained for the standard molar entropy of the formation of the C_{60} adduct with L-arginine (equation 11):

$$\Delta_f S_m^o(298,15K) = -(10234 \pm 7)\ J \cdot K^{-1} \cdot mol^{-1} \ . \qquad (11)$$

Table 5 presents the standard molar thermodynamic functions of the C_{60} fullerene adduct with L-arginine, calculated in the temperature range T = 5–320 K.

Table 5. Standard molar thermodynamic functions of the light fullerene adduct C_{60}-L-arginine. $S_m°$ is the standard molar entropy, $[H_m°(T) - H_m°(0)]$ is the enthalpy, and $[\Phi_m°(T) - \Phi_m°(0)]$ is the Gibbs function at 0.1 mPa.

T / K	$C_{p,m}^{\circ}(T)$ / $J \cdot K^{-1} \cdot mol^{-1}$	$\Delta_0^T H_m^{\circ}(T)$ / $kJ \cdot mol^{-1}$	$\Delta_0^T S_m^{\circ}(T)$, $J \cdot K^{-1} \cdot mol^{-1}$	$\Delta_0^T \Phi_m^{\circ}(T)$ / $kJ \cdot mol^{-1}$
5	1.049	0.00135	0.364	0.094
10	7.790	0.0199	2.699	0.699
15	32.15	0.110	9.64	2.31
20	70.20	0.360	23.80	5.79
25	113.3	0.818	44.04	11.32
30	161.1	1.50	68.84	18.79
35	213.8	2.44	97.58	27.94
40	269.5	3.64	129.7	38.63
45	326.1	5.13	164.7	50.67
50	382.2	6.90	202.0	63.93
70	596.2	16.71	364.9	126.3
90	827.1	30.92	542.3	198.7
110	1025.9	49.51	728.1	287.0
130	1201.2	71.8	913.9	361.6
150	1366.8	97.49	1097.5	447.5
170	1527.7	126.4	1278.4	534.6
190	1685.6	158.6	1457.0	622.4
210	1842.1	193.9	1633.4	710.3
230	1999.1	232.3	1808.0	798.1
250	2159.1	273.8	1981.2	885.9
270	2325.4	318.7	2153.7	973.4

273.15	2352.4	326.0	2180.8	987.2
290	2501.7	366.9	2326.0	1060.7
298.15	2577.4	387.6	2396.4	1096.3
310	2692.4	418.8	2499.0	1147.9
320	2794.5	446.3	2586.1	1191.5

Using the DFT method, in the DMol^3 program within the framework of the harmonic approximation, A. V. Petrov, a researcher at the Department of Solid State Chemistry of the Institute of Chemistry of St. Petersburg State University, calculated the heat capacity values for the adduct of C_{60} with L-arginine. At low temperatures, good agreement was obtained between calculated and experimental data for two isomers of the C_{60} adduct with L-arginine with a uniform (Fig. 58*a*) and equatorial ('Saturn-like') (Fig. 58*b*) distribution of functional groups.

(*a*)

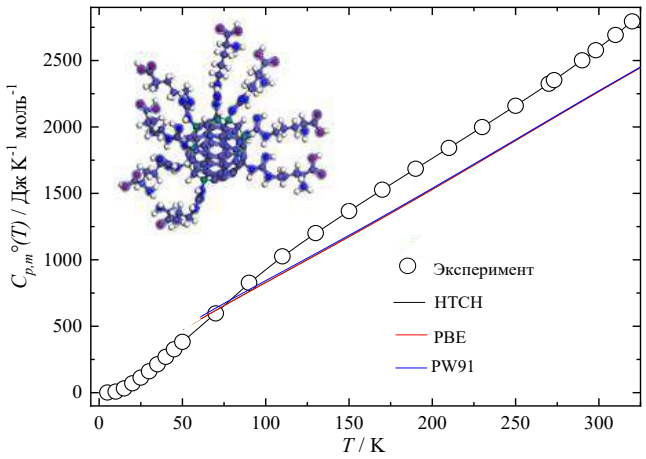

(*b*)

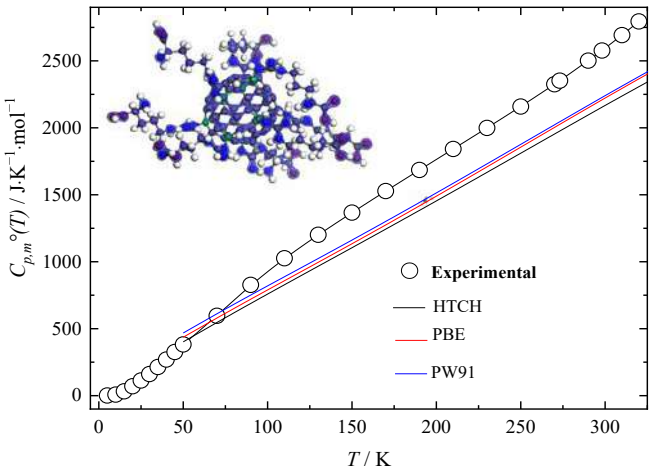

Fig. 58. Comparison of experimental and calculated isobaric heat capacities of the C_{60} adduct with L-arginine with uniform (*a*) and 'Saturn-like' (*b*) distribution of functional groups. HCTH functional — black line, PBE functional — red line, PW91 functional — blue line.

As the temperature increases, a discrepancy is observed between the experimental and calculated data, which is associated with the anharmonicity of the vibrations (the heat capacity values are calculated in the harmonic approximation). In addition, we can conclude that there is no significant difference in the heat capacity values for the C_{60} fullerene adduct molecules with L-arginine with different distributions of amino acid residues, calculated using the PBE, PW91 and HCTH functionals [122].

3.3. Physicochemical properties of aqueous solutions of the adduct of light fullerene C_{60} with L-arginine

3.3.1. Densities of aqueous adduct solutions

The results of an experimental study of the density of aqueous solutions of the adduct of fullerene C_{60} with L-arginine in the temperature range T = 278.15–323.15 K and the concentration range C = 3–40 g·dm^{-3}) are presented in Table 6 and Fig. 59.

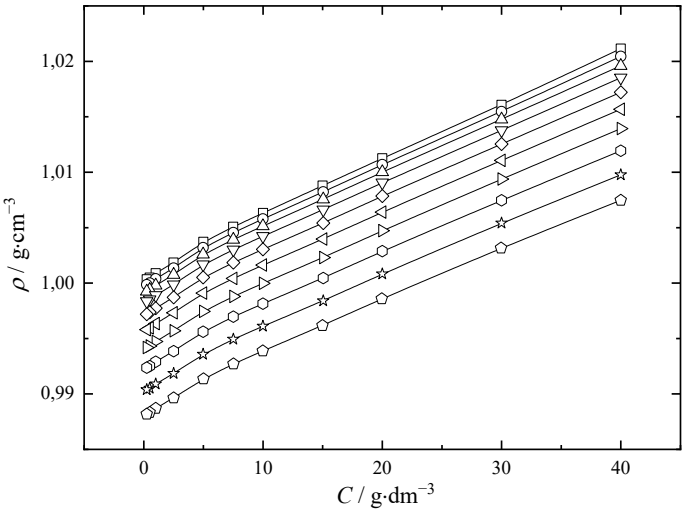

Fig. 59. Concentration dependences of the density (ρ) of aqueous solutions of the C_{60} adduct with L-arginine at (□) 278.15 K; (○) 283.15 K; (△) 288.15 K; (▽) 293.15 K; (◇) 298.15 K; (◁) 303.15 K; (▷) 308.15 K; (⬡) 313.15 K; (☆) 318.15 K; (⬠) 323.15 K. C is volume concentration.

From Fig. 59 shows an increase in density with increasing concentration of the C_{60} adduct with L-arginine.

The obtained data on the concentration and temperature dependences of density (Table 6) were used to calculate the average molar volumes ($\overline{V}$) of solutions according to equation 12:

$$\overline{V} = \frac{V}{n_{H_2O} + n_{\mathrm{C_{60}\text{-L-arginine}}}}, \qquad (12)$$

where V is volume of aqueous solution of C_{60} adduct with L-arginine; $n_{\mathrm{H_2O}}$ and $n_{C_{60}-\mathrm{L\text{-}arginine}}$ are number of moles of water and C_{60}-L-arginine in 1 dm^3 solution.

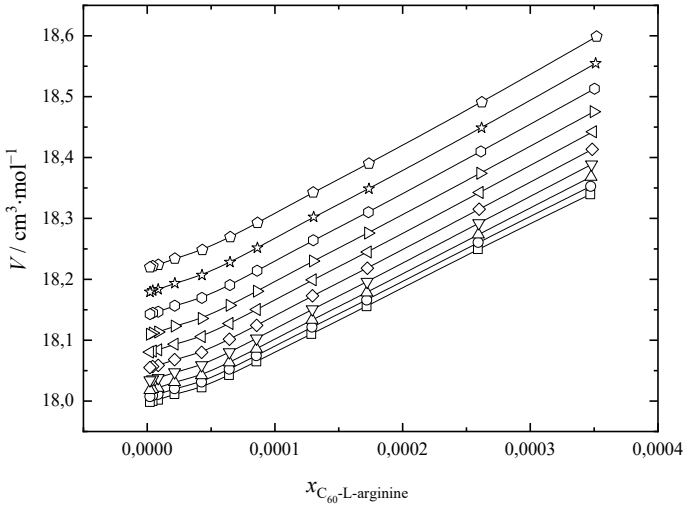

Fig. 60. Concentration dependences of the average molar volume ($\overline{V}$) of aqueous solutions of the C_{60} adduct with L-arginine at (□) 278.15 K; (○) 283.15 K; (△) 288.15 K; (▽) 293.15 K; (◇) 298.15 K; (◁) 303.15 K; (▷) 308.15 K; (⬡) 313.15 K; (☆) 318.15 K; (⬠) 323.15 K. *x* is the mole fraction of the dissolved substance.

Using equations 13 and 14, the partial molar volumes of the solution components were calculated (V_{H_2O} and $V_{C_{60}-\text{L-arginine}}$):

Table 6. Temperature and concentration dependences of density (ρ) of aqueous solutions of C_{60} with L-arginine. C is the volume concentration of the adduct in an aqueous solution.

C / g·dm^{-3}	ρ / g·cm^{-3}									
	278.15 K	283.15 K	288.15 K	293.15 K	298.15 K	303.15 K	308.15 K	313.15 K	318.15 K	323.15 K
0.3	1.00033	0.99983	0.99924	0.99834	0.99718	0.99579	0.99418	0.99236	0.99038	0.98817
0.5	1.00045	0.99995	0.99936	0.99847	0.99732	0.99592	0.99428	0.99246	0.99047	0.98828
1	1.00069	1.00020	0.99960	0.99871	0.99755	0.99616	0.99454	0.99272	0.99071	0.98852
2.5	1.00139	1.00089	1.00029	0.99940	0.99826	0.99686	0.99523	0.99340	0.99139	0.98918
5	1.00262	1.00210	1.00149	1.00058	0.99942	0.99800	0.99636	0.99451	0.99248	0.99026
7.5	1.00388	1.00336	1.00274	1.00182	1.00065	0.99923	0.99760	0.99578	0.99375	0.99152
10	1.00505	1.00452	1.00388	1.00296	1.00178	1.00036	0.99872	0.99688	0.99485	0.99262
15	1.00744	1.00687	1.00621	1.00527	1.00406	1.00263	1.00096	0.99911	0.99705	0.99482
20	1.00985	1.00928	1.00861	1.00766	1.00645	1.00500	1.00333	1.00147	0.99942	0.99718
30	1.01464	1.01404	1.01333	1.01234	1.01111	1.00963	1.00795	1.00604	1.00398	1.00173
40	1.01972	1.01901	1.01817	1.01709	1.01577	1.01425	1.01250	1.01051	1.00834	1.00603

$$V_{H_2O} = \left(\frac{\partial V}{\partial n_{H_2O}} \right)_{T,P,n_{\text{C}_{60}\text{-L-arginine}}} \qquad V_{\text{C}_{60}\text{-L-arginine}} = \left(\frac{\partial V}{\partial n_{\text{C}_{60}\text{-L-arginine}}} \right)_{T,P,n_{H_2O}}, \tag{13}$$

$$V_{H_2O} = \overline{V} - x_{\text{C}_{60}\text{-L-arginine}} \left(\frac{\partial \overline{V}}{\partial x_{\text{C}_{60}\text{-L-arginine}}} \right)_{T,P} \qquad V_{\text{C}_{60}\text{-L-arginine}} = \overline{V} - x_{H_2O} \left(\frac{\partial \overline{V}}{\partial x_{H_2O}} \right)_{T,P}. \tag{14}$$

Figs. 61 and 62 show the concentration dependences of the partial molar volumes of water and the C_{60} adduct with L-arginine ($V_{\text{H}_2\text{O}}$ and $V_{C_{60}-\text{L-arginine}}$) in the temperature range $T = 278.15–323.15$ K.

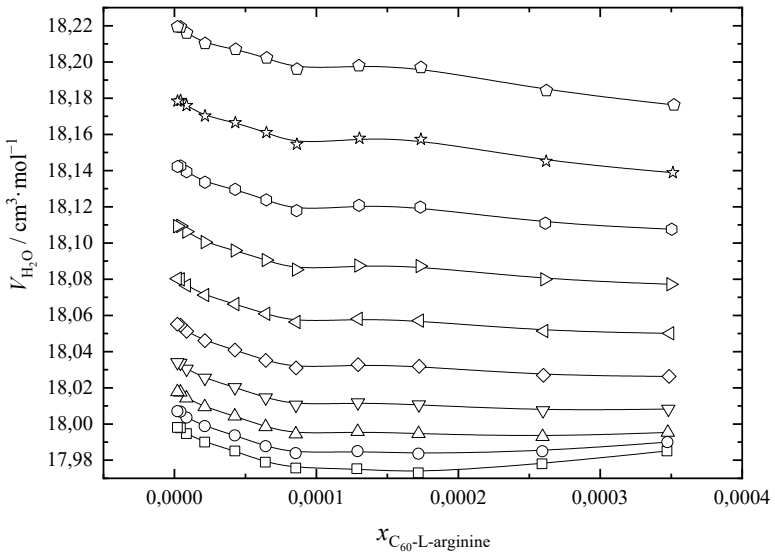

Fig. 61. Concentration dependence of the partial volume of water at (□) 278.15 K; (○) 283.15 K; (△) 288.15 K; (▽) 293.15 K; (◇) 298.15 K; (◁) 303.15 K; (▷) 308.15 K; (⬡) 313.15 K; (☆) 318.15 K; (⬠) 323.15 K. x is the mole fraction of the solute in the solution.

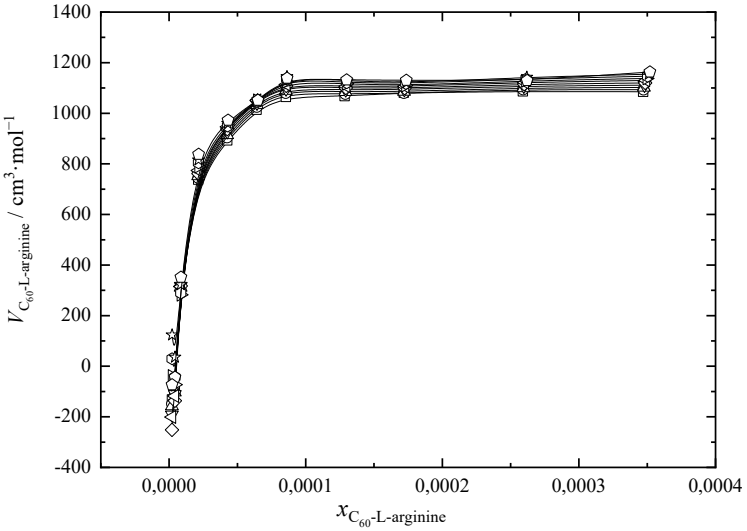

Fig. 62. Concentration dependence of the partial volume of C_{60}-L-arginine at (□) 278.15 K; (○) 283.15 K; (△) 288.15 K; (▽) 293.15 K; (◇) 298.15 K; (◁) 303.15 K; (▷) 308.15 K; (⬡) 313.15 K; (☆) 318.15 K; (⬠) 323.15 K. *x* is the mole fraction of the dissolved substance.

It can be seen that at all studied temperatures, the concentration dependences of the partial molar volumes of C_{60} with L-arginine are complex: in the region of low concentrations of the adduct, the partial molar volumes are negative and take on high modulus values (Fig. 63). This means that the addition of even a small amount of C_{60} adduct with L-arginine leads to significant compaction and structuring of aqueous solutions.

The second derivatives of the Gibbs potential, corresponding to the first derivatives of volume or entropy, are much more sensitive to changes in the structure of the solution than low-order partial derivatives. Mixed second-order derivatives of the Gibbs potential were determined from experimental data on the densities of aqueous solutions of C_{60} with L-arginine using Maxwell's relations:

$$\frac{\partial^2 \overline{G}}{\partial P \partial T} = \frac{\partial^2 \overline{G}}{\partial T \partial P} = \left(\frac{\partial \overline{V}}{\partial T}\right)_{P,X} = -\left(\frac{\partial \overline{S}}{\partial P}\right)_{T,X}, \quad (15)$$

where $\overline{G}, \overline{V}, \overline{S}$ are average molar quantities (Gibbs potential, volume and entropy).

It can be seen that in the studied temperature range the function $\left(\partial\overline{V}/\partial T\right)_P\left(x_{\text{C}_{60}\text{-L-arginine}}\right)$ passes through an extremum at $x_{\text{C}_{60}\text{-L-arginine}} \approx 2\cdot10^{-5}$ (Fig. 63).

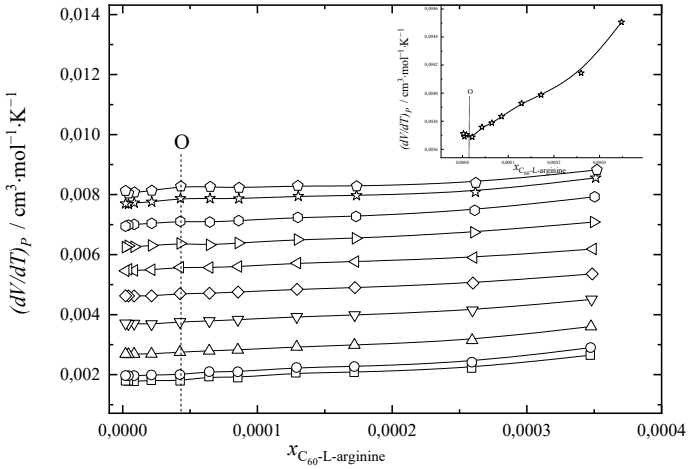

Fig. 63. Concentration dependence of the derivative $\left(\frac{\partial V}{\partial T}\right)_{P,X}$ at (□) 278.15 K; (○) 283.15 K; (△) 288.15 K; (▽) 293.15 K; (◇) 298.15 K; (◁) 303.15 K; (▷) 308.15 K; (⬡) 313.15 K; (☆) 318.15 K; (⬠) 323.15 K. *O* is an extremum point ($\left(\frac{\partial^2 V}{\partial x \partial T}\right)_P = 0, x = 5\cdot10^{-6}$).

This concentration corresponds to the loss of thermodynamic stability of aqueous solutions of the C_{60} adduct with L-arginine. The latter fact is associated with the complex and hierarchical type of adduct association in solution, namely the formation of second-order associates with linear dimensions of thousands of nm (see section 3.3.4.).

Similar results were obtained using another mixed derivative of the Gibbs potential:

$$\frac{\partial^2\overline{G}}{\partial P\partial x} = \frac{\partial^2\overline{G}}{\partial x\partial P} = \left(\frac{\partial\overline{V}}{\partial x}\right)_{T,P} = \left(\frac{\partial\mu_{\text{C}_{60}\text{-L-arginine}}}{\partial P}\right)_T - \left(\frac{\partial\mu_{H_2O}}{\partial P}\right)_T = V_{\text{C}_{60}\text{-L-arginine}} - V_{H_2O}, \quad (16)$$

where μ_i, V_i are chemical potential and partial molar volume of the *i*-component.

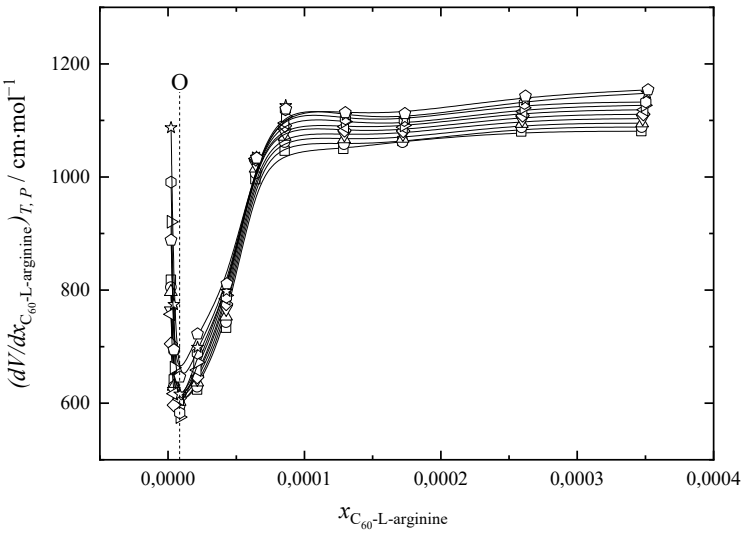

Fig. 64. Concentration dependence of the derivative $\frac{\partial V}{\partial x_{C_{60}\text{-L-arginine}}}$ at (□) 278.15 K; (○) 283.15 K; (△) 288.15 K; (▽) 293.15 K; (◇) 298.15 K; (◁) 303.15 K; (▷) 308.15 K; (⬡) 313.15 K; (☆) 318.15 K; (⬠) 323.15 K. *O* is an extremum point ($\left(\frac{\partial^2 V}{\partial x \partial T}\right)_P = 0, x = 5 \cdot 10^{-6}$).

As can be seen from Fig. 64 the dependence $\left(\partial \overline{V} / \partial x\right)_{P,T} (x_{C_{60}\text{-L-arginine}})$ also passes through a minimum at $x_{C_{60}\text{-L-arginine}} \approx 5 \cdot 10^{-6}$.

Fig. 65 shows the calculated concentration and temperature dependences of the isobaric thermal expansion coefficient (α_P) of aqueous solutions of the C_{60} adduct with L-arginine in the temperature range T = 283.15–323.15 K:

$$\alpha_P = -\left(\frac{1}{\rho}\right)\left(\frac{\partial \rho}{\partial T}\right)_P, \quad (17)$$

where ρ are densities of aqueous solutions of the C_{60} adduct with L-arginine and T is absolute temperature.

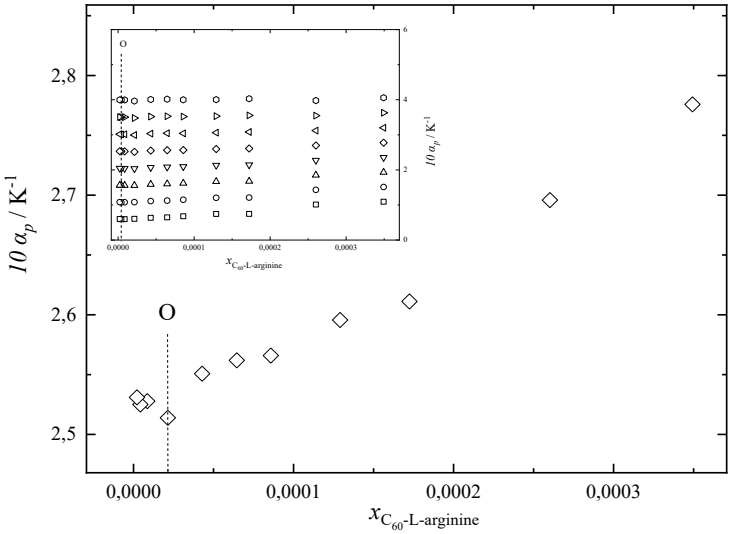

Fig. 65. Concentration dependence of the coefficient of isobaric thermal expansion (α_P) of the binary system C_{60}-L-arginine–H_2O at (□) 278.15 K; (○) 283.15 K; (△) 288.15 K; (▽) 293.15 K; (◇) 298.15 K; (◁) 303.15 K; (▷) 308.15 K; (⬡) 313.15 K; (☆) 318.15 K; (⬠) 323.15 K; *x* is mole fraction; *O* is the extremum point.

It can be seen that in the temperature range T = 283.15–318.15 K the coefficients of isobaric thermal expansion have a similar concentration dependence as the mixed derivatives of the Gibbs energy $\left(\partial \overline{V} / \partial T\right)_{P,X}$ and $\left(\partial \overline{V} / \partial x\right)_{P,T}$.

3.3.2. Temperature dependence of the viscosity of aqueous adduct solutions

The concentration dependences of the dynamic viscosity $\eta(C)$ of aqueous solutions of the C_{60} adduct with L-arginine are presented in Table 7 and Fig. 66.

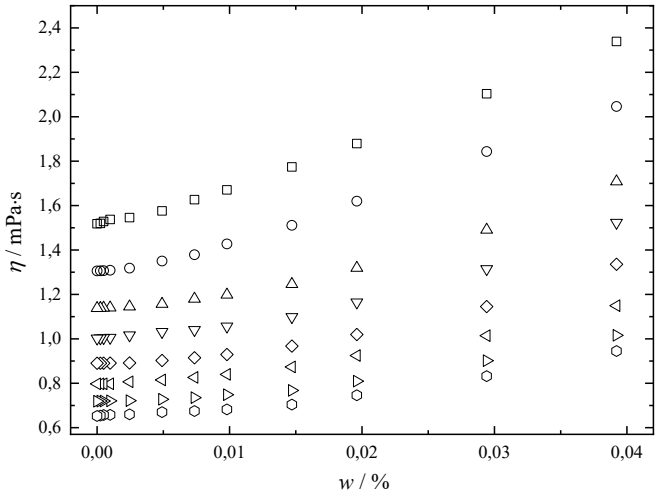

Fig. 66. Concentration dependence of viscosities of aqueous solutions of the C_{60}-L-arginine adduct at (□) 278.15 K; (○) 283.15 K; (△) 288.15 K; (▽) 293.15 K; (◇) 298.15 K; (◁) 303.15 K; (▷) 308.15 K; (⬡) 313.15 K. *w* is the mass fraction of the C_{60} adduct with L-arginine.

From Fig. 66, it can be seen that with increasing concentration of the adduct, the viscosity increases, with the maximum increase (22 % compared to water) observed at T = 283.15 K at C = 40 g·dm^{-3}.

Thermodynamic parameters of flow viscosity were calculated using the Eyring equation:

$$\eta = \frac{hN_A}{V} \exp\left(\frac{\Delta G}{RT}\right)_P, \tag{18}$$

where η is dynamic viscosity, V is molar volume, h is Plank's constant, N_A is Avogadro's number.

Table 7. Temperature and concentration dependences of viscosity (η) of aqueous solutions of the C_{60} adduct with L-arginine. C is volume concentration.

C / g·dm^{-3}	η / mPa·s									
	278.15 K	283.15 K	278.15 K	293.15 K	278.15 K	303.15 K	278.15 K	313.15 K	278.15 K	323.15 K
0.25	1.525	1.312	1.143	1.006	0.895	0.802	0.725	0.659	0.604	0.556
0.5	1.529	1.316	1.146	1.010	0.897	0.805	0.727	0.661	0.606	0.558
1	1.539	1.324	1.154	1.017	0.904	0.810	0.732	0.666	0.609	0.561
2.5	1.560	1.343	1.170	1.031	0.917	0.822	0.743	0.676	0.618	0.569
5	1.610	1.386	1.208	1.063	0.946	0.850	0.767	0.697	0.635	0.582
7.5	1.628	1.402	1.221	1.077	0.957	0.858	0.775	0.705	0.646	0.594
10	1.651	1.423	1.238	1.090	0.969	0.869	0.785	0.713	0.653	0.599
15	1.748	1.504	1.313	1.158	1.031	0.923	0.833	0.759	0.692	0.634
20	1.822	1.570	1.369	1.205	1.072	0.960	0.867	0.787	0.718	0.657
30	2.032	1.753	1.527	1.345	1.199	1.076	0.972	0.882	0.808	0.741
40	2.274	1.902	1.653	1.456	1.292	1.157	1.043	0.947	0.865	0.791

ΔH and ΔS provide structural information about the interaction between solute and solvent. Analysis of Table 8 indicates the stability of the values of ΔH and ΔS of viscous flow over the entire concentration range (C = 0.25–40 g·dm^{-3}) taking into account the accuracy of numerical differentiation [123].

Positive ΔH values indicate the presence of specific interactions between the adduct and solvent molecules, negative ΔS values indicate that the formation of an activated complex leads to molecular ordering in solution. Using the logarithmic form of the Frenkel–Andrade equation, the activation energy of viscous flow and the pre-exponential factor were calculated (Table 8):

$$\ln \eta = \ln A_S + \frac{E_a}{R}\frac{1}{T}, \tag{19}$$

where A_S is the pre-exponential factor, E_a is the activation energy of viscous flow, R is the universal gas constant, T is the absolute temperature.

Viscous flow activation temperatures were determined according to equation 20 (Table 8):

$$T_A = \frac{-E_a}{R \ln A_S}, \tag{20}$$

Additionally, van't Hoff coefficients for the viscosity (γ_n) of the binary system C_{60}-L-arginine–H_2O were calculated in accordance with equation 21:

$$\gamma_n^{\frac{\Delta T}{10}} = \frac{\eta_{T-\Delta T}}{\eta_T} = \frac{\eta_{T-10}}{\eta_T} = 1.22 \pm 0.03, \tag{21}$$

where γ_n is the van't Hoff coefficient (Fig. 67).

Table 8. Concentration dependences of the thermodynamic characteristics of viscous flow: activation energy (E_a), logarithm of the pre-exponential factor ($\ln A_S$), activation temperature of viscous flow (T_A), change in enthalpy (ΔH) and entropy (ΔS). C is the volume concentration.

C / g·dm^{-3}	E_a / J·mol^{-1}	$\ln A_S$ / mPa·s	T_A / K	ΔH / kJ·mol^{-1}	ΔS / J·mol^{-1}·K^{-1}
0.25	16588.70	−6.4236	310.61	16.34	−94.17
0.5	16660.01	−6.5227	307.21	16.44	−93.18
1	16835.63	−6.7060	301.96	16.62	−91.60
2.5	16732.98	−6.7044	300.19	16.47	−91.13
5	16760.54	−6.7744	297.58	16.53	−90.69
7.5	16678.75	−6.7538	297.03	16.52	−90.66
10	16776.16	−6.8055	296.50	16.57	−90.69
15	16687.06	−6.8004	295.15	16.48	−90.71
20	16690.47	−6.8157	294.54	16.49	−90.58
30	16686.59	−6.8210	294.25	16.48	−90.54
40	16697.48	−6.8283	294.12	16.50	−90.47

From Fig. 67, it is clear that there is a high stability of van't Hoff coefficients.

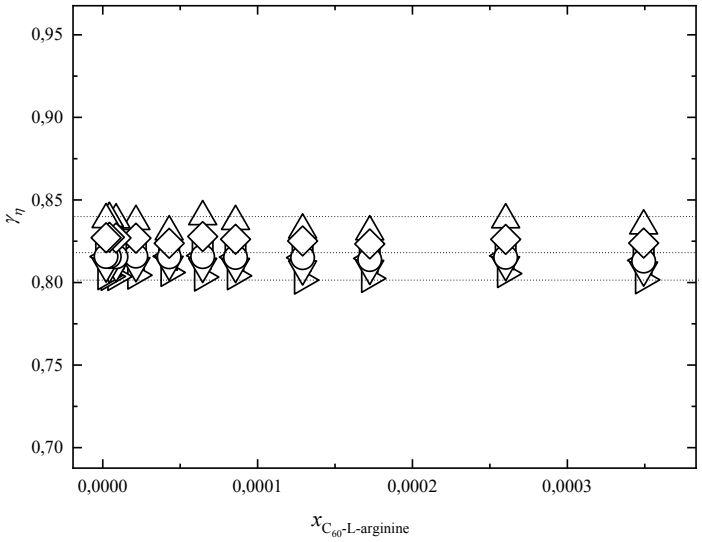

Fig. 67. Concentration dependences of Van't Hoff coefficients for viscosity (γ_n = 1.22 ± 0.03) of a binary system C_{60}-L-arginine–H_2O. (□) $\left(\frac{\eta_{298,15}}{\eta_{313,15}}\right)^{\frac{10}{\Delta T}}$, (○) $\left(\frac{\eta_{293,15}}{\eta_{308,15}}\right)^{\frac{10}{\Delta T}}$, (△)$\left(\frac{\eta_{288,15}}{\eta_{303,15}}\right)^{\frac{10}{\Delta T}}$; (▽) $\left(\frac{\eta_{303,15}}{\eta_{313,15}}\right)^{\frac{10}{\Delta T}}$; (◁)$\left(\frac{\eta_{298,15}}{\eta_{308,15}}\right)^{\frac{10}{\Delta T}}$; (▷)$\left(\frac{\eta_{293,15}}{\eta_{303,15}}\right)^{\frac{10}{\Delta T}}$. x is the mole fraction of the C_{60} adduct with L-arginine.

Fig. 68 shows the temperature dependences of the dynamic viscosities of the binary system C_{60}-L-arginine–H_2O. The obtained dependencies were described using the three-parameter Vogel–Fulcher–Tammann equation (VFT):

$$\lg \eta(T) = \lg \eta_0 + \frac{A}{T - B}, \tag{22}$$

where η_0, A and B are correlation parameters.

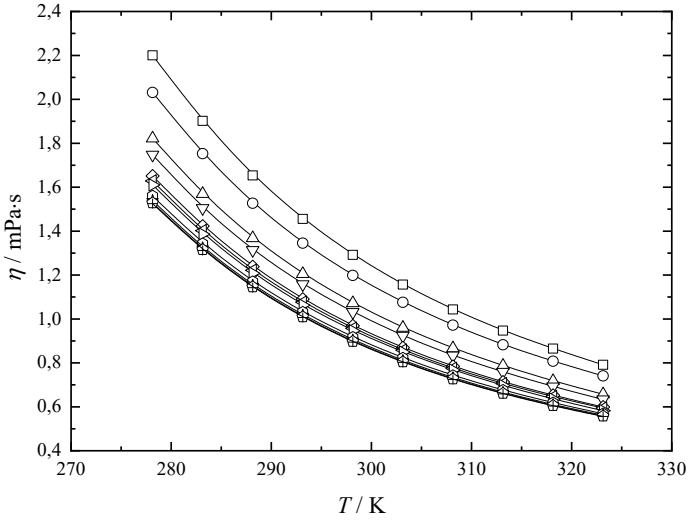

Fig. 68. Temperature dependences of the dynamic viscosity of aqueous solutions containing the adduct of fullerene C_{60} with L-arginine: dots are experimental values, solid lines are results of approximation using the VFT equation (equation 22): (□) 40 g·dm^{-3}; (○) 30 g·dm^{-3}; (△) 20 g·dm^{-3}; (▽) 15 g·dm^{-3}; (◇) 10 g·dm^{-3}; (◁) 7.5 g·dm^{-3}; (▷) 5 g·dm^{-3}; (⬡) 2.5 g·dm^{-3}; (☆) 0.5 g·dm^{-3}; (⬠) 0.25 g·dm^{-3}; (+) water.

The absolute average deviation (*AAD*) and standard deviation (*SD*) between the experimental and calculated values were determined from equations 23 and 24:

$$AAD = \left[\sum_{i=1}^{n} \left(\frac{\eta_{\exp,i} - \eta_{cal,i}}{\eta_{\exp,i}} \right) \right] \cdot \frac{100}{n}, \tag{23}$$

$$SD = \left[\frac{\sum_{i=1}^{n} \left(\eta_{\exp,i} - \eta_{cal,i} \right)^2}{(n-p)} \right]^{\frac{1}{2}}, \tag{24}$$

where $\eta_{exp,i}$ and $\eta_{cal,i}$ are experimental and calculated values of dynamic viscosities of aqueous adduct C_{60} with L-arginine solutions; n is number of measurements, p is the number of specified parameters. The values of the parameters of the VFT equation, as well as the *SD* and *AAD* values, are presented in Table 9.

Table 9. Correlation parameters of the VFT equation. *C* is the concentration of the C_{60} adduct with L-arginine in an aqueous solution, *SD* is the standard deviation, *AAD* is the absolute average deviation.

	$C_{C_{60}\text{-L-arginine}}$ / g·dm^{-3}											
	0	0.25	0.5	1	2.5	5	7.5	10	15	20	30	40
A / K	332.57	332.57	332.57	332.68	332.76	333.02	333.52	333.90	334.58	334.74	335.12	335.21
B / K	116.51	116.51	116.51	116.94	117.21	118.18	120.07	121.57	124.23	124.90	126.44	126.70
η_0 / mPa·s	0.0132	0.0132	0.0132	0.0131	0.0131	0.0129	0.0124	0.0121	0.0117	0.0121	0.0130	0.0144
SD / mPa·s	0.003	0.003	0.004	0.004	0.004	0.006	0.006	0.008	0.010	0.011	0.011	0.008
AAD / %	0.42	0.46	0.60	0.72	0.66	0.81	0.98	1.25	1.58	1.80	1.58	1.37

3.3.3. Refraction of aqueous adduct solutions

Experimental values of refractive indices (n_D) of aqueous solutions of C_{60} with L-arginine adduct in the temperature range T = 283.15–323.15 K are presented in Table 10.

The concentration dependences of the specific and molar refractions of aqueous solutions of the C_{60} adduct with L-arginine were calculated using the Lorentz–Lorenz equation:

$$r = \left(\frac{n_D^{T\,2} - 1}{n_D^{T\,2} + 2} \right) \cdot \frac{1}{\rho}, \tag{25}$$

$$R = \left(\frac{n_D^{T\,2} - 1}{n_D^{T\,2} + 2} \right) \cdot \frac{\overline{M}}{\rho}, \tag{26}$$

where r, R are specific and molar refraction, $\overline{M}$ is average molecular weight of the solution: $\overline{M} = x_{H_2O} \cdot M_{H_2O} + x_{\text{C}_{60}\text{-L-arginine}} \cdot M_{\text{C}_{60}\text{-L-arginine}}$. Table 11 shows the obtained specific and molar refractions of the studied aqueous solutions of the C_{60} adduct with L-arginine.

Table 10. Concentration dependences of the refractive index (n_D) of aqueous solutions of the C_{60} adduct with L-arginine in the temperature range T = 278.15–323.15 K.

C / g·dm^{-3}	n_D								
	283.15	288.15	293.15	298.15	303.15	308.15	313.15	318.15	323.15
0.06	1.33374	1.33345	1.33305	1.33256	1.33200	1.33137	1.33067	1.32992	1.32909
0.13	1.33381	1.33351	1.33311	1.33262	1.33207	1.33144	1.33074	1.32998	1.32916
0.25	1.33397	1.33368	1.33328	1.33278	1.33224	1.33161	1.33092	1.33014	1.32933
0.5	1.33438	1.33410	1.33371	1.33320	1.33269	1.33199	1.33130	1.33054	1.32971
1	1.33515	1.33489	1.33450	1.33397	1.33351	1.33275	1.33206	1.33129	1.33043
2.5	1.33573	1.33551	1.33512	1.33460	1.33416	1.33337	1.33269	1.33192	1.33106
5	1.33625	1.33607	1.33569	1.33519	1.33475	1.33395	1.33327	1.33251	1.33163
10	1.33732	1.33716	1.33682	1.33635	1.33591	1.33509	1.33443	1.33366	1.33278
15	1.33841	1.33824	1.33795	1.33754	1.33706	1.33629	1.33564	1.33487	1.33401
20	1.34052	1.34031	1.34007	1.33983	1.33927	1.33858	1.33794	1.33718	1.33636
30	1.34327	1.34292	1.34248	1.34197	1.34139	1.34074	1.34001	1.33921	1.33838

Table 11. Refractive properties of aqueous solutions of the C_{60} adduct with L-arginine at 298.15 K. C is the volume concentration, n_D is the refractive index, r and R are the specific and molar refractions of aqueous solutions of the C_{60} adduct with L-arginine, $r_{C_{60}\text{-L-arginine}}$ and $R_{C_{60}\text{-L-arginine}}$ are specific and molar refractions of the C_{60} adduct with L-arginine.

C / g·dm^{-3}	n_D	r / cm^3·g^{-1}	R / cm^3·mol^{-1}	$r_{C_{60}\text{-L-arginine}}$ / cm^3·g^{-1}	$R_{C_{60}\text{-L-arginine}}$ / cm^3·mol^{-1}
0.25	1.33257	0.20603	3.70944	0.246	519
0.5	1.33264	0.20604	3.71051	0.243	513
1	1.33281	0.20606	3.71272	0.244	516
2.5	1.33328	0.20612	3.71935	0.245	518
5	1.33412	0.20622	3.73039	0.246	519
7.5	1.33478	0.20632	3.74152	0.246	519
10	1.33539	0.20641	3.75235	0.245	518
15	1.33659	0.20659	3.77432	0.244	516
20	1.33777	0.20675	3.79596	0.243	513
30	1.34006	0.20705	3.83951	0.241	509
40	1.34238	0.20737	3.88408	0.240	508

The values of the molar ($R_{C_{60}\text{-L-arginine}}$) and specific ($r_{C_{60}\text{-L-arginine}}$) refractions of the C_{60} adduct with L-arginine (Table 11) were calculated in accordance with the refraction additivity rule (equations 27 and 28):

$$r = \left(r_{H_2O} \cdot w_{H_2O} + r_{C_{60}\text{-L-arginine}} \cdot w_{C_{60}\text{-L-arginine}}\right) \cdot \frac{1}{100}, \quad (27)$$

$$R = \left(R_{H_2O} \cdot x_{H_2O} + R_{C_{60}\text{-L-arginine}} \cdot x_{C_{60}\text{-L-arginine}}\right), \quad (28)$$

where r_i, R_i and specific and molar refractions of the i-component, w_i, x_i are mass and mole fractions of the i-component.

Fig. 69 shows the specific and molar refractions of the C_{60} adduct with L-arginine in aqueous solutions at T = 298.15 K, calculated using the refraction additivity rule.

(*a*)

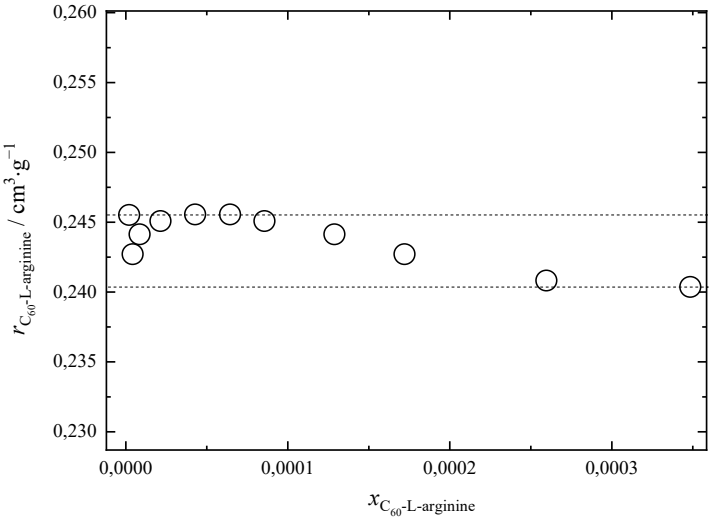

(*b*)

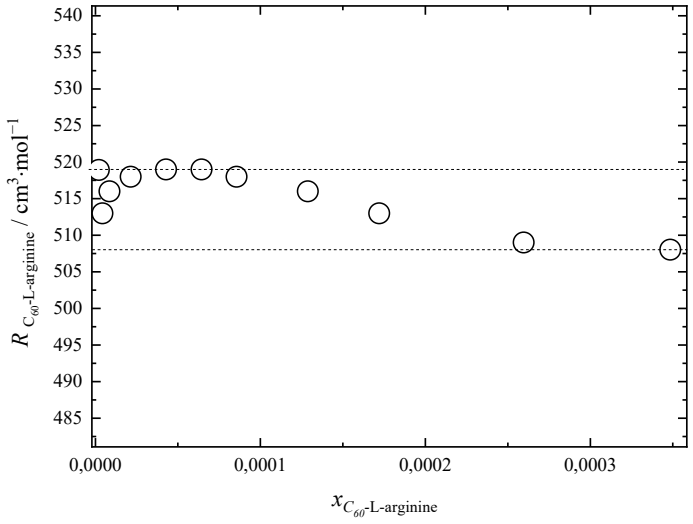

Fig. 69. Concentration dependences of specific (*a*) and molar (*b*) refraction of C_{60}-L-arginine in an aqueous solution at 298.15 K; *x* is the mole fraction.

In addition, using the Eisenlohr additivity rule, based on data on atomic refractions and increments of chemical bonds, the value of the molar refraction of the C_{60} adduct with L-arginine was calculated:

$$R^{add} = 60\,R_c + 8\cdot(3R_c + 3R_{CH_2} + 8R_H + 2R_{N(=NH_2)} + 2R_{N(NH)} + R_{O(C=O)} + R_{O(-OH)}) \approx 512 \pm 7 \text{ cm}^3 \cdot \text{mol}^{-1} \quad (29)$$

It has been established that the discrepancy in the calculation of molar refraction is associated with the choice of spectral lines (H_a [λ = 658.3 nm]) and H_γ [λ = 436.1 nm]). The specific refraction value of the C_{60} adduct with L-arginine was calculated according to equation 30:

$$r^{add} = \frac{R^{add}}{M(C_{60}\text{-L-arginine})} \approx 0.242 \pm 0.03\ \text{m}^3 \cdot \text{g}^{-1}. \quad (30)$$

The specific and molar refraction values of the C_{60} fullerene adduct with L-arginine, calculated using the Eisenlohr additivity rule, are in good agreement with the data calculated from the refractive indices of solutions.

3.3.4. Particle sizes in aqueous solution and ζ-potentials

Table 12 and Fig. 70 shows the concentration dependence of the size distribution of associates of the C_{60} adduct with L-arginine in aqueous solutions in the concentration range C = 0.001–10 g·dm^{-3} at T = 298.15 K.

Table 12. Size distribution of associates of the C_{60} adduct with L-arginine in aqueous solutions at 298.15 K. δ_0, δ_I, δ_{II}, δ_{III} are the average diameters of the monomer molecule and associates of the first, second and third orders; $N_{0\to1}$, $N_{0\to2}$, $N_{0\to3}$ are the average numbers of monomeric molecules of the C_{60} adduct with L-arginine in first, second and third order associates, ζ_I, ζ_{II}, ζ_{III} are the zeta potentials of first, second and third order associates.

C / g·dm^{-3}	δ_0 / nm	δ_I / nm	δ_{II} / nm	δ_{III} / μm	$N_{0\to1}\cdot10^{-4}$	$N_{0\to2}\cdot10^{-5}$	$N_{0\to2}\cdot10^{-9}$	ζ_I / mV	ζ_{II} / mV	ζ_{III} / mV
0.001	—	50–70	200–300	—	0.8–2	3–7	—	−30	−40	—
0.01	—	50–70	200–300	—	0.8–2	3–7	—	−30	−40	—
0.1	—	—	200–300	—	—	3–7	—	−30	−40	—
0.2	—	—	200–300	—	—	3–7	—	—	−40	—
0.3	—	—	200–300	5–6	—	3–7	2–4	—	−40	—
0.4	—	—	200–300	5–6	—	3–7	2–4	—	−40	—
0.5	—	—	200–300	5–6	—	3–7	2–4	—	−40	—
1.0	—	—	200–300	5–6	—	3–7	2–4	—	−40	—
3.0	—	—	200–300	5–6	—	3–7	2–4	—	−40	—
5.0	—	—	200–300	5–6	—	3–7	2–4	—	−40	−60
7.0	—	—	200–300	5–6	—	3–7	2–4	—	−40	−60
10.0	—	—	200–300	5–6	—	3–7	2–4	—	−40	−60

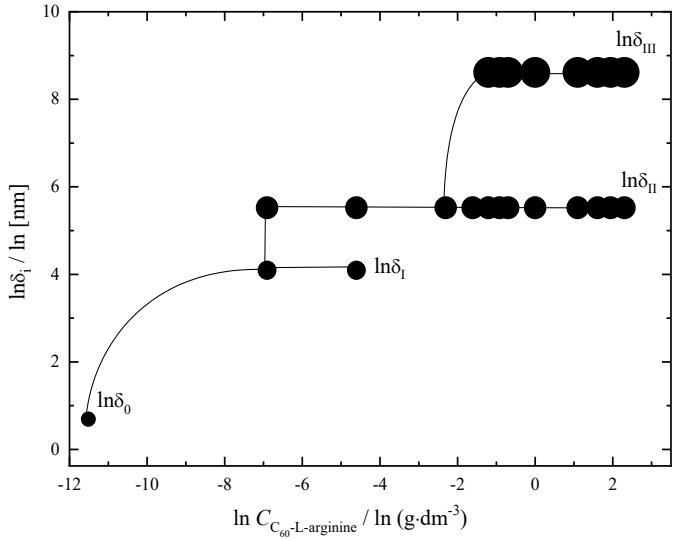

Fig. 70. Concentration dependence of the size distribution of associates of the C_{60} adduct with L-arginine in aqueous solutions at 298.15 K; $C_{C_{60}\text{-L-arginine}}$ is volume concentration of the adduct of C_{60} with L-arginine.

Analysis of Table 12 and Fig. 70 shows the following:

(*1*) monomeric molecules of the C_{60} adduct with L-arginine with linear dimensions of ~2 nm were not detected in the concentration range C = 0.001–10 g·dm^{-3};

(*2*) in the concentration range C = 0.001–0.1 g·dm^{-3}, the simultaneous presence of first- and second-order associates with linear sizes of 50–70 nm and 200–300 nm, respectively, is observed. It should be noted that the formation of second-order associates causes the loss of thermodynamic stability of the solution [124];

(3) in the concentration range C = 0.1–0.2 g·dm^{-3}, only second-order clusters with linear sizes of 200–300 nm are present in the solution;

(4) in the concentration range C = 0.3–10 g·dm^{-3}, associates of the second and third orders with sizes of 200–300 nm and 5–6 μm, respectively, are simultaneously present in the solution;

(5) using equation 31, the average number of monomer molecules in clusters of the first ($N_{0\to1}$), second ($N_{0\to2}$) and third order ($N_{0\to3}$) was calculated (see Table 12):

$$N_{0\to i} = \left(\frac{d_i}{d_0}\right)^3 \cdot K_{\text{pack}}, \qquad (31)$$

where K_{pack} is a formal packing factor corresponding to the packing of 'small spheres' into a 'large sphere'. Due to the relatively large size and the presence of charge on amino acid residues, a packing factor corresponding to a primitive cubic cell was chosen (K_{pack} = 0.52).

In addition, using the Helmholtz–Smoluchowski equation, the values of ζ-potentials were estimated based on the experimental values of electrophoretic mobility (see Table 12 and Fig. 71).

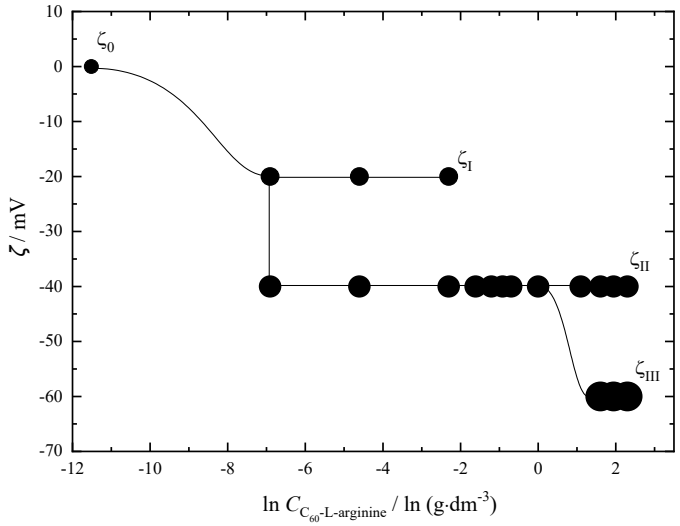

Fig. 71. Concentration dependences of the ζ-potentials of associates of the C_{60} adduct with L-arginine of the first, second and third orders in aqueous solutions at 298.15 K; $C_{C_{60}\text{-L-arginine}}$ is a volume concentration.

Analysis of the concentration dependence of ζ-potentials (see Table 12 and Fig. 71) shows the following:

(*1*) in the concentration range C = 0.001–10 g·dm^{-3}, the values of ζ-potentials are negative and equal to −(60–20) mV;

(*2*) over the entire concentration range, solutions of the C_{60} adduct with L-arginine are electrokinetically stable;

(*3*) in the concentration range C = 0.001–0.1 g·dm^{-3}, the ζ-potential distribution includes two peaks corresponding to first- and second-order associates. In the concentration range C = 0.2–5 g·dm^{-3}, the distribution of ζ-potentials includes one peak corresponding to second-order associates. In turn, in the concentration range C = 5–10

g·dm^{-3}, two peaks corresponding to second- and third-order associates are clearly visible in the ζ-potential distribution (see Table 12).

(*4*) comparison of experimental data presented in Figs. 69 and 70, shows a discrepancy in the size of associates in the concentration range C = 0.1–3 g·dm^{-3} (see Table 12). Most likely, this is due to the fact that, under the influence of an electric potential, charged particles of the C_{60} adduct with L-arginine can associate or dissociate depending on the ratio of surface charges and the degree of hydration of the clusters.

3.3.5. Solubility

Fig. 72 shows the temperature dependence of solubility in the binary system C_{60} adduct with L-arginine–water in the temperature range 293.15–333.15 K.

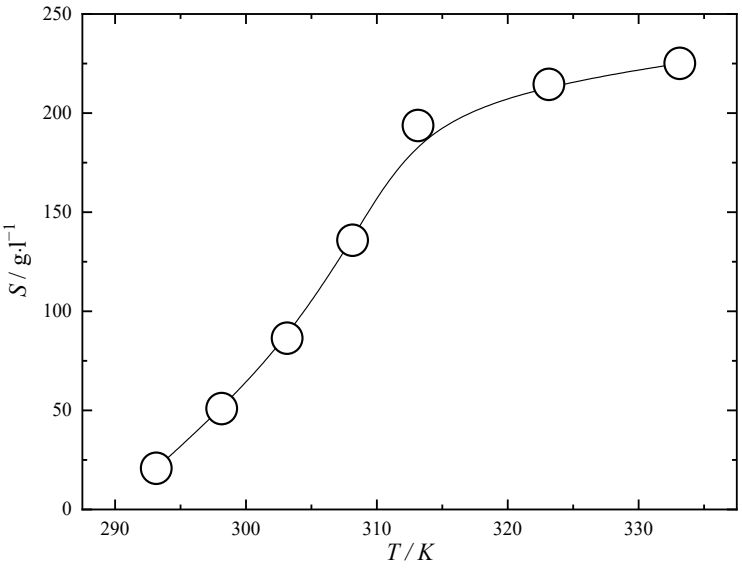

Fig. 72. Temperature dependence of the solubility of the C_{60} adduct with L-arginine in water in the temperature range 293.15–333.15 K.

From the presented data it is clearly seen that the solubility of the adduct ranges from tens to hundreds of grams per liter (depending on temperature), such solubility values are in good agreement with experimental data obtained for such well-known water-soluble adducts as fullerenols [94], carboxylated fullerenes [95]. The solubility diagram has a sigmoidal character. This type of dependence is common for systems containing fullerenes and their derivatives [95].

3.3.6. Description of *T–x* dependences of physical properties

The temperature and concentration dependences of the physicochemical properties of solutions (*M*) of the C_{60} adduct with L-arginine (density, viscosity and refractive indices) are described using a second-order polynomial, *M* (*T*, *x*) (Fig. 73):

$$M = A + \sqrt{x}\sum_{i=1}^{3} b_i \cdot T^{i-1} + \sqrt{1-x}\sum_{i=4}^{6} b_i \cdot T^{i-4}, \quad (32)$$

where *x* is mole fraction of the adduct of C_{60} with L-arginine, *T* is the absolute temperature, *A*, b_i (i = 1–6) are correlation parameters calculated by the least squares method using Origin 9 software.

The agreement between the experimental and calculated values of the physicochemical properties of aqueous solutions of the C_{60} adduct with L-arginine was assessed by calculating the standard deviation (*SD*) and the coefficient of determination (R^2) according to equations 33, 34:

$$SD = \left[\frac{\sum_{i=1}^{n} \left(x_{\exp,i} - x_{cal,i} \right)^2}{n} \right]^{1/2}, \quad (33)$$

$$R^2 = \frac{\sum_{i=1}^{n} \left(x_{cal,i} - \frac{1}{n}\sum_{i=1}^{n} x_{\exp,i} \right)^2}{\sum_{i=1}^{n} \left(x_{\exp,i} - \frac{1}{n}\sum_{i=1}^{n} x_{\exp,i} \right)^2}, \quad (34)$$

where $x_{cal,i}$ and $x_{exp,i}$ are calculated and experimental values, *n* is the number of measurements. Tables 13 and 14 summarise the correlation parameters, as well as the R^2 and *SD* values for the *T–x* dependences of density, viscosity and refractive index.

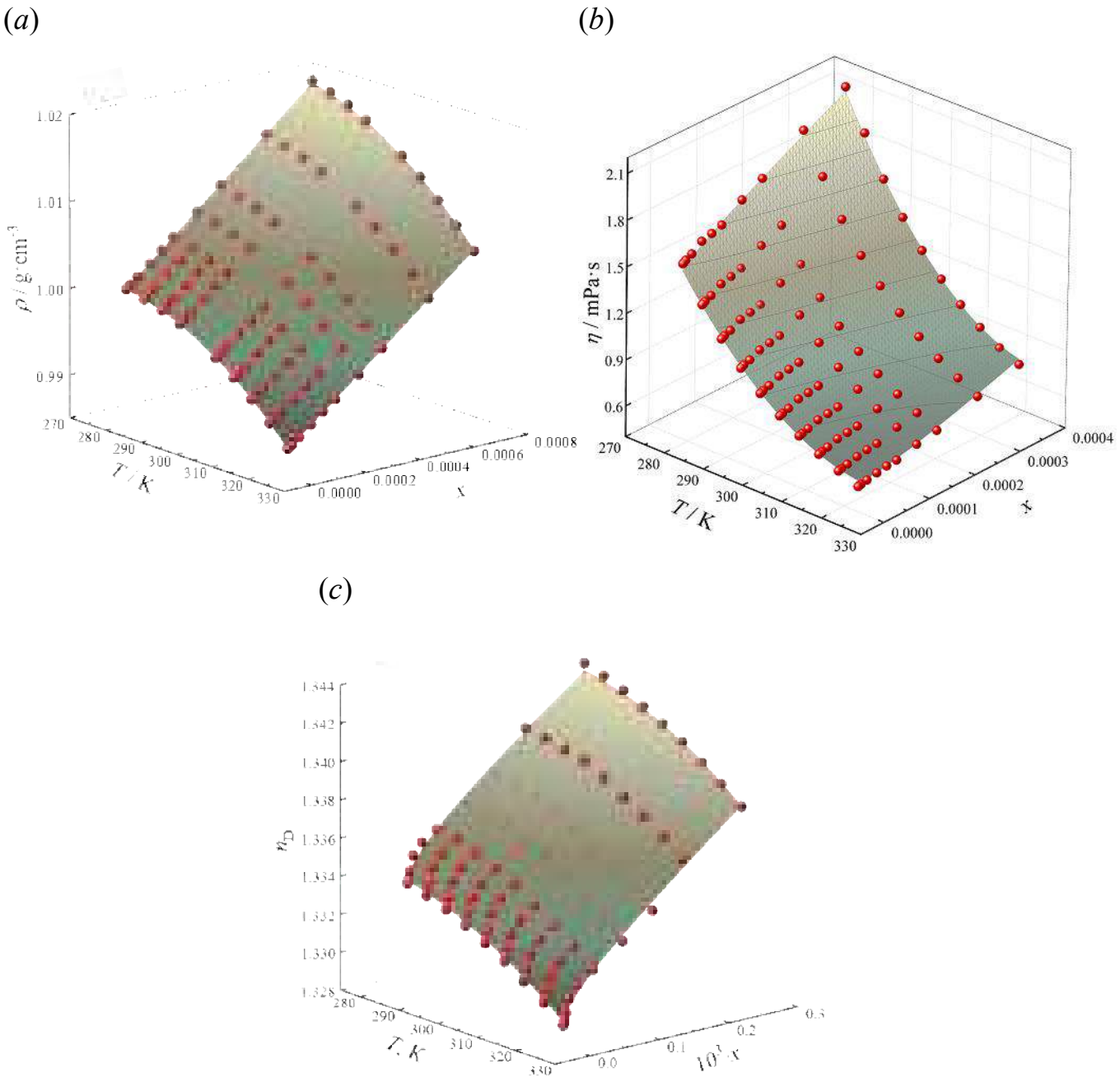

Fig. 73. Temperature and concentration dependence of density (*a*), viscosity (*b*) and refractive index (*c*) of aqueous solutions of the C_{60} adduct with L-arginine; ρ is the density of the solution, η is the dynamic viscosity, n_D is the refractive index, T is the absolute temperature, x is the mole fraction. Experimental data are represented by red spheres, surfaces are data calculated using equation 32.

Table 13. Correlation parameters A, b_i (i = 1–6) polynomial equation 32 to describe the temperature and concentration dependences of density (ρ), dynamic viscosity (η) and refractive indices (n_D) of aqueous solutions of the C_{60} adduct with L-arginine. R^2 is the coefficient of determination (equation 34).

Property of the solution	A	b_1	b_2	b_3	b_4	b_5	b_6	R^2
ρ / g·cm^{-3}	101.681	1.574	$-8.57\cdot10^{-3}$	$1.16\cdot10^{-3}$	−101.017	$2.48\cdot10^{-3}$	$-4.57\cdot10^{-6}$	0.9998
η / mPa·s	2654.894	828.853	−5.052	$7.58\cdot10^{-3}$	−2616.051	−0.2338	$3.57\cdot10^{-4}$	0.9968
n_D	48.637	2.998	−0.0203	$3.46\cdot10^{-5}$	−47.412	$8.26\cdot10^{-4}$	$-1.56\cdot10^{-6}$	0.9996

Table 14. Standard deviations (*SD*) for the calculated values of density (ρ), dynamic viscosity (η), and refractive index (n_D) of aqueous solutions of the C_{60} adduct with L-arginine (equation 33).

T / K	*SD*		
	ρ / g·cm^{-3}	η / mPa·s	n_D
278.15	0.00009	0.0033	—
283.15	0.00008	0.0022	0.00005
288.15	0.00005	0.0024	0.00004
293.15	0.00006	0.0018	0.00005
298.15	0.00004	0.0008	0.00004
303.15	0.00004	0.0012	0.00004
308.15	0.00006	0.0019	0.00004
313.15	0.00008	0.002	0.00004
318.15	0.00009	0.0015	0.00004
323.15	0.00011	0.0025	0.00007

3.4. Biocompatibility and biological activity of the adduct of light fullerene C_{60} with L-arginine

3.4.1. Cytotoxicity

The cytotoxicity of the adduct was studied using the MTT reagent (3-(4,5-dimethylthiazol-2-yl)-2,5-diphenyltetrazolium bromide) on the HEK293 cell line (human embryonic kidney cells). As a result of the interaction of the MTT reagent with NAD(P)H-dependent cellular oxidoreductases, a coloured product is formed — formazan, with an absorption maximum at a wavelength of 540 nm, the content of which is proportional to the number of viable cells (Fig. 74).

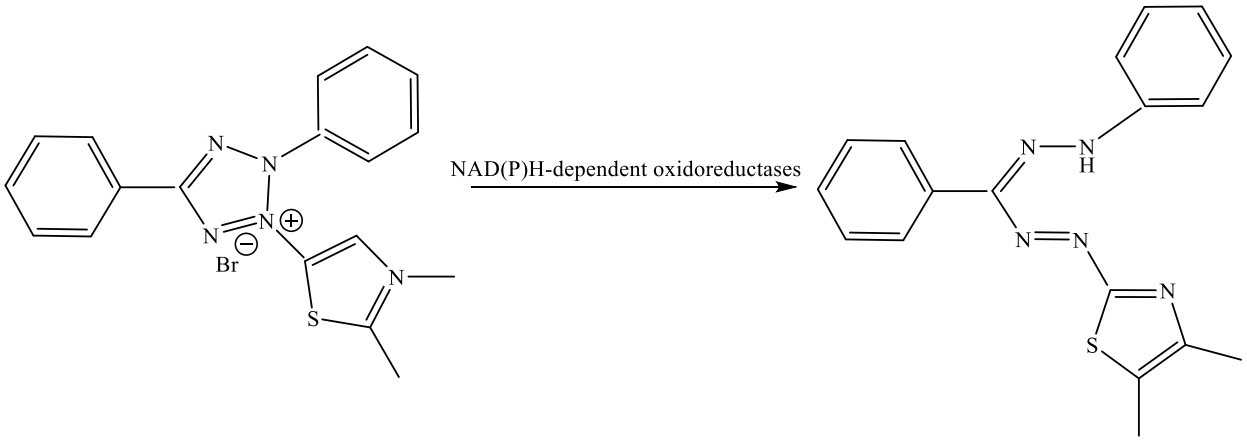

Fig. 74. Scheme of the reduction reaction of the tetrazolium dye MTT.

It was found that the adduct of C_{60} with L-arginine in a concentration range of 1–200 μM did not cause a decrease in cell viability and did not have a toxic effect on HEK293 cells (Fig. 75).

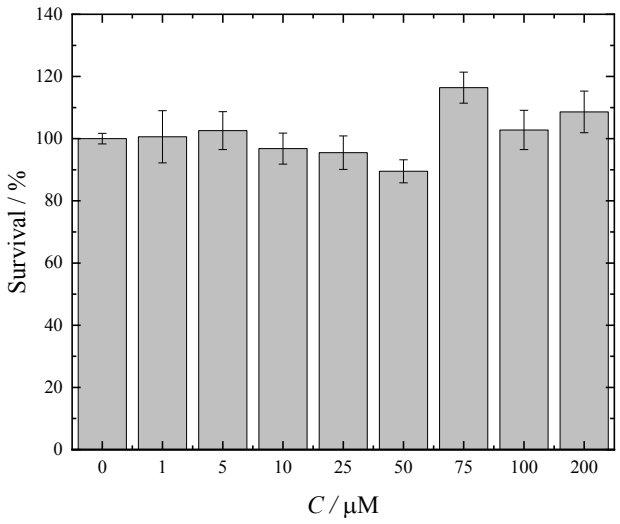

Fig. 75. Dependence of the viability of the cell line (HEK293) on the concentration of the C_{60} adduct with L-arginine. *C* is the molar concentration of the adduct.

3.4.2. Genotoxicity

The DNA-damaging effect of the C_{60} adduct with L-arginine was studied in human peripheral blood monocyte cells. The average values of DNA content in comet tails (%), tail length and tail moment of comets are presented in Table 15.

Table 15. Concentration dependence of the genotoxicity of the C_{60} adduct with L-arginine.

Characteristic being studied	Control (phosphate buffer)	Amplitude / %				
		$C(H_2O_2)$ / μM	$C(C_{60}$-L-arginine) / μM			
		100.0	10.0	50.0	75.0	100.0
% Tail DNA	3.3 ± 0.4	89.1 ± 6.7*	3.4 ± 0.3	4.7 ± 1.4	2.5 ± 0.5	5.6 ± 1.2
Tail length / μM	14.0 ± 3.0	492.8 ± 20.6*	9.5 ± 2.3	16.1 ± 3.2	11.0 ± 2.2	19.1 ± 2.9
Tail momentum	0.50 ± 0.01	43.1 ± 1.4*	0.30 ± 0.01	0.80 ± 0.04	0.30 ± 0.01	1.07± 0.03

*$p < 0.05$ compared to control.

It was found that the amount of DNA damage in human peripheral blood monocytes in the presence of H_2O_2 is significantly greater than in control cells incubated in phosphate buffer. The adduct of C_{60} with L-arginine in the concentration range of 10–100 μM did not have a genotoxic effect on the DNA of human peripheral blood monocytes. As an example, Fig. 76 shows photographs of DNA comets obtained by incubating cells in the presence of H_2O_2, phosphate buffer, and the C_{60} adduct with L-arginine.

(*a*) (*b*) (*c*)

Fig. 76. Comet DNA after electrophoresis in cell microgel: (*a*) — positive control (H_2O_2), (*b*) negative control (phosphate buffer), (*c*) — C_{60} adduct with L-arginine (*C* = 100 μM).

3.4.3. Binding to HSA

Fig. 77 shows the dependence of the thermal effect of the interaction of the adduct of fullerene C_{60} with L-arginine with HSA at 298.15 K depending on the volume of the titrant.

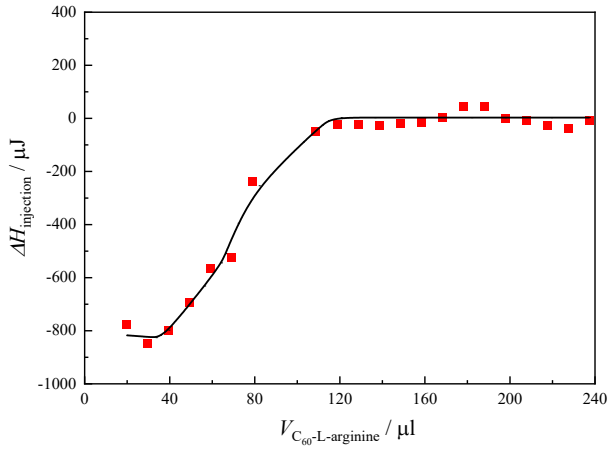

Fig. 77. Dependence of the thermal effect of the reaction of the interaction of the adduct of fullerene C_{60} with L-arginine with HSA at 298.15 K. ΔH is the thermal effect of the reaction, $V_{C_{60}\text{-L-arginine}}$ is the volume of the titrant.

Based on the experimental data obtained, the interaction parameters of the C_{60} fullerene adduct with L-arginine with HSA were calculated based on the thermodynamic model of independent binding [125]. The obtained value of the stoichiometry of the interaction shows that at the equivalence point there is 0.7 mol of titrant (adduct) per 1 mol of the titrated substance (HSA) (Table 16). This fact can be explained by the structural features of the protein under study, namely the inaccessibility of some binding sites due to the steric factor. The calculated binding constant of HSA to the adduct (K_a = $6.0 \cdot 10^5$ M^{-1}) is in the effective range of 10^4–10^5 mol·dm^{-3}, necessary for albumin to perform its transport function in the bloodstream. In turn, at lower values of the binding constant the complexes will not be strong enough, and at larger values, irreversible binding will occur and the adduct will not be released from the complex with HSA [126].

Table. 16. Thermodynamic characteristics of the interaction of the adduct C_{60} with L-arginine with HSA at 298.15 K. K_d is the dissociation constant, K_a is the binding constant, n is the stoichiometric coefficient, ΔH, ΔS, ΔG are the changes in enthalpy, entropy and Gibbs energy in the reaction of interaction of the adduct with HSA, T is absolute temperature.

K_d / M^{-1}	n	ΔH / kJ·mol^{-1}	ΔS / J·mol^{-1}·K^{-1}	ΔG / kJ·mol^{-1}	$-T\Delta S$ / kJ·mol^{-1}	K_a / M^{-1}
$1.7 \cdot 10^{-6}$	0.7 ± 0.07	-85.3 ± 8.5	-175 ± 17.5	-33.0 ± 3.3	-52.3 ± 5.2	$6.0 \cdot 10^{5}$

From the presented values of thermodynamic parameters (Table 16) it is clear that the interaction of the adduct with HSA is an exothermic process. Negative values of ΔH and ΔS are typical for the formation of hydrogen bonds, therefore, the binding of the adduct to HSA occurs due to the arginine residues of the fullerene adduct.

3.4.4. Antiradical activity

Fig. 78 shows the proposed reaction mechanism for the interaction of the C_{60} adduct with L-arginine with DPPH.

(*a*)

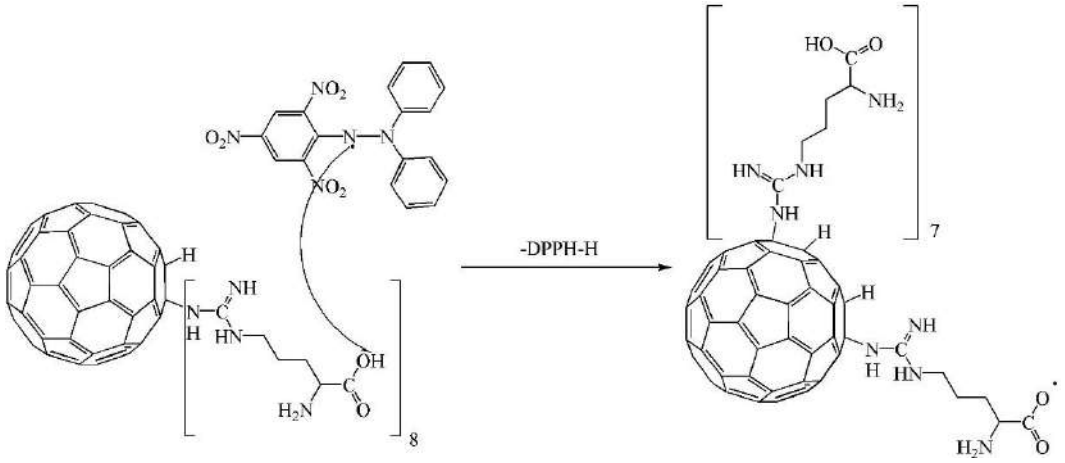

(*b*)

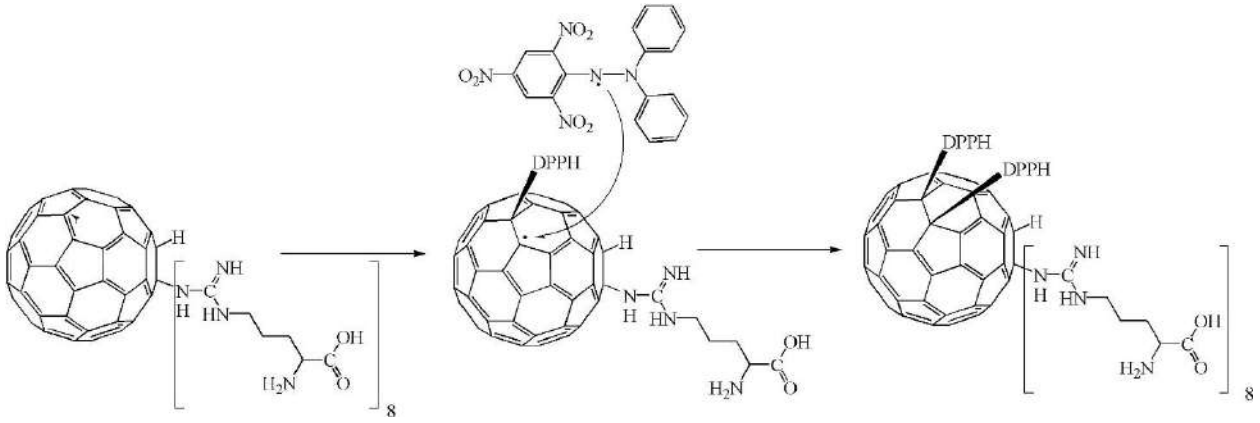

Fig. 78. The proposed mechanism of interaction of the C_{60} fullerene adduct with L-arginine with DPPH: (*a*) transfer of hydrogen to the DPPH radical (fast stage) and (*b*) nucleophilic attack of the C=C bond (slow stage).

A pseudo-first order model was used to quantify the reaction rate between the C_{60} adduct with L-arginine and DPPH [127]:

$$\ln\frac{A_\infty - A_t}{A_\infty - A_0} = -kt\,, \tag{35}$$

where A_∞, A_t and A_0 are optical densities of the solution after 'infinity' (six days after the start of the experiment), at time t and at the initial time, respectively. The kinetic dependence of the reduction reaction of the DPPH radical by the adduct of C_{60} with L-arginine is presented in Fig. 79.

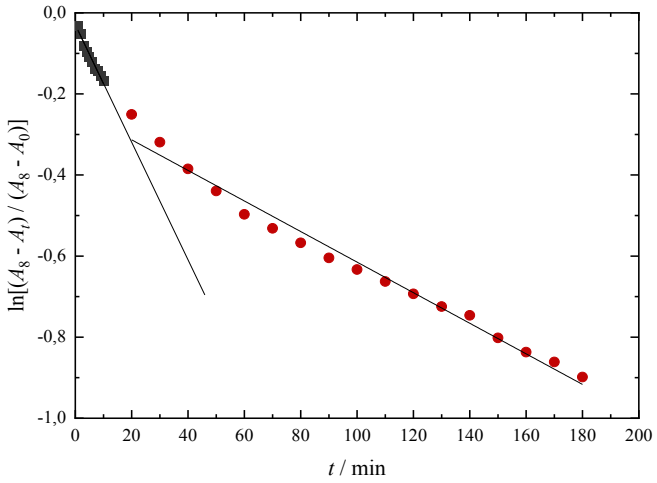

Fig. 79. Kinetic dependence of the reduction reaction of the DPPH radical by a fullerene adduct.

Using equation 35 the rate constants were calculated for two stages of the reaction of DPPH with the C_{60} adduct with L-arginine: $k_1 = 0.0151$ min^{-1} (fast stage) and $k_2 = 0.0038$ min^{-1} (slow stage).

Analysis of the literature [127] showed that for fullerene C_{60} (concentration 100 μM) the rate constant is $k_2 = 0.0007$ min^{-1}, for $C_{60}(OH)_{30}$ $k_1 = 0.0063$ min^{-1} and $k_2 = 0.0014$ min^{-1}. In addition, it was found that the calculated reaction rate constants are comparable to the rate constants of the first and second stages for other fullerene adducts with amino acids (Table 17).

Table 17. Values of the rate constants for the reduction of DPPH by water-soluble adducts of light fullerenes with amino acids.

Compound	k_1 / min^{-1}	k_2 / min^{-1}
C_{60}-L-arginine	0.0151	0.0038
C_{70}-L-lysine [128]	0.0313	0.00238
C_{70}-L-threonine [128]	0.0112	0.00127
C_{60}-glycine [129]	0.0352	0.00112
C_{60}-L- hydroxyproline [129]	0.0835	0.00131
C_{60}-L- methionine [129]	0.0301	0.00112
C_{60}-L- cysteine [129]	0.0931	0.00105

The fraction of reduced radical (*RRF*) was also calculated using the formula:

$$RRF = \frac{(A_{\text{DPPH}} - A_{\text{sample}})}{A_{\text{DPPH}}} \cdot 100\%, \quad (36)$$

where A_{DPPH} = 0.302, A_{sample} are optical densities of DPPH solutions one hour after the start of measurements in the absence and presence of an antioxidant (sodium ascorbate and C_{60}-L-arginine), respectively. As a result, the following *RRF* values were obtained: *RRF* (C_{60}-L-arginine) = 64.2 %, *RRF* (sodium ascorbate) = 86.8%. In addition, the value of antioxidant efficiency (*AE*) was calculated for the adduct using the formula:

$$AE = \frac{1}{EC_{50} \cdot T_{EC_{50}}}, \quad (37)$$

where EC_{50} is the amount of antioxidant required to reduce half of the radicals, $T_{EC_{50}}$ is reduction time for half of the radicals.

Calculations showed that the *AE* value for the adduct is 2.39 l·mol^{-1}·s^{-1} ($T_{EC_{50}}$ = 4189 s, EC_{50} = 100 μM). According to literature data [130], for the synthetic industrial antioxidant ionol, the *AE* value is 0.58 l·mol^{-1}·s^{-1} ($T_{EC_{50}}$ =2100 s, EC_{50} = 82 μM). From the data obtained, it follows that the adduct has pronounced antiradical properties.

Chapter 4. Main results and conclusions

1. A new method has been developed for the preparation of a water-soluble adduct of fullerene C_{60} with L-arginine, which allows obtaining the final product with a yield of more than 90 %. The resulting compound was identified using a complex of physicochemical methods of analysis: ^{13}C NMR, IR spectroscopy, thermogravimetric analysis, elemental analysis and HPLC.

2. The thermodynamic properties of the C_{60} fullerene adduct with L-arginine were studied in a wide temperature range T = 13–326 K using adiabatic vacuum calorimetry. It has been established that no phase transitions are observed in the studied temperature range; Based on experimental data on the temperature dependence of isobaric heat capacity, the standard thermodynamic functions $S_m°(T)$, $[H_m°(T) - H_m°(0)]$ and $[\Phi_m°(T) - \Phi_m°(0)]$ were calculated.

3. A study was carried out of the physicochemical properties of aqueous solutions of the adduct of fullerene C_{60} with L-arginine: densities, viscosities, refractive indices, particle size distribution and ζ-potentials were studied. It has been established that the adduct of fullerene C_{60} with L-arginine has large negative values of partial molar volumes in aqueous solutions, which indicates a strong structuring of solutions. It was shown that aqueous solutions of the adduct are associated and the size of the associates varies from 50 nm to 6 μm depending on the concentration.

4. The biocompatibility of the C_{60} fullerene adduct with L-arginine was studied. The adduct was shown to bind to HSA and exhibit no cyto- or genotoxicity.

5. The interaction of the C_{60} fullerene adduct with L-arginine with the stable DPPH radical was studied. It was found that the adduct has antiradical activity, which is comparable to the antiradical activity of the industrial antioxidant ionol.

Abbreviations list

A172 — human glioblastoma cell line

A549 — human lung carcinoma cell line

AE — antioxidant effectiveness

AFM — atomic force microscopy

Aib — α-aminoisobutyric acid

Boc — *tert*-butyloxycarbonyl group

BSA — bovine serum albumin

CAT — catalase

CD4 — cluster of differentiation

CMV — cytomegalovirus infection

COP — C_{60}-peptide

CP/MAS — cross-polarisation sequence of exciting pulses

CPD — cytopathic effect

CV — cyclic voltammetry

Cys3 — cystathione gamma lyase

DCC/HOBt — *N*,*N*'-dicyclohexylcarbodiimide/1-hydroxybenzotriazole

DFT — density functional theory

DFT-MD — molecular dynamics method based on density functional theory

DiGln — diglucuronide

DMAP — 4-dimethylaminopyridine

DMEM — Dulbecco's Modified Eagle Medium

$DMol^3$ — DFT method implemented using atomic wave functions using the PCM model

DMSO — dimethyl sulphoxide

RRF — fraction of reduced radical

Fab — antigen binding fragment

FBO — determination of bond orders for 'fuzzy' atoms

Fgu — fulleropyrrolidinoglutamic acid

Fmoc — fluorenylmethyloxycarbonyl group

Fmoc-Cl — 9-fluorenyl methyl chloroformate

FOX — catalytic oxidation of iron

Fpr — 3,4-fuleroproline

GlcNac — N-acetylglucosamine

GluEg — ethylene glycol modified side chain of glutamic acid

GSH-Px — glutathione peroxidase

HaCaT — cell line of immortalised human skin cells

HEK 293 — human embryonic kidney cells

HeLa — human cervical adenocarcinoma cell line

HEPES — (4-(2-hydroxyethyl)-1-piperazine ethanesulphonic acid)

HEWL — lysozyme isolated from chicken egg white

HF — Hartree–Fock method

HMP — *p*-benzyloxybenzyl alcohol

HPLC — high performance liquid chromatography

HSA — human serum albumin

HSA — human serum albumin

HSV — herpes simplex virus

Hyp — hydroxyproline

IC_{50} — concentration of half-maximal inhibition

Lm8 — mouse osteosarcoma tumour cell line

MT-4 — human lymphoblastoid cells

MurNac — N-acetylmuramic acid

MWCO — molecular weight cutoffs

NAD(P)H — nicotinamide-β-adenine dinucleotide phosphate

NADH — reduced nicotinamide adenine dinucleotide

Nle — norleucine

PAL — peptide amide linker

PBE — Perdue–Burk–Ernzerhof functional

Pbf — 2,2,4,6,7-pentamethyldihydrobenzofuran-5-sulfonyl

PC12 — rat pheochromocytoma cell line

PCM — polarisable continuum model

PEG — polyethylene glycol

PEKC — porcine embryonic kidney cells

Peptide T — synthetically produced protein based on the gp 120 protein of the HIV 1 virus, capable of binding to CD4 receptors of T lymphocytes

Peptide T(4–8) — pentapeptide analogue in the V2 region of the gp120 protein, which blocks the viral activity of HIV (amino acid sequence Thr-Thr-Asn-Tyr-Thr)

Phl — phenylalaninol

Pmc — 2,2,5,7,8-pentamethylchroman-6-sulfonyl

POEPOP — polyoxyethylene polyoxypropylene

PS — polystyrene

ROS — reactive oxygen species

$Ru(bpy)_3]^{2+}$ — ruthenium-tris(2,2'-bipyridyl)

SMMC-7721 — human hepatocarcinoma cell line

TEMPO — (2,2,6,6-tetramethylpiperidin-1-yl)oxyl

TFA — trifluoroacetic acid

TG — thermogravimetry

TOAC — 2,2,6,6-tetramethyl-*N*-oxyl-4-amino-4-carboxylic acid

VFT — Vogel–Fulcher–Tammann equation

Acknowledgments

I express my deep gratitude to my scientific supervisors — Doctor of Biological Sciences, leading researcher of the Department of Solid State Chemistry Vladimir Vladimirovich Sharoyko and Doctor of Chemical Sciences, Professor of the Department of Solid State Chemistry Konstantin Nikolaevich Semenov — for their help and support in organising and conducting the dissertation research. I express my special gratitude to Doctor of Chemical Sciences, Professor, Head of the Department of Solid State Chemistry Igor Vasilievich Murin for his assistance in organising the dissertation research at the department and to the staff of the Department of Solid State Chemistry.

Identification and study of the physicochemical properties of the C_{60} fullerene adduct with L-arginine were carried out using the equipment of the resource centres ‘Innovative technologies of composite nanomaterials’, ‘Magnetic resonance research methods’, ‘Methods for analysing the composition of matter’, ‘Thermogravimetric and calorimetric research methods’, Science Park of Saint Petersburg State University and the Centre for the collective use of scientific equipment ‘New materials and resource-saving technologies’ of Nizhny Novgorod State University named after. N. I. Lobachevsky. Biomedical research was carried out on the basis of the Department of General and Bioorganic Chemistry and the Laboratory of Biomedical Materials Science of PSPbSMU named after I. P. Pavlov, Ministry of Health of Russia.

References

1. Kroto H.W. et al. C_{60}: Buckminsterfullerene // Nature. Nature Publishing Group, 1985. Vol. 318, № 6042. P. 162–163.

2. Krätschmer W. et al. Solid C_{60}: a new form of carbon // Nature. 1990. Vol. 347, № 6291. P. 354–358.

3. Krokosz A. et al. Carbon nanoparticles as possible radioprotectors in biological systems // Radiation Physics and Chemistry. 2016. Vol. 128. P. 143–150.

4. Ghasemzadeh P. et al. Protective effect of ^{25}Mg-porphyrin-fullerene nanoparticles on oxygen-glucose deprivation/reperfusion injury in PC12 cells // Acta Med Iran. 2016. Vol. 54, № 8. P. 478–484.

5. Rašović I. Water-soluble fullerenes for medical applications // Materials Science and Technology. Taylor & Francis, 2017. Vol. 33, № 7. P. 777–794.

6. Goodarzi S. et al. Fullerene: Biomedical engineers get to revisit an old friend // Materials Today. Elsevier, 2017. Vol. 20, № 8. P. 460–480.

7. Hsieh F.-Y. et al. Water-Soluble Fullerene Derivatives as Brain Medicine: Surface Chemistry Determines If They Are Neuroprotective and Antitumor // ACS Appl Mater Interfaces. 2017. Vol. 9, № 13. P. 11482–11492.

8. Miao, Y., Zhao, H., Chen, J., Wang, M., Wen L.-P. The Application of *In Vivo* Extracellular Recording Technique to Study the Biological Effects of Nanoparticles in Brain // Use of Nanoparticles in Neuroscience / ed. Santamaria F., Peralta X. Humana Press, 2018. P. 171–186.

9. Mahdi J.F. et al. Effect of Viscosity and Density of Substance on Dielectric Properties of Medicinal Compounds in Solution // Nano Biomed Eng. 上海交通大学, 2020. Vol. 12, № 4. P. 351–357.

10. Jiang G., Yang Y. Preparation and tribology properties of water-soluble fullerene derivative nanoball // Arabian Journal of Chemistry. Elsevier, 2017. Vol. 10. P. S870–S876.

11. Gao J. et al. Polyhydroxy Fullerenes (Fullerols or Fullerenols): Beneficial Effects on Growth and Lifespan in Diverse Biological Models // PLoS One / ed. Willson R.C. 2011. Vol. 6, № 5. P. e19976.

12. Yang J. et al. Fullerene-Derivatized Amino Acids: Synthesis, Characterization, Antioxidant Properties, and Solid-Phase Peptide Synthesis // Chemistry - A European Journal. 2007. Vol. 13, № 9. P. 2530–2545.

13. Bianco A. et al. Fullerene-based amino acids and peptides // Journal of Peptide Science. 2001. Vol. 7, № 4. P. 208–219.

14. Toniolo C. et al. A Bioactive Fullerene Peptide // J Med Chem. American Chemical Society, 1994. Vol. 37, № 26. P. 4558–4562.

15. Marastoni M. et al. Structure-activity relationships of peptide T-related pentapeptides. // Arzneimittelforschung. 1989. Vol. 39, № 8. P. 926–928.

16. Sofou P. et al. Synthesis of a proline-rich [60]fullerene peptide with potential biological activity // Tetrahedron. 2004. Vol. 60, № 12. P. 2823–2828.

17. Bianco A. et al. Solid-phase synthesis and characterization of a novel fullerene-peptide derived from histone H3 // Org Biomol Chem. The Royal Society of Chemistry, 2003. Vol. 1, № 23. P. 4141–4143.

18. Zhang Y. et al. Potentiation of antimicrobial photodynamic inactivation mediated by a cationic fullerene by added iodide: *in vitro* and *in vivo* studies. // Nanomedicine (Lond). NIH Public Access, 2015. Vol. 10, № 4. P. 603–614.

19. Li Q., Liu C., Li H. Induction of Endogenous Reactive Oxygen Species in Mitochondria by Fullerene-Based Photodynamic Therapy // J Nanosci Nanotechnol. 2016. Vol. 16, № 6. P. 5592–5597.

20. Nishizawa C. et al. Pyrrolidinium-type fullerene derivative-induced apoptosis by the generation of reactive oxygen species in HL-60 cells // Free Radic Res. Taylor & Francis, 2009. Vol. 43, № 12. P. 1240–1247.

21. Iwase Y. et al. Antitumor effect of sonodynamically activated pyrrolidine tris-acid fullerene // Jpn J Appl Phys. IOP Publishing, 2016. Vol. 55, № 7S1. P. 07KF02.

22. Hardt J.I. et al. Pharmacokinetics and Toxicology of the Neuroprotective e,e,e-Methanofullerene(60)-63-tris Malonic Acid [C3] in Mice and Primates // Eur J Drug Metab Pharmacokinet. Springer International Publishing, 2018. P. 1–12.

23. Mashino T. et al. Human immunodeficiency virus-reverse transcriptase inhibition and hepatitis C virus RNA-dependent RNA polymerase inhibition activities of fullerene

derivatives. // Bioorg Med Chem Lett. Elsevier Limited, 2005. Vol. 15, № 4. P. 1107–1109.

24. Kumarasamy N., Krishnan S. Beyond first-line HIV treatment regimens // Curr Opin HIV AIDS. 2013. Vol. 8, № 6. P. 586–590.

25. Paydary K. et al. The emergence of drug resistant HIV variants and novel anti-retroviral therapy. // Asian Pac J Trop Biomed. China Humanity Technology Publishing House, 2013. Vol. 3, № 7. P. 515–522.

26. Liu Q. et al. Fullerene-Induced Increase of Glycosyl Residue on Living Plant Cell Wall // Environ Sci Technol. American Chemical Society, 2013. Vol. 47, № 13. P. 7490–7498.

27. Yin J.-J. et al. The scavenging of reactive oxygen species and the potential for cell protection by functionalized fullerene materials // Biomaterials. 2009. Vol. 30, № 4. P. 611–621.

28. Kole C. et al. Nanobiotechnology can boost crop production and quality: first evidence from increased plant biomass, fruit yield and phytomedicine content in bitter melon (Momordica charantia) // BMC Biotechnol. BioMed Central, 2013. Vol. 13, № 1. P. 37.

29. Troshin P.A., Lyubovskaya R.N. Organic chemistry of fullerenes: the major reactions, types of fullerene derivatives and prospects for practical use // Russian Chemical Reviews. 2008. Vol. 77, № 4. P. 323–369.

30. Hirsch A., Li Q., Wudl F. Globe-trotting Hydrogens on the Surface of the Fullerene Compound $C_{60}H_6(N(CH_2CH_2)_2O)_6$ // Angewandte Chemie International Edition in English. Wiley-Blackwell, 1991. Vol. 30, № 10. P. 1309–1310.

31. Hu Z. et al. Photodynamic anticancer activities of water-soluble C_{60} derivatives and their biological consequences in a HeLa cell line // Chem Biol Interact. Elsevier, 2012. Vol. 195, № 1. P. 86–94.

32. Romanova V.S. et al. Addition of amino acids and dipeptides to fullerene C_{60} giving rise to monoadducts // Russian Chemical Bulletin. 1994. Vol. 43, № 6. P. 1090–1091.

33. Vol'pin M.E., Parnes Z.N., Romanova V.S. Amino acid and peptide derivatives of fullerene // Russian Chemical Bulletin. Kluwer Academic Publishers-Plenum Publishers, 1998. Vol. 47, № 5. P. 1021–1025.

34. Kotelnikova R.A. et al. Nanobionics of Pharmacologically Active Derivatives of Fullerene C_{60} // Journal of Nanoparticle Research. Kluwer Academic Publishers, 2003. Vol. 5, № 5/6. P. 561–566.

35. Kotel'nikova R.A. et al. Antioxidant properties of water-soluble amino acid derivatives of fullerenes and their role in the inhibition of herpes virus infection // Russian Chemical Bulletin. Springer US, 2011. Vol. 60, № 6. P. 1172–1176.

36. Frog E.S., Kotelnikova RA, Bogdanov GN, Shtolko VN F.I., Kushch AA, Fedorova NE, Medzhidova AA R.V. Effect of amino acid derivatives of fullerene C_{60} on the development of cytomegalovirus infection [Electronic resource] // Technologies of living systems. 2003. P. 42–46.

37. Belavtseva E.M. et al. Investigation of structures of micelles of a fullerene derivative of alanine in aqueous solutions by tunneling scanning microscopy // Russian Chemical Bulletin. 1996. Vol. 45, № 4. P. 831–833.

38. Jiang G. et al. Synthesis and properties of novel water-soluble fullerene–glycine derivatives as new materials for cancer therapy // J Mater Sci Mater Med. Springer US, 2015. Vol. 26, № 1. P. 24.

39. Li Z. et al. Preparation and Characterization of Fullerene (C_{60}) Amino Acid Nanoparticles for Liver Cancer Cell Treatment // J Nanosci Nanotechnol. 2014. Vol. 14, № 6. P. 4513–4518.

40. Hu Z. et al. Synthesis of glutathione C_{60} derivative and its protective effect on hydrogen peroxide-induced apoptosis in rat pheochromocytoma cells. // Neurosci Lett. 2007. Vol. 429, № 2–3. P. 81–86.

41. Hu Z. et al. Synthesis of β-alanine C_{60} derivative and its protective effect on hydrogen peroxide-induced apoptosis in rat pheochromocytoma cells // Cell Biol Int. Wiley-Blackwell, 2007. Vol. 31, № 8. P. 798–804.

42. Hu Z. et al. Synthesis of amphiphilic amino acid C_{60} derivatives and their protective effect on hydrogen peroxide-induced apoptosis in rat pheochromocytoma cells // Carbon N Y. 2008. Vol. 46, № 1. P. 99–109.

43. Hu Z. et al. The protective activities of water-soluble C(60) derivatives against nitric oxide-induced cytotoxicity in rat pheochromocytoma cells. // Biomaterials. 2010. Vol. 31, № 34. P. 8872–8881.

44. Khalikov Sh.Kh. et al. Synthesis and Characterization of Fullero-C_{60} α-Amino Acids with Antiviral Properties // Chem Nat Compd. Springer US, 2017. Vol. 53, № 1. P. 121–127.

45. Rasnetsov L.D. The agent for inhibiting the reproduction of enveloped viruses, process of its preparing, pharmaceutical composition and method for inhibiting viral infections.: pat. RU2236852 USA. Russia, 2004.

46. Rasnetsov L.D. Hydrated n-fullerene-amino acid derivatives, method for preparing them and based pharmaceutical compositions.: pat. RU2458046 USA. Russia, 2012.

47. Maggini M., Scorrano G., Prato M. Addition of azomethine ylides to C_{60}: synthesis, characterization, and functionalization of fullerene pyrrolidines // J Am Chem Soc. American Chemical Society, 1993. Vol. 115, № 21. P. 9798–9799.

48. Watanabe L.A. et al. Synthesis of novel fullerene amino acids and their multifullerene peptides // Tetrahedron Lett. 2004. Vol. 45, № 38. P. 7137–7140.

49. Zhang J., Yuan L., Zhang Y.D. Synthesis of Fullerene-Acid Conjugates // Adv Mat Res. Trans Tech Publications, 2012. Vol. 463–464. P. 538–542.

50. Naixing Wang et al. A C_{60}-derivatized dipeptide // Tetrahedron Lett. Pergamon, 1995. Vol. 36, № 3. P. 431–434.

51. Prato M. et al. Synthesis and characterization of the first fullerene-peptide // J Org Chem. American Chemical Society, 1993. Vol. 58, № 21. P. 5578–5580.

52. König W., Geiger R. A new method for synthesis of peptides: activation of the carboxyl group with dicyclohexylcarbodiimide using 1-hydroxybenzotriazoles as additives. // Chem Ber. 1970. Vol. 103, № 3. P. 788–798.

53. Zhmak O.M., Volpina M.A., Kupriyanova T.M., Andronova E.A., Makarov V.S., Romanova Z.N., Parnes M.E., Volpin V.T. Glycopeptide fullerene derivative showing adjuvant activity: pat. RU2124022 USA. 1997.

54. Polese A. et al. Solvent-Dependent Intramolecular Electron Transfer in a Peptide-Linked $[Ru(bpy)_3]^{2+}$–C_{60} Dyad // J. Am. Chem. Soc. American Chemical Society, 1999. Vol. 121. P. 3446–3452.

55. Ousaka N. et al. “Helix-in-Helix” Superstructure Formation through Encapsulation of Fullerene-Bound Helical Peptides within a Helical Poly(methyl methacrylate) Cavity // Angewandte Chemie International Edition. John Wiley & Sons, Ltd, 2017. Vol. 56, № 3. P. 791–795.

56. Mazzoni M., Conti F., Corvaja C. The sign of the exchange interaction between triplet excited fullerene and nitroxide free radicals // Appl Magn Reson. Springer-Verlag, 2000. Vol. 18, № 3. P. 351–361.

57. Kurz A. et al. A fullerene-modified protein // Chemical Communications. Royal Society of Chemistry, 1998. Vol. 0, № 3. P. 433–434.

58. Prato M. et al. Synthesis and electrochemical properties of substituted fulleropyrrolidines // Tetrahedron. Pergamon, 1996. Vol. 52, № 14. P. 5221–5234.

59. Kim K.-H. et al. Protein-directed self-assembly of a fullerene crystal // Nat Commun. Nature Publishing Group, 2016. Vol. 7. P. 11429.

60. Grigoryan G. et al. Computational Design of Virus-Like Protein Assemblies on Carbon Nanotube Surfaces // Science (1979). 2011. Vol. 332, № 6033. P. 1071–1076.

61. Xu D. et al. A Novel method for the preparation of fluorescent C_{60} poly(amino acid) composites and their biological imaging // J Colloid Interface Sci. 2018. Vol. 516. P. 392–397.

62. Jung G. et al. Template-free self-assembling fullerene and lipopeptide conjugates of alamethicin form voltage-dependent ion channels of remarkable stability and activity // Journal of Peptide Science. Wiley-Blackwell, 2003. Vol. 9, № 11–12. P. 784–798.

63. Bianco A. et al. Synthesis, Chiroptical Properties, and Configurational Assignment of Fulleroproline Derivatives and Peptides // J. Am. Chem. Soc. American Chemical Society, 1996. Vol. 118, № 17. P. 4072–4080.

64. Pellarini F. et al. A Novel [60]Fullerene Amino Acid for Use in Solid-Phase Peptide Synthesis // Org. Lett. American Chemical Society, 2001. Vol. 3, № 12. P. 1845–1848.

65. Pantarotto D. et al. Solid-Phase Synthesis of Fullerene-peptides // J. Am. Chem. Soc. American Chemical Society, 2002. Vol. 124, № 42. P. 12543–12549.

66. Xu Y. et al. Synthesis and immunomodulatory activity of [60]fullerene–tuftsin conjugates // Biomaterials. Elsevier, 2011. Vol. 32, № 36. P. 9940–9949.

67. Dostalova S. et al. Antiviral activity of fullerene C_{60} nanocrystals modified with derivatives of anionic antimicrobial peptide maximin H5 // Monatshefte für Chemie - Chemical Monthly. 2016. Vol. 147, № 5. P. 905–918.

68. Jennepalli S. et al. Synthesis of Mono and Bis[60]fullerene-Based Dicationic Peptoids // European J Org Chem. Wiley-Blackwell, 2015. Vol. 2015, № 1. P. 195–201.

69. Aroua S., Schweizer W.B., Yamakoshi Y. C_{60} Pyrrolidine Bis-carboxylic Acid Derivative as a Versatile Precursor for Biocompatible Fullerenes // Org Lett. American Chemical Society, 2014. Vol. 16, № 6. P. 1688–1691.

70. Strom T.A., Barron A.R. A simple quick route to fullerene amino acid derivatives // Chemical Communications. The Royal Society of Chemistry, 2010. Vol. 46, № 26. P. 4764.

71. Tsumoto H. et al. Preparation of C_{60}-based active esters and coupling of C_{60} moiety to amines or alcohols. // Bioorg Med Chem Lett. 2008. Vol. 18, № 2. P. 657–660.

72. Reiriz C. et al. α,γ-Peptide Nanotube Templating of One-Dimensional Parallel Fullerene Arrangements // J Am Chem Soc. 2009. Vol. 131, № 32. P. 11335–11337.

73. Garbuio L. et al. Effect of Orientation of the Peptide-Bridge Dipole Moment on the Properties of Fullerene–Peptide–Radical Systems // J Am Chem Soc. American Chemical Society, 2012. Vol. 134, № 25. P. 10628–10637.

74. Fujii S., Morita T., Kimura S. Photoinduced electron transfer in thin layers composed of fullerene-cyclic peptide conjugate and pyrene derivative. // Langmuir. 2008. Vol. 24, № 10. P. 5608–5614.

75. Fujii S., Morita T., Kimura S. Fabrication of Langmuir–Blodgett Film of a Fullerene Derivative with a Cyclic Peptide as an Anchor // Bioconjug Chem. American Chemical Society, 2007. Vol. 18, № 6. P. 1855–1859.

76. Stewart M.H. et al. Competition between Förster Resonance Energy Transfer and Electron Transfer in Stoichiometrically Assembled Semiconductor Quantum Dot–Fullerene Conjugates // ACS Nano. 2013. Vol. 7, № 10. P. 9489–9505.

77. Minois P. et al. [60]Fullerene L-Amino Acids and Peptides: Synthesis under Phase-Transfer Catalysis Using a Phosphine–Borane Linker. Electrochemical Behavior // J Org Chem. 2017. Vol. 82, № 21. P. 11358–11369.

78. Siepi M. et al. Modified denatured lysozyme effectively solubilizes fullerene c60 nanoparticles in water // Nanotechnology. 2017. Vol. 28, № 33. P. 335601.

79. Chen B.-X. et al. Antigenicity of fullerenes: Antibodies specific for fullerenes and their characteristics // Proceedings of the National Academy of Sciences. 1998. Vol. 95, № 18. P. 10809–10813.

80. Benyamini H. et al. Interaction of C_{60}-Fullerene and Carboxyfullerene with Proteins: Docking and Binding Site Alignment // Bioconjugate Chem. American Chemical Society, 2006. Vol. 17, № 2. P. 378–386.

81. Lebedev B. V. et al. Thermodynamics of C_{60} fullerene in the 0–340 K range // Russian Chemical Bulletin. Kluwer Academic/Plenum Publishers, 1996. Vol. 45, № 9. P. 2113–2117.

82. Lebedev B.V., Bykova T.A., Lobach A.S. Thermodynamic properties of hydrofullerene C60H36 from 5 to 340 K // J Therm Anal Calorim. Kluwer Academic Publishers, 2000. Vol. 62, № 1. P. 257–265.

83. Lelet M.I. et al. Thermodynamic and thermal properties of the C60-l-lysine derivative // J Chem Thermodyn. 2017. Vol. 115. P. 7–11.

84. Podolsky N.E. et al. Thermodynamic properties from calorimetry and density functional theory and the thermogravimetric analysis of the fullerene derivative $C_{60}(OH)_{40}$ // J Chem Eng Data. American Chemical Society, 2019. Vol. 64, № 4. P. 1480–1487.

85. Podolsky N.E. et al. Thermodynamic properties of the $C_{70}(OH)_{12}$ fullerenol in the temperature range T = 9.2 K to 304.5 K // Journal of Chemical Thermodynamics. Academic Press, 2020. Vol. 144, № 3. P. 106029.

86. Timofeeva G.I., Romanova V.S., Lopanova L.A. Molecular characteristics of water-soluble fullerene derivatives of amino acids and peptides // Russian Chemical Bulletin. Springer New York, 1996. Vol. 45, № 4. P. 834–837.

87. Timofeeva G.I. et al. A study of the behavior of disubstituted methyl esters of peptide derivatives of fullerene C_{60} in aqueous solutions // Russian Chemical Bulletin. Springer US, 2012. Vol. 61, № 8. P. 1635–1637.

88. Timofeeva G.I., Romanova V.S. Dependence of the degree of association of mono- and disubstituted biologically active derivatives of fullerene C_{60} in aqueous solutions on the concentration and nature of substituents // Russian Chemical Bulletin. Springer US, 2007. Vol. 56, № 12. P. 2389–2393.

89. Timofeeva G.I., Kuleshova E.F., Romanova V.S. Dependence of the degree of association of water-soluble amino acid and peptide derivatives of fullerene[60] on pH and the ionic strength of a solution // Russian Chemical Bulletin. Kluwer Academic Publishers-Plenum Publishers, 1997. Vol. 46, № 3. P. 472–475.

90. Charykov N.A. et al. Excess thermodynamic functions in aqueous systems containing soluble fullerene derivatives // J Mol Liq. 2018. Vol. 256. P. 305–311.

91. Serebryakov E.B. et al. Physico-chemical properties of the C_{70}-L-lysine aqueous solutions // J Mol Liq. 2018. Vol. 256. P. 507–518.

92. Meshcheriakov A.A. et al. Physicochemical properties, biological activity and biocompatibility of water-soluble C_{60}-Hyp adduct // Colloids Surf B Biointerfaces. Elsevier B.V., 2020. Vol. 196. P. 111338.

93. Sharoyko V. V. et al. Physicochemical investigation of water-soluble $C_{60}(C_2NH_4O_2)_4H_4$ (C_{60}-Gly) adduct // J Mol Liq. Elsevier, 2021. Vol. 344. P. 117658.

94. Semenov K.N. et al. Fullerenols: Physicochemical properties and applications // Progress in Solid State Chemistry. Elsevier Ltd, 2016. Vol. 44, № 2. P. 59–74.

95. Semenov K.N. et al. Carboxylated fullerenes: Physico-chemical properties and potential applications // Progress in Solid State Chemistry. Pergamon, 2017. Vol. 47–48. P. 19–36.

96. Pochkaeva E.I. et al. Fullerene derivatives with amino acids, peptides and proteins: From synthesis to biomedical application // Progress in Solid State Chemistry. 2020. Vol. 57. P. 100255.

97. Nikolaev D.N. et al. Thermodynamic and quantum chemical investigation of the monocarboxylated fullerene $C_{60}CHCOOH$ // Journal of Chemical Thermodynamics. 2020. Vol. 140.

98. Semenov K.N. et al. Fullerenol-d solubility in fullerenol-d–inorganic salt–water ternary systems at 25 °C // Ind Eng Chem Res. American Chemical Society, 2013. Vol. 52, № 46. P. 16095–16100.

99. Semenov K.N., Charykov N.A., Keskinov V.N. Fullerenol synthesis and identification. Properties of the fullerenol water solutions // J Chem Eng Data. American Chemical Society, 2011. Vol. 56, № 2. P. 230–239.

100. Semenov K.N. et al. Physico-chemical properties of the fullerenol-70 water solutions // J Mol Liq. Elsevier, 2015. Vol. 202. P. 1–8.

101. Semenov K.N. et al. Phase equilibria in fullerene-containing systems as a basis for development of manufacture and application processes for nanocarbon materials // Russian Chemical Reviews. IOP Publishing, 2016. Vol. 85, № 1. P. 38–59.

102. Semenov K.N. et al. Solid-liquid phase equilibria in the fullerenol-d–$CuCl_2$–H_2O system at 25 °C // Russian Journal of Physical Chemistry A. Maik Nauka-Interperiodica Publishing, 2014. Vol. 88, № 6. P. 1073–1075.

103. Semenov K.N. et al. Solubility and some properties of aqueous solutions of fullerenol-d and composition of crystal hydrates // Russian Journal of Applied Chemistry. SP MAIK Nauka/Interperiodica, 2011. Vol. 84, № 1. P. 44–49.

104. Semenov K.N. et al. Fullerenol–70-d: synthesis, identification, polythermal solubility and density of aqueous solutions // Nanosystems: physics, chemistry, mathematics. 2012. Vol. 3, No. 6. P. 146–156.

105. Semenov K.N., Charykov N.A. Solubility Diagram of a Fullerenol-d-NaCl-H_2O System at 25°C // Russian Journal of Physical Chemistry A. Springer, 2012. Vol. 86, № 10. P. 1636–1638.

106. Sidorov L.N. et al. Fullerenes. Study Guide / ed. Yanovsky D.V. Moscow: Publishing House “Exam,” 2005. 688 p.

107. Semenov K.N., Charykov N.A. Temperature dependence of solubility of individual light fullerenes and industrial fullerene mixture in 1-chloronaphthalene and 1-bromonaphthalene // J Chem Eng Data. American Chemical Society, 2010. Vol. 55, № 7. P. 2373–2378.

108. Semenov K.N. et al. Solubility, thermal analysis and association of bis-adducts of light fullerene C_{60} and amino acids: lysine, threonine and hydroxyproline in aqueous solutions // Journal of Physical Chemistry. Pleiades Publishing Ltd, 2019. Vol. 93, No. 7. P. 1015–1022.

109. Strom T.A. et al. Fullerene-based inhibitors of HIV-1 protease // Journal of Peptide Science. 2015. Vol. 21, № 12. P. 862–870.

110. Rafalsky V.V. Clinical pharmacology of atazanavir // Farmateka. 2008. Vol. 4. P. 18–26.

111. Nakamura S., Mashino T. Biological activities of water-soluble fullerene derivatives // J Phys Conf Ser. IOP Publishing, 2009. Vol. 159, № 1. P. 012003.

112. Castro E. et al. Fullerenes in biology and medicine // J Mater Chem B. The Royal Society of Chemistry, 2017. Vol. 5, № 32. P. 6523–6535.

113. Slater T.F. Free-radical mechanisms in tissue injury. // Biochem J. Portland Press Ltd, 1984. Vol. 222, № 1. P. 1–15.

114. Orlova M.A. et al. Fullerene and apoptosis: Ingenta Connect // Onlogematologia. 2013. Vol. 8, № 1. P. 65-71(7).

115. Mroz P. et al. Photodynamic therapy with fullerenes // Photochemical & Photobiological Sciences. The Royal Society of Chemistry, 2007. Vol. 6, № 11. P. 1139.

116. Kotelnikova R.A. et al. Membranotropic properties of the water soluble amino acid and peptide derivatives of fullerene C_{60} // FEBS Lett. Wiley-Blackwell, 1996. Vol. 389, № 2. P. 111–114.

117. Kotel'nikova R.A. et al. Luminescent techniques in investigation of the biological properties of fullerene-based hybrid nanostructures // High Energy Chemistry. 2009. Vol. 43, № 7. P. 582–586.

118. Kumar A., Rao M. V., Menon S.K. Photoinduced DNA cleavage by fullerene–lysine conjugate // Tetrahedron Lett. 2009. Vol. 50, № 47. P. 6526–6530.

119. Yang L.-Y. et al. Characterization of fullerenol-protein interactions and an extended investigation on cytotoxicity // Colloids Surf B Biointerfaces. 2017. Vol. 157. P. 261–267.

120. Ji H., Sun H., Qu X. Antibacterial applications of graphene-based nanomaterials: Recent achievements and challenges // Advanced Drug Delivery Reviews. Elsevier B.V., 2016. Vol. 105. P. 176–189.

121. Mahmoudi T., Wang Y., Hahn Y.B. Graphene and its derivatives for solar cells application // Nano Energy. Elsevier Ltd, 2018. Vol. 47. P. 51–65.

122. Iurev G.O. et al. Thermodynamic and thermal properties of the C_{60}-L-Arg derivative // J Chem Thermodyn. 2018. Vol. 127. P. 39–44.

123. Pochkaeva E.I. et al. Polythermal density and viscosity, nanoparticle size distribution, binding with human serum albumin and radical scavenging activity of the C_{60}-L-arginine ($C_{60}(C_6H_{13}N_4O_2)_8H_8$) aqueous solutions // J Mol Liq. Elsevier B.V., 2020. Vol. 297. P. 111915.

124. Semenov K.N. et al. Thermodynamic Functions in the Binary System of a C_{60} Fullerene Derivative with Methionine Amino Acid–H_2O // Russian Journal of Physical Chemistry A. 2020. Vol. 94, № 4. P. 698–703.

125. Herrera I., Winnik M.A. Differential Binding Models for Isothermal Titration Calorimetry: Moving beyond the Wiseman Isotherm // J Phys Chem B. American Chemical Society, 2013. Vol. 117, № 29. P. 8659–8672.

126. Pochkaeva E.I. et al. Isothermal Calorimetric Titration of Human Serum Albumin with The Fullerene C60–L-Arginine Adduct // Russian Journal of General Chemistry. 2019. Vol. 89, № 8. P. 1309−1312.

127. Awan F. et al. Enhanced radical scavenging activity of polyhydroxylated C_{60} functionalized cellulose nanocrystals // Cellulose. Springer Netherlands, 2016. Vol. 23, № 6. P. 3589–3599.

128. Serebriakov E.B. Physicochemical study of adducts of C_{70} fullerene adducts with L-lysine and L-threonine. 2023.

129. Meshcheriakov A.A. Functionalisation of fullerene C_{60} for obtaining materials for biomedical purposes. 2023.

130. Alinkina E.S., Misharina T.A., Fatkullina D.L. Antiradical Properties of Oregano, Thyme, and Savory Essential Oils // Appl Biochem Microbiol. Akademiia nauk SSSR, 2013. Vol. 49, № 1. P. 82–87.